19ENG03 MefHySto

Metrology for Advanced Hydrogen Storage Solutions

D6: Report on a method for measuring and calculating heat conductivity of hydrogen ab/adsorbed in an intermetallic material or porous materials as a function of temperature, pressure, hydrogen absorption capacity and rate, considering dynamic heat flux impact and a harmonised method (< 1 % uncertainty) for stored hydrogen.

Lead partner: MAHYTEC

Contributing partners: BAM, FHA, MPG

Work package: 4

Due date: November 2023

Actual submission date: February 2024

This project has received funding from the EMPIR programme co-financed by the Participating States and from the European Union's Horizon 2020 research and innovation programme.

The EMPIR initiative is co-funded by the European Union's Horizon 2020 research and innovation programme and the EMPIR Participating States

TABLE OF CONTENTS

1 Summary

In reversible hydrogen storage technologies, the temperature is one of the important influencing factors. The correct assessment of the thermodynamic parameters (such as heat conductivity, enthalpy of ab/adsorption, desorption) are crucial for forecasting the storage capacity. In addition, the performance of reversible hydrogen storage technologies can be affected by the quality of hydrogen. Therefore, the assessment of the influence of hydrogen pollutants on the capacity of storage as well as the lifetime of these technologies is essential.

Concerning deviations from the original plan, the development of reference materials and methods for hydrogen ad/absorption capacity by a harmonised method with a precision better than <1% was not engaged. After the bibliography studies and dedicated analysis, we concluded that within from the actual state of knowledge in hydride systems there are no methods that can attain a resolution better than 1%. The dispersion inherent to material sciences studies may justify the dispersion of results attained during round robin test of MgH_2 absorption [1]. On the other hand, a deeper understanding of pollutants in hydrides, both as a function of pollutant concentration and number of cycles, is a subject that was developed as it is both feasible with actual experimental means, and is relevant from the point of view of commercial implementation of hydride solutions.

2 Objectives

The aim of this work package is to provide a validated method for measuring and calculating heat conductivity of hydrogen ab/adsorbed in an intermetallic material or porous materials as a function of temperature, pressure, hydrogen absorption capacity and rate, considering dynamic heat flux impact and to develop a harmonised method (< 1 % uncertainty) for stored hydrogen.

The specific aims of each Task are:

- To develop a method for measuring thermal capacity for dynamic storage methods for hydrogen ab/adsorption and desorption.
- To assess the influence of pollutants in hydrogen gas using the metal hydride assembly/metal hydride and cryo adsorbents reference materials from Task 4.1.
- To develop reference materials and reference methods for hydrogen ad/absorption capacity

3 Introduction

WP4. METROLOGY FOR REVERSIBLE HYDROGEN STORAGE TECHNOLOGIES

- Intro about the WP and description of tasks.

(Please leave this section blank. This section will be completed by the EURAMET MSU using text from the final Publishable Summary.)

4 Assessing thermal conductivity for dynamic storage methods for hydrogen ab/adsorption and desorption

4.1 Technology survey

In order to understand the state-of-the-art measuring technologies for hydrogen uptake and thermal properties in either intermetallic alloys or porous adsorbents, the MefHySto participants MAHYTEC, MPG, BAM, and FHA prepared and distributed two technology surveys among external expert participants. Questions about the current best technologies, shortcomings, best materials, and procedures were asked in these surveys, where pre-defined answers were provided for a higher simplicity, and additionally, open slots where experts can provide specific details.

The survey about metal hydrides focused on their properties as a technology for hydrogen storage. Participants were asked about the used materials in studies, the most remarkable properties of interest, the key advantages or disadvantages as hydrogen storage materials, the used methods to measure both hydrogen capacity and sorption/desorption kinetics, the influence of pollutants, and the measured thermal properties. The survey about cryoadsorbents mainly focuses on the relevant information to select reference materials (RM) and methods. The questions were about the most studied materials, the preferentially used characterization techniques, measurement techniques and conditions of the hydrogen uptake, and calculation or measurement of thermal properties. Finally, participants were asked about the necessity of a hydrogen cryoadsorbent RM and their suggestions.

4.1.1 Results from technology survey: Metal hydride storage

A survey with 16 questions was distributed to eight expert participants involved in the field of metal hydrides. All the participants use AB_5 alloys (see Figure 1), followed, by more than 70 % of the experts, by AB and AB_2. A_2B and MgH families are also often studied (more than 50 %). The most studied properties by the participants are the hydrogen capacity and pressure plateau (87 %), followed by lifetime, kinetic, and hydride formation/decomposition enthalpy (75 %). Hysteresis, swelling, and thermal conductivity are other commonly studied properties (62,5 % of participants). Less than a third of the participants show interest in pollutants' tolerance, granulometry, or entropy.

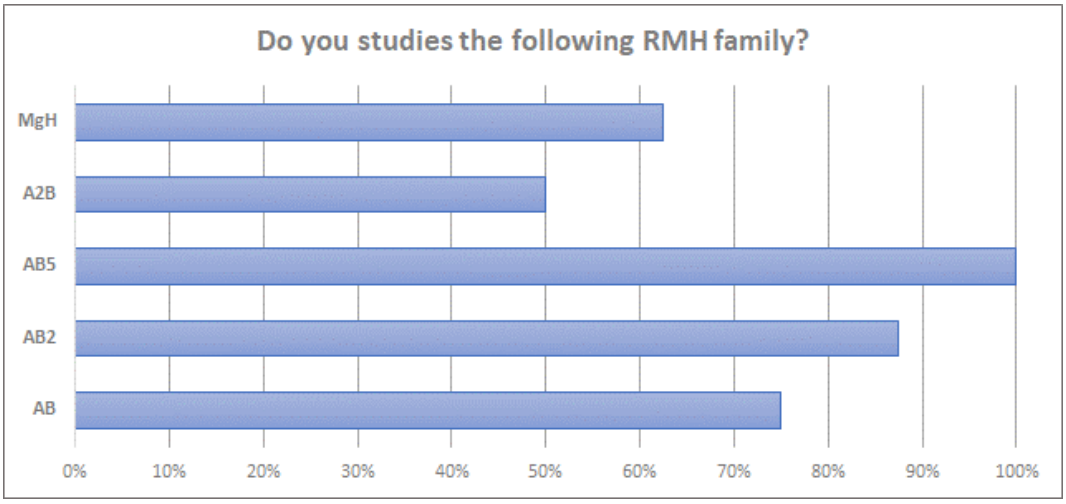

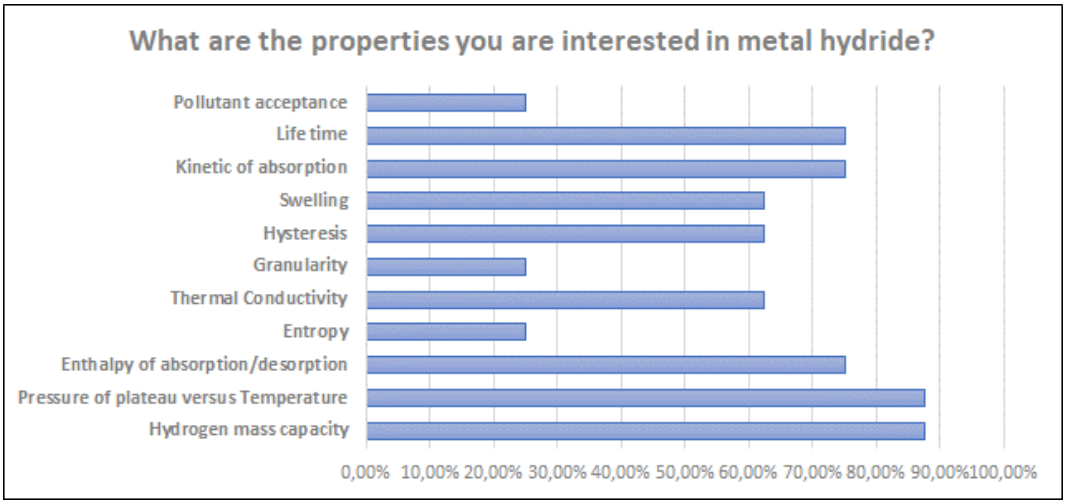

Figure 1 : Studied metal hydride families and interesting properties.

Figure 2 shows the answers about the advantages and disadvantages of metal hydrides from the participants. Volumetric uptakes and low necessary pressure values are the most advantageous features of metal hydrides compared with compressed gas storage. Less than half of the participants remarked the recyclability, adaptability (of, for example, pressure and temperature), cost, kinetics, and thermal behavior. On the other hand, the participants indicated that cost, thermal behavior, gravimetric uptake, and dynamic desorption/absorption of metal hydrides are the major inconveniences. However, the thermal behavior could also be an advantage, depending on the use.

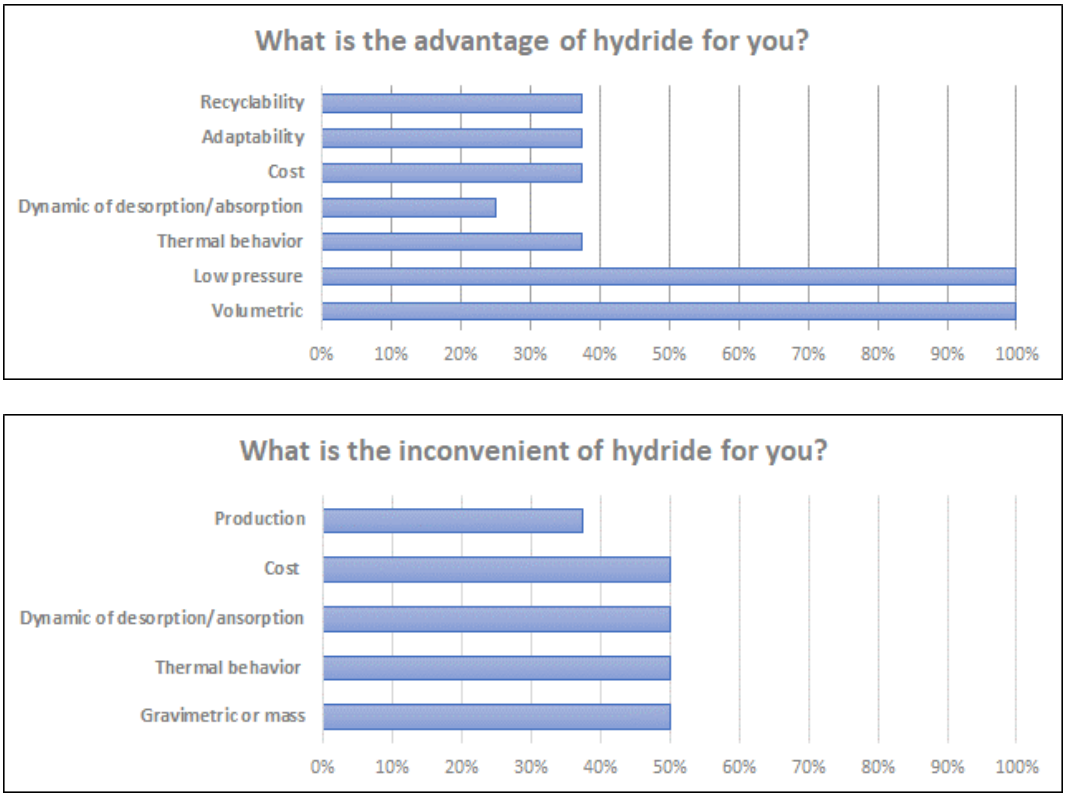

Figure 2 : Advantages and inconveniences of metal hydrides.

Figure 3 shows the results about the used measurement methods of the hydrogen uptake, one of the most relevant parameters for the rest of the project. Most participants use Sieverts-like volumetric

methods, followed by gravimetric methods, to record the PCT (pressure-concentration-temperature) curves relating the hydrogen concentration in materials at different temperatures and pressure values in equilibrium. Also, volumetric techniques are more frequently used to measure adsorption-desorption kinetics. Changes in sorption/desorption kinetics are related to pollution effects and can be associated with kinetic reduction previous to the loss of gravimetric capacity.

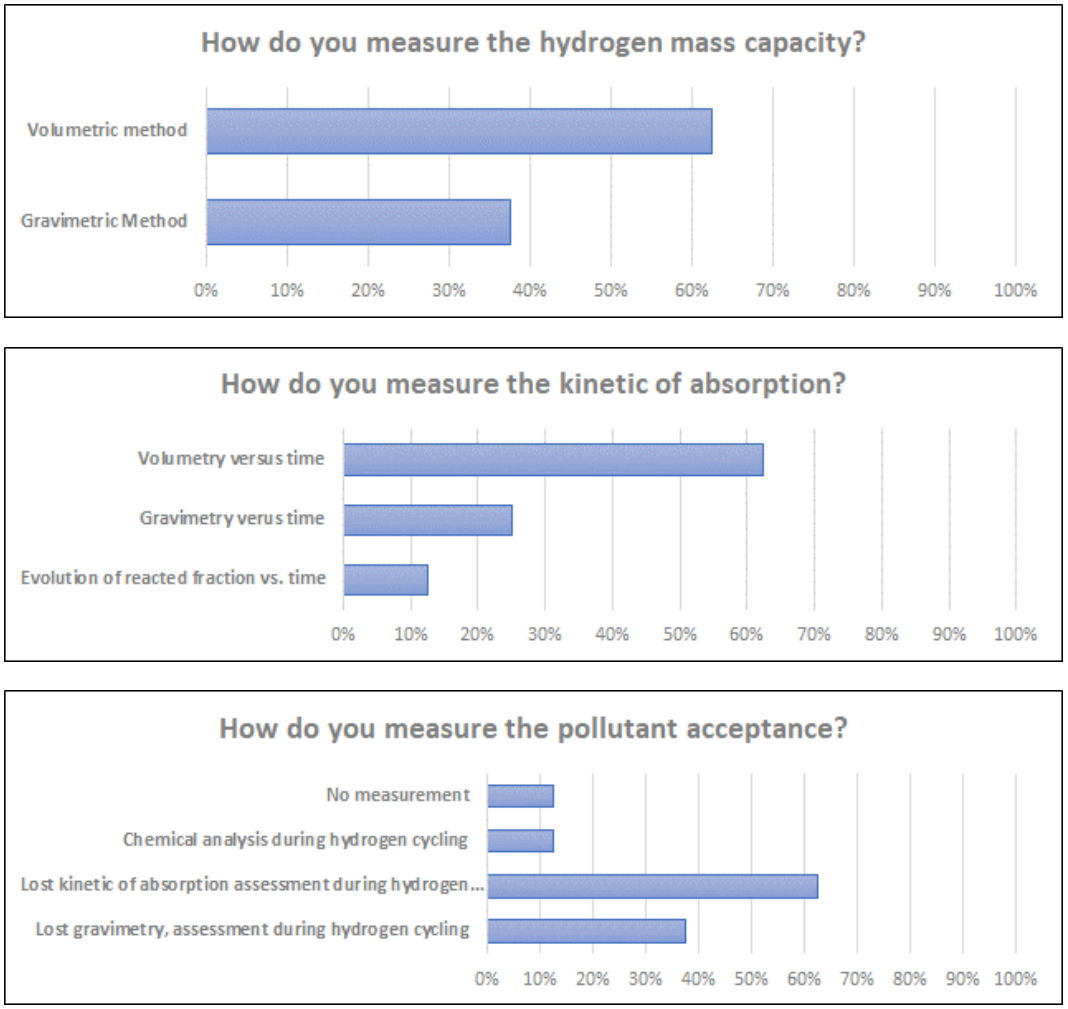

Figure 3 : Global measurement of some characteristics.

Besides capacity and kinetics, thermal properties like enthalpy and entropy of sorption/desorption are also measured indirectly via PCT methods (see Figure 4). Half of the participants do not measure thermal conductivity, and 9 % of those who do it use the indirect methods (without specifying which ones), or they do it directly by transient hot-wire method.

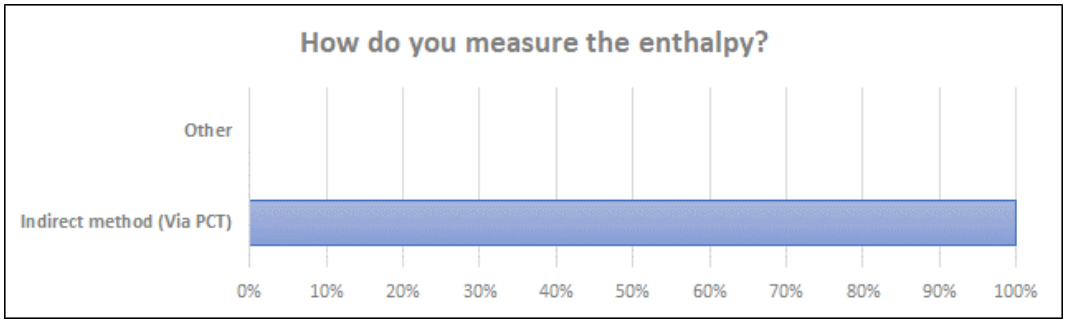

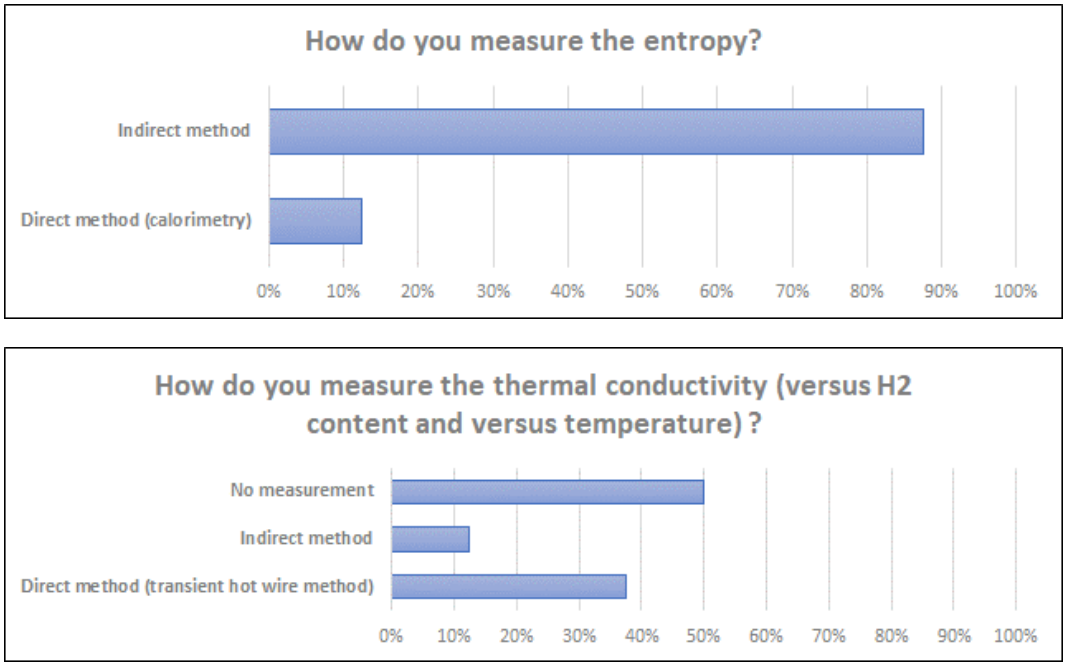

Figure 4 : Measurement of thermal characteristics.

4.2 Literature review

One of the main questions regarding hydrogen storage using reversible metal hydride (MH) is the regarding the flow of hydrogen. Considering two thermodynamic state S0 and S1 of a hydride, this state is governed by: internal variables of the crystal such as the hydrogen concentration, temperature of hydride and surrounding pressure.
The volume of hydrogen provides by a tank where hydride change from S0 to S1 is then provide by the change of hydrogen concentration of the hydride, while the flow is driven by the temperature kinetics and pressure. The temperature is controlled by the heat exchange. This heat exchange is related with the thermal conductivity. Inside the tank, the thermal conductivity is due to local convection and conduction phenomena in the MH bed. From macroscopic point of view, to design a heat exchanger, it is useful to use an Effective Thermal Conductivity (ECT) [2].

To determine ECT, several theoretical models have been presented, including the Yagi and Kunii model [3], Deissler and Boegli model [4], Masamune and Smith model [5], Zehner P, Schlunder EU [6], However, the theoretical models mentioned above were developed to describe the behaviour of non-reactive packed beds. Some models try to take into account this phenomenon for instance Madaria *et al.* [7] extended the models developed by Yagi and Kunii [3].

Nevertheless, none of these theoretical models can precisely estimate the ETCs of MH beds under different conditions. Thus, many experimental methods for measuring the ETC have been proposed, as experimental measurements are an irreplaceable tool to validate theoretical models.
Zhao *et Al* [2] in a review of the experimental methods describe several ways to assess the ECT and summarise the various method in the following figure.

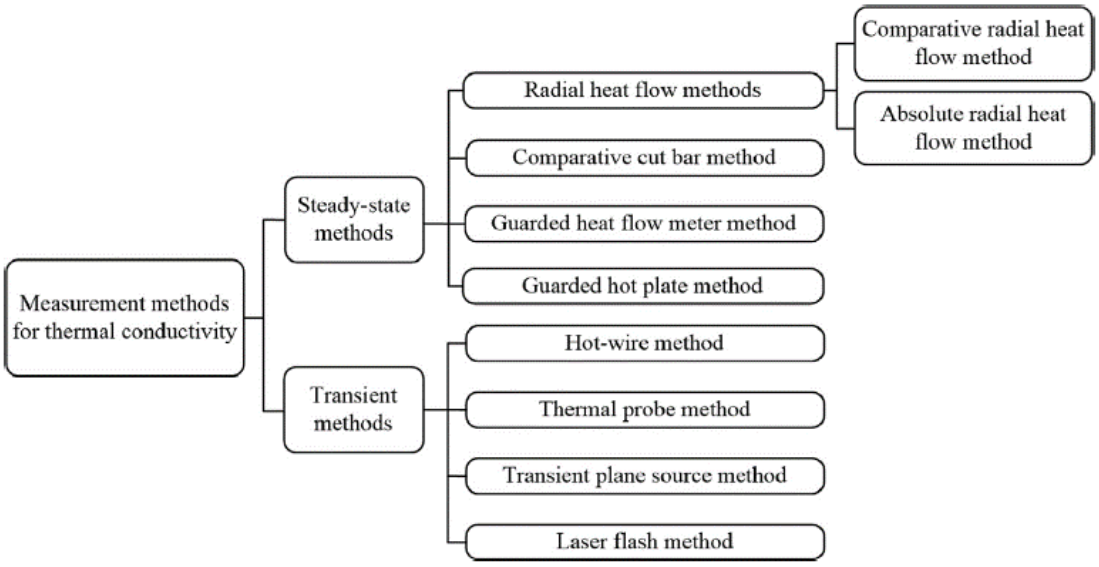

Figure 5 : The various method for ECT Measurement [2]

4.2.1 State of the art: Experimental method for ECT measurement

Various methods have been used to determine the thermal conductivity of bulk and powdered solids. A number of methods for measuring the thermal conductivity of MH beds have been developed. These thermal conductivity measurement methods for thermal conductivity can be classified into two main categories: steady-state methods and transient methods. The range of materials to which each method can be applied is limited based on the fundamental laws of heat conduction.

4.2.2 Steady-state methods

- Radial heat flow method

In the radial heat flow method, one-dimensional radial heat flow must be maintained across a cylindrical sample, while the undesired axial and circumferential heat flows should be minimized [9]. The ISO 8497: 1994[10] cover the relevant measurement requirements and testing procedure about this method. Fig 2. presents a schematic of a steady-state radial heat flow method for determining thermal conductivity.

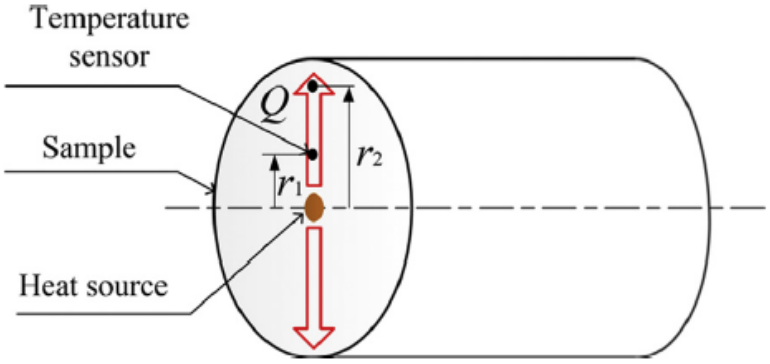

Figure 6 : Radial Heat Flow method [2]

In a typical radial heat flow apparatus, a cylindrical heater is placed at the central axis of a cylindrical test sample, and a steady-state temperature gradient is established in the radial direction.

By measuring the heat flux and temperature at different known radii, the thermal conductivity can be derived from Fourier's heat conduction equation for one-dimensional radial heat flow, which is given as :

$$\lambda = \frac{Q}{2\pi l(T1 - T2)} ln \frac{R2}{R1}$$

Where λ is the ECT

Recently Yang et al [8] propose the following experimental device and use several gases for the measurement.

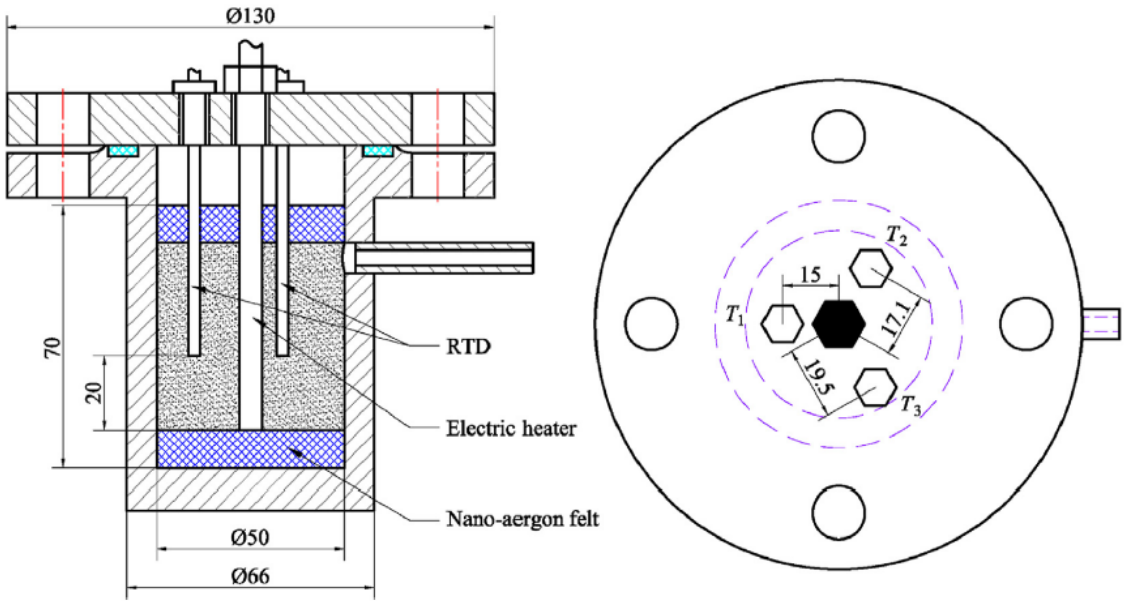

Figure 7 : ECT measurement cell [8]

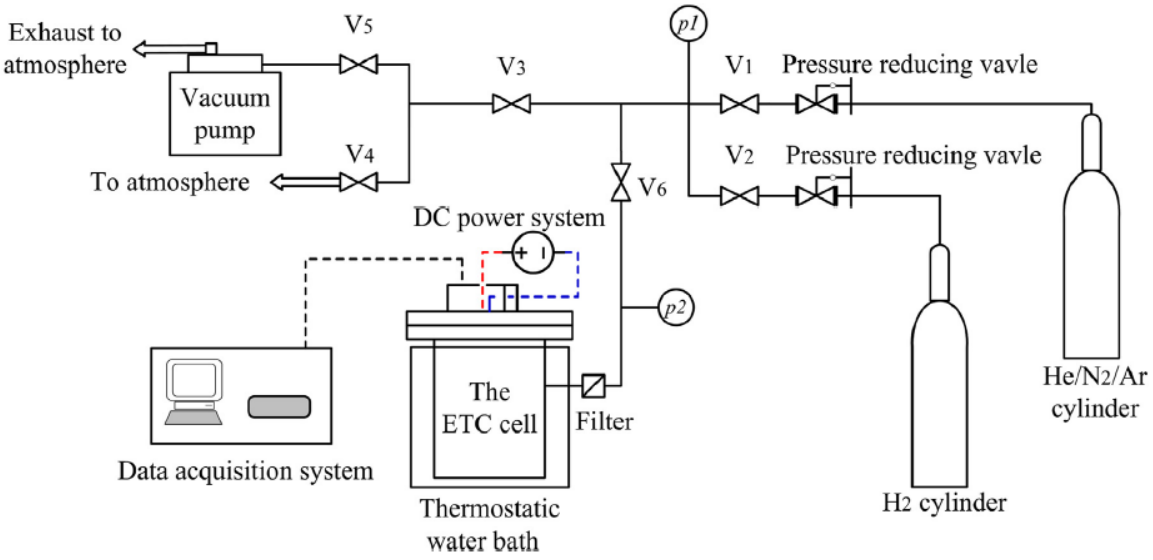

Figure 8 : Experimental Apparatus for ECT Measurment with Radial Flow Method [7]

The main conclusion on this last study is :

"The experimental results indicate that the ETC of the LaNi5 powder bed decreases gradually during the activation process due to the pulverization of the LaNi5 particle. At a hydrogen pressure of 1.0 MPa and average temperature of 36.7°C, the ETC of the LaNi5 powder bed decreases from 1.68 to 0.91 W /(m K) when the number of hydrogenation dehydrogenation cycles increases from 1 to 5. Before and after activation, the ETCs of the dehydrogenated LaNi5 powder under a helium pressure of 1.5 MPa are 1.63 and 0.84 W/ (m K), respectively. Correspondingly, the mean particle diameter of activated LaNi5 powder reduced to 11.8 μm, which is only 3.1% of that in the unactuated state [8].

- Other steady state method

Other steady state method has been investigated; however, theses method seems more complex and not more efficient to assess ECT Among this method we can noted mainly Comparative cut bar method [11,12]. This method is explained Figure 9.

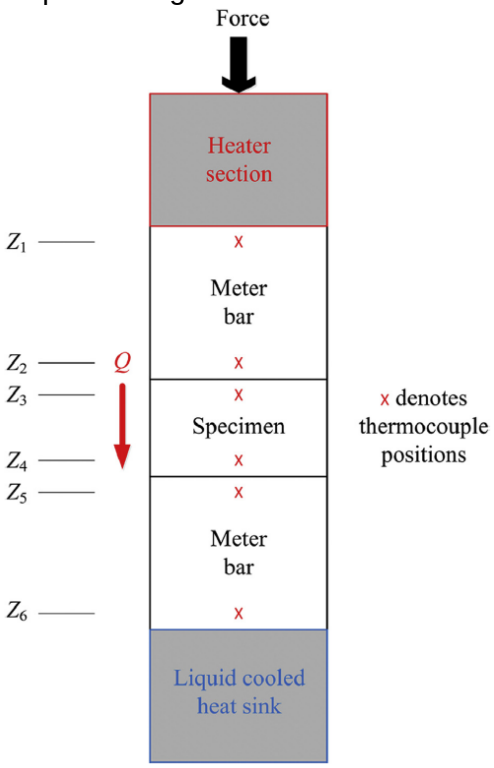

Figure 9 : Schematic of the comparative cut bar method for determining thermal conductivity

If λ_R is the conductivity of reference material, then :

$$\lambda = \frac{Z4 - Z3}{T4 - T3}\frac{\lambda_R}{2}\left[\frac{T2 - T1}{Z2 - Z1}\frac{T6 - T5}{Z6 - Z5}\right]$$

4.2.3 Transient methods

- Hot wire method

Figure 10 presents a schematic of the hot wire method for determining thermal conductivity. This method is based on measuring the temperature change at a known distance from a linear heat source (hot wire) encased in the test sample. The hot wire is assumed to have an infinite length and an infinitesimal diameter, as well as a negligible heat capacity [13]. ASTM C1113/C1113M 09 [14] and ISO 8894-1: 2010 [15] provide further details regarding the apparatus and test procedure for the

hot wire method. An abrupt electrical pulse is applied to the hot wire, and the thermal conductivity is derived from the resulting rise in temperature as a function of the elapsed time over a known time interval at a defined distance from the hot wire. The equation of the calculation of the thermal conductivity of the sample using the transient hot wire method is :

$$\lambda = \frac{P}{4\pi(T(t2) - T(t1))} ln \frac{t2}{t1}$$

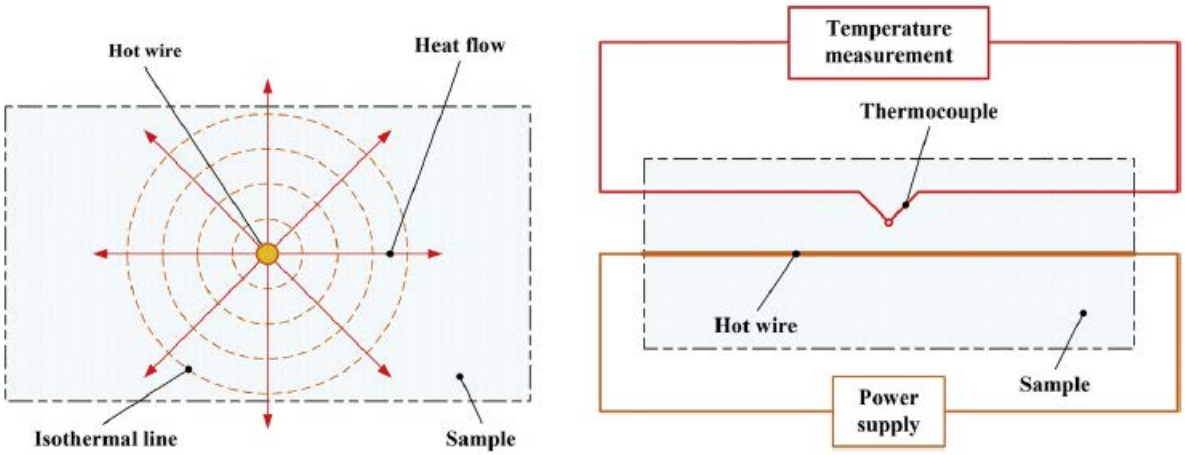

Figure 10 : Schematic of the hot wire method for determining thermal conductivity

- Other transient methods

Other method such as Thermal probe method seems less efficiency. ASTM D5334-14 [16] specifies the test apparatus and procedure for the thermal probe method. The physical model of this method is similar to that of the hot wire method, except that the hot wire is replaced by a probe containing an electric heater and a temperature sensor. A typical thermal probe is shown in Figure 11 in this method.

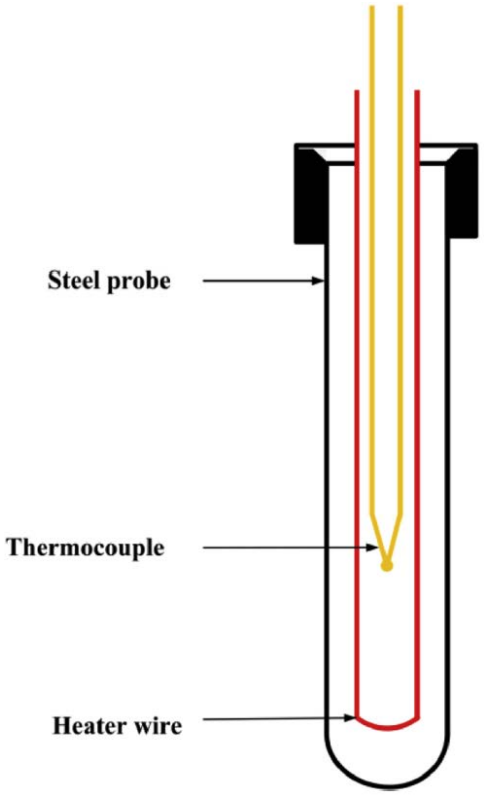

Figure 11 : Schematic of Schematic of a thermal probe for determining thermal conductivity.

The probe is inserted into an isothermal sample (generally a soft or granular material). After the specimen reaches equilibrium at the selected testing temperature, a known heat is applied to the heater wire; the temperature change should be less than 10 K over 1000 s. Based on an approximation of the solution for the boundary value problem describing the physical situation, the temperature response can be given by:

$$\Delta T \cong \frac{P}{4\pi\lambda} Ln(t)$$

where ΔT is change in temperature relative to time.

- Identification

Among the various method of identification, the use of inverse method could be used to assess the thermal property of MH bed. Ghafir *et al* use this methodology.

These authors concluded :

“The effective thermal conductivity λeff of metal hydride beds can be determined directly by experiments, but not that of the discrete hydrided particles, λd. The conductivity of the particles, as a function of absorbed hydrogen concentration, is the important property for heat diffusion in the hydride and is in fact the property that needs to be used for calculation of rates and process times during cycles of charging and discharging. This property λd of the discrete metal hydride particles changes dynamically during sorption and desorption of hydrogen. It can be estimated by the selection of a suitable model and inverse calculation procedures.”

4.2.4 Conclusion

Two main kinds of method for measurement of ECT are existing Steady state and transient method. Among this type of experiment for steady state method, Radial heat flow method could be use and with transient, hot wire method should be preferred.

Several theoretical models are also existing to assess the ECT. However, both experimental methods could be simulated with theoretical model, and by using inverse method the model parameter could be estimated.

4.2.5 References

1. P. Moretto. Round Robin Test exercise on hydrogen absorption/desorption properties of a magnesium hydride based material. P. Moretto C. Zlotea, F. Dolci, A. Amieiro, J.-L. Bobet, A. Borgschulte, D. Chandra, H. Enoki, P. De Rango, D. Fruchart, J. Jepsen, M. Latroche, I. Llamas Jansa, D. Moser, S. Sartori, S.M. Wang, J.A. Zan. International Journal of Hydrogen Energy. Volume 38, Issue 16, 30 May 2013, Pages 6704-6717
2. W. Zhao et al : Methods for measuring the effective thermal conductivity of metal hydride beds: A review, International Hydrogen Energy 2020(45) 6680-6700
3. Yagi S, Kunii D. Studies on effective thermal conductivities in packed beds. AIChE J 1957;3(3):373-81
4. Deissler RG, Boegli JS. An investigation of effective thermal conductivities of powders in various gases. Trans ASME 1958;80:1417-25.
5. Masamune S, Smith JM. Thermal conductivity of beds of spherical particles. Ind Eng Chem Fundam1963;2:136-43.
6. Zehner P, Schlunder EU. Thermal conductivity of granular materials at moderate temperatures. Chemie Ingr Tech 1970;42:933-41.
7. Madaria Y, Anil Kumar E, Maiya P, Srinivasa Murthy S. Simulation of effective thermal conductivity of metal hydride packed beds. Heat Transf Eng 2016;37:616-24.
8. Yang et al : Measurement and analysis of effective thermal conductivity of LaNi5 and its hydride under different gas atmospheres International Hydrogen Energy 2021(46) 19467-77
9. Fave L, Pouchon MA, Hebert C. A radial heat flow apparatus for thermal conductivity characterisation of cylindrical samples. J Therm Anal Calorim 2017;130(3):1855-63
10. ISO 8497:1994. Thermal insulation determination of steady-state thermal transmission properties of thermal insulation for circular pipes. International Organization for Standardization (ISO); 1994.
11. Jensen C, Xing C, Folsom C, Ban H, Phillips J. Design and validation of a high-temperature comparative thermalconductivity measurement system. Int J Thermophys 2012;33(2):311-29.
12. ASTM E1225-13. Standard test method for thermal conductivity of solids by means of the guarded comparative- longitudinal heat flow technique. ASTM International; 2009.
13. Zhao D, Qian X, Gu X, Jajja SA, Yang R. Measurement techniques for thermal conductivity and interfacial thermal conductance of bulk and thin film materials. J Electron Packag 2016;138(4):1-64.
14. ASTM C1113/C1113M-09. Standard test method for thermal conductivity of refractories by hot wire (platinum resistance thermometer technique). West Conshohocken, PA: ASTM International; 2019
15. ISO 8894-1: 2010. Refractory materials determination of thermal conductivity e Part 1: hot-wire methods (cross array and resistance thermometer). Paris: ISO_Editions; 2010.
16. ASTM D5334-14. Standard test method for determination of thermal conductivity of soil and soft rock by thermal needle probe procedure. West Conshohocken, PA: ASTM International; 2014.
17. Mohd Fahmi Abdul Ghafir et al ,Prediction of the thermal conductivity of metal hydrides – The inverse problem, International Hydrogen Energy Journal 2009(34); 7125-30

4.3 Metal hydride test tank

To carry out thermal conductivity tests with the selected method, MAHYTEC designed the test tank with FHA support, which takes care of the assembly of the test bench in parallel.

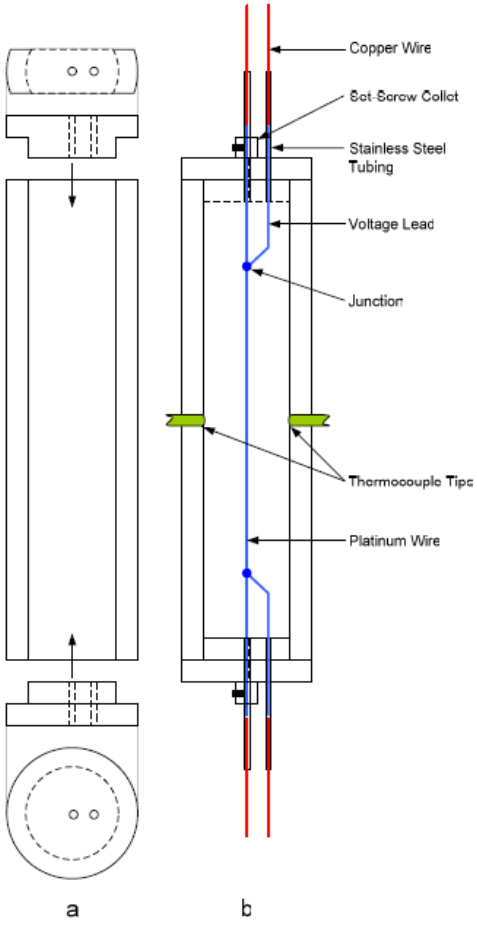

The test tank includes the following elements:

- A shell with caps that will hold up to temperature and pressure
- A heating wire
- Temperature sensors
- Sealing elements for the passage of the wire and temperature sensors
- Valve and filter

The shell and the caps were designed by MAHYTEC. The choice of 316L steel material was for its compatibility with hydrogen, its mechanical resistance and its resistance to temperature.

The sizing of the chamber which contains the metal hydride is dependent on several parameters. Have the largest possible ratio of length to chamber diameter (around 4) and the quantity of hydride can be absorbed around 100 Nl of hydrogen.

The minimum diameter of the chamber was set at 43 mm in order to be able to insert the heating wire and the thermocouples into the test chamber. Which include the sealing elements that allow them to pass through the caps.

From the diameter we were able to calculate different possibilities for the length of the chamber until we obtained a good ration and had the right quantity of hydrogen absorbed by the metal hydride.

Ration L/D	Length (mm)	Volume (cm3)	Quantity of metal hydride (g)	Quantity of hydrogen absorb (Nl)
3	129	184	503	82
3,5	150,5	214	586	95
4	172	246	672	109

Once the choice of the ratio of 4 was validated, we were able to size the rest of the tank so that it could withstand an operating pressure of 200 bar.

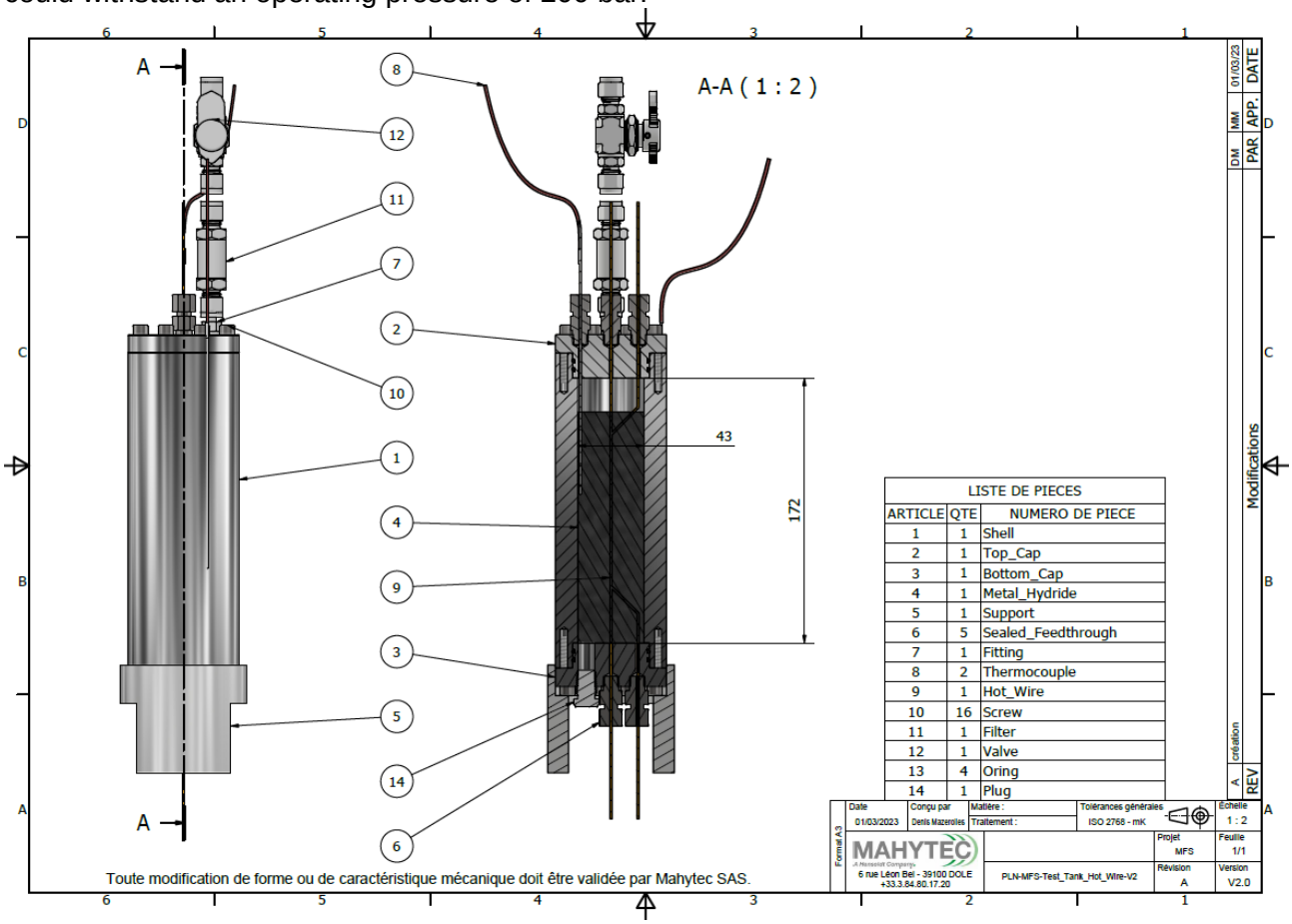

Figure 12 : Test Tank Plan & Nomenclature

The heating wire has been chosen in platinum. The heating wire was initially tested with a bed of sand to define the ranges of voltage, intensity and times necessary for the following tests. These first trials allowed to define the main parameters of the control loop monitoring the tests.

One of the important elements of installing the heating wire is to insulate it electrically from the metal hydride. Indeed, this being an electrical conductor, not insulating the wire would create a short circuit when a current is passed through the wire.

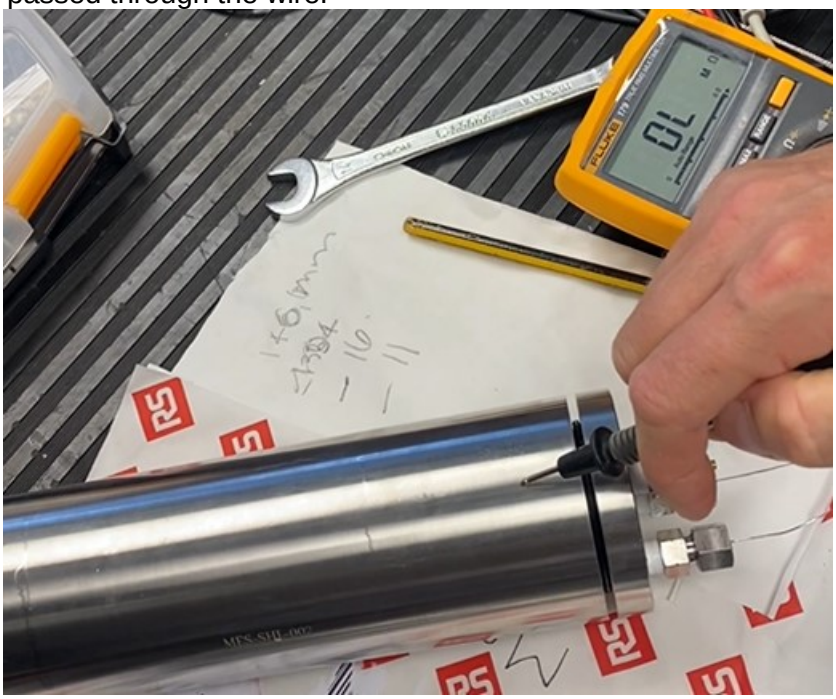

Figure 13 : Electrical conductivity test between tank and heating wire

Wire insulation was done with a classic electrical wire insulation spray. In addition to the waterproof elements that allow the heating wire to pass through the plugs with a ceramic tube.

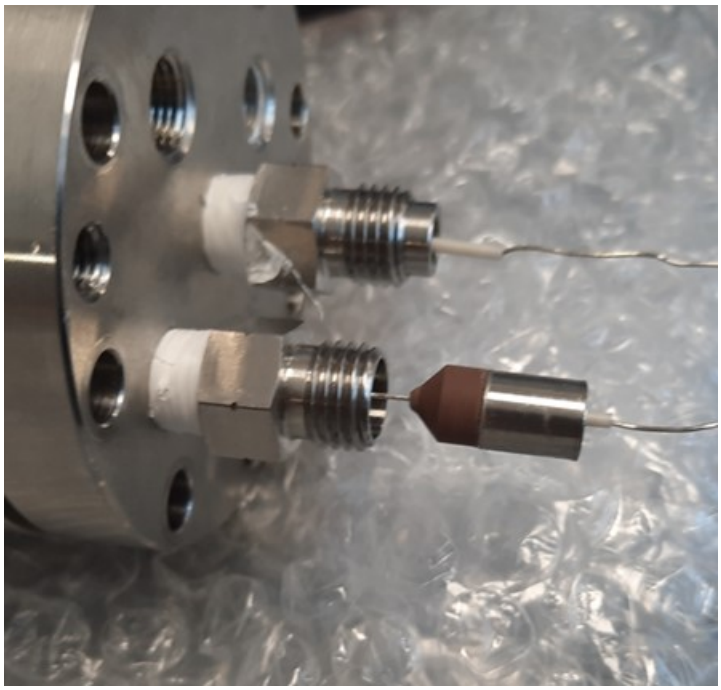

Figure 14 : Electrical insulation of sealing elements

Figure 15 : Hydride damaged heating wire insulation

Unfortunately, during the activation under hydrogen of the metal hydride, it damaged the insulation. Indeed, metal hydride is abrasive during absorption/desorption of hydrogen. After disassembly of the tank in a glove box in order to preserve the activated metal hydride. New insulation with an orange Kapton film was done to resist the abrasive swelling of the metal hydride.

Figure 16 : New heating wire insulation

The insulation problem solved, the tank was completely assembled with a filter which prevents the metal hydride from leaving the test chamber and a valve which allows the tank to be isolated from the test bench.

Figure 17 : Test tank assembled at MAHYTEC

To carry out thermal conductivity tests with the selected method, MAHYTEC designed the test tank with FHA support, which takes care of the assembly of the test bench in parallel.

4.4 Test bench

4.4.1 Introduction

FHa's test bench is based on thermal mass flow controllers (Bronkhorst) and enables loading and unloading hydrogen in the hydride tank with a maximum flow rate of 120 NmL/min between 0 to 30 barg. The test bench is piloted through an Labview interface that allows to control and monitor all the flow, pressure and temperature variables, registering all necessary values for data post-processing.

4.4.2 P&ID

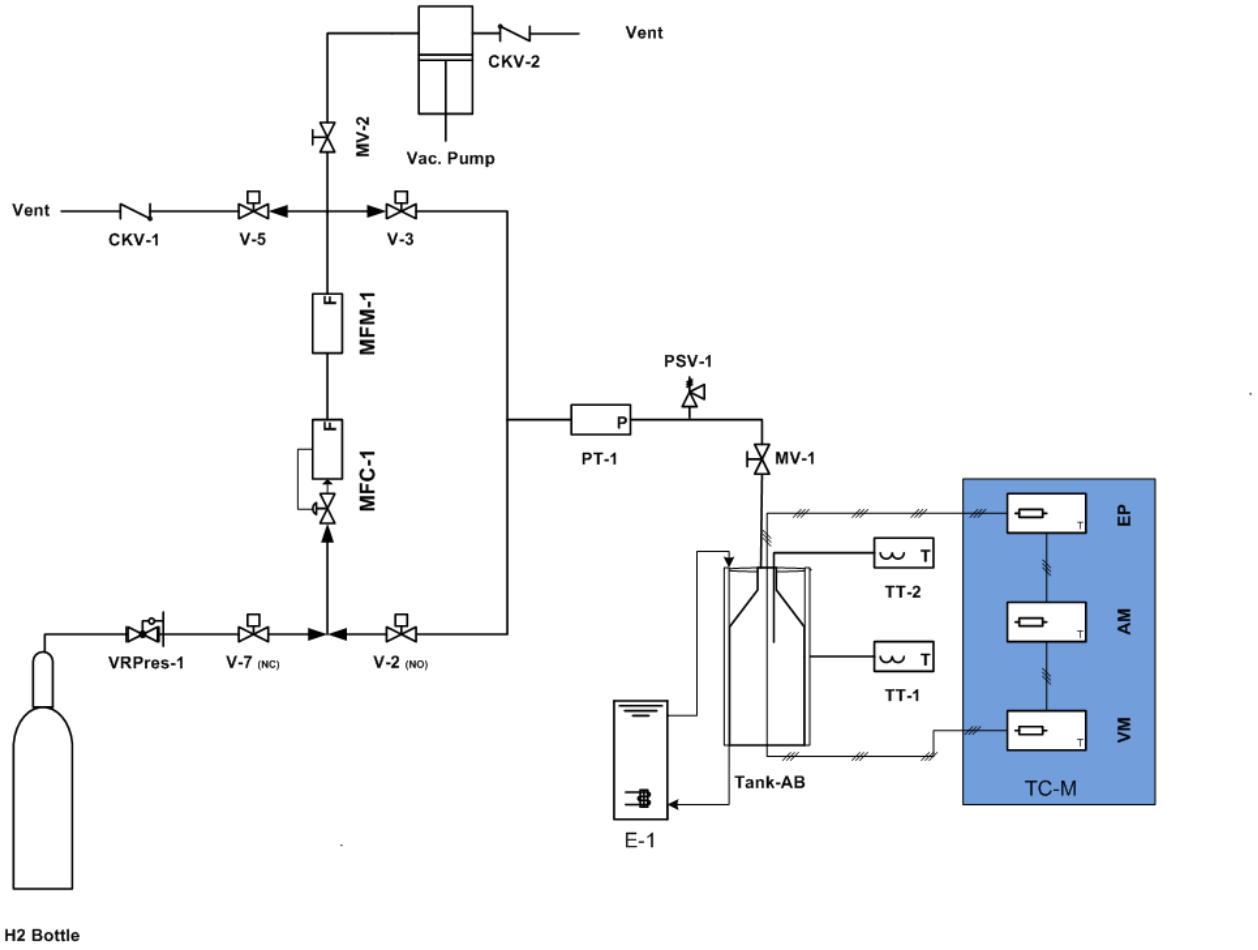

Figure 18. P&ID scheme of set-up built at FHa's facilities

Table 1. Explanatory legend of P&ID in Figure 39

Tag	Description
VRPres-1	Regulator Redline, simple stage, flammables. P_{in}= 200 bar, P_{out}= 2.5-50 bar 1/4"NPTH (Seal included)
V-2	Selenoid valve 2/2 NC G1/8". Spool 24V/DC ATEX Ref. F3111AV20
V-3	Selenoid valve 2/2 NC G1/8". Spool 24V/DC ATEX Ref. F3111AV20
V-5	Selenoid valve 2/2 NC G1/8". Spool 24V/DC ATEX Ref. F3111AV20
V-7	Selenoid valve 2/2 NC G1/8". Spool 24V/DC ATEX Ref. F3111AV20
MFC-1	MFC SLA5850S 0-120 mL/min. Pamount= 1-27 bar(g), Paval= 1-22 bar(g). T= 0-40C. 1/8"DB_4-20 mA, Signal RS485
MFM-1	MFC SLA5860S 0-20 mL/min. P= 1-22 bar(g). T= 0-40C. 1/8"DB_4-20 mA, Signal RS485
PT-1	PT, Pressure transmisor Barksdale. Conectror socket 3 pol. Ref. BT5-T5-08BG-P7W
MV-2	Ball-valve OD 1/8". Inox 316. Ref, V82A-D-2T-S
CKV-1	Check valve OD 1/8"
CKV-2	Check valve OD 1/8"
PSV-1	Relief valve 1/4"NOTMXH CE Inox 316 ref: V66-MF-4N-CE. Calibration at 35 bar.
Vac.Pump	Agilent IDP-7 Dry pump, 152 l/min, 2.0 x 10-2 mbar
E-1	Water bath
E-1-2	Cooling zone cooling jacket with FLUXWRAP Insulation Banket
VM	Digital multimeter TT 1705
AM	Digital multimeter FLUKE 8846A
EP	Programable power supply GwINSTEK psm 6003
TT-1	Temperature transmitter for thermocouple J, K, T
TT-2	Temperature transmitter for thermocouple J, K, T

4.4.3 Working principle

Hydrogen for the tests is supplied via bottle at the desired testing pressure. The hydrogen used to supply the test bench is quality 6.0 (99.9999% vol. H_2). A vacuum pump enables removing any traces of air before beginning the cycling tests, A set of electrovalves enable the direction of the flow to load or unload the tank. The flow of hydrogen fed to the tank or discharged from it is controlled by a flow controller (Bronkhorst). Since the flow at the end of the desorption process is too low and below the detection limit of the controller, a flow meter is installed in series to measure such values at low range.

The pressure inside the tank during the tests is measured with the pressure transmitter, while the temperature inside the tank, as well as on its wall, is measured with to thermocouples. A water bath allows to control the temperature of the test, which can be set from 10 to 30 °C

4.4.4 Cycle testing

The cycling testing consists in an initial conditioning of the system under vacuum followed by several absorption and desorption processes.

Starting procedure

Before starting the test air is removed from the system following procedure described below:

- V-5 is closed while V-2, V-3 and V-7 are open.

- MV-1 is opened.
- The vacuum pump is started and valve MV-2 slowly opened.
- The pump is maintained in operation for 2h.
- At the end of this period, all valves are closed.
- The tank is now ready for the absorption tests.

Hydrogen absorption

Hydrogen is supplied to the tank following the procedure described below to perfom the absotion part of the cycling test:

- Valve MV-2 is closed and valve MV-1 is opened.
- Valves V-7 and V-3 are opened while V-2 and V-5 are maintained closed.
- The setpoint of the flow controller is defined as 100 Nml/min.
- Values of flow, pressure and temperature are registered during the tests
- The test is considered as finished once the flow meter displays no flow value and pressure inside the tank has reached the supply pressure value.

Hydrogen desorption

Hydrogen is removed from the tank (desoption) following the procedure described below to perfom this second part of the cycling test:

- Valve MV-2 is closed and valve MV-1 is opened.
- Valves V-2 and V-5 are opened while V-3 and V-7 are maintained closed.
- The setpoint of the flow controller is defined as 100 Nml/min.
- Values of flow, pressure and temperature are registered during the tests.
- The test is considered as finished once the flow meter displays no flow value and pressure inside the tank has reached a negative value.

Corrections regarding dead volume

During the absorption and desopton tests there is some volume of hydrogen that is counted by the mass flow controller, but that has not entered inside the tank. This is the so called dead volume of the setup. This volume has to be withdrawn from the volume measured by the mass flow controller to provide a corrected valur of the real apacity of the hydride tank.
The dead volume in the setup is calculated with the following procedure:

- Once an adorption test is finished, valve MV-1 and MV-2 are closed.
- Valves V-2 and V-5 are opened while V-3 and V-7 are maintained closed.
- The setpoint of the flow controller is defined as 100 Nml/min.
- Values of flow, pressure and temperature are registered during the tests until the flow meter displays no flow value.

The dead volume results in V1 = **85.90 ml**

4.5 First thermal conductivity measurements – A4.1.7

4.5.1 Description of Pt wire tests

In a first stage, some tests were conducted with the platinum wire (outside the tank) in order to calibrate the control system. A 3D printer was used at FHA facilities for the manufacturing of a support for the wire and the two measurement points.
The tests consisted in supplying an intensity between 1 and 4 A at 10 V by a power supply. During the test, a multimeter recorded the potential difference and resistance against time for later data postprocessing.

Several tests were conducted due to a bad resolution in the voltage measurement. work was carried out related to the noise filtering. Since the hydride of the tank is highly conductive, several isolation strategies were followed (Plastik 70 isolation spray and Kapton film).

The material used for the voltage leads for these first experiments was copper. The use of this material is not relevant since this doesn't affect to the final measurement. During the test, the supported wire was submerged in the reference medium whose thermal conductivity wanted to be measured.

Figure 19. Example of Kapton-insulated wire for testing thermal conductivity in the calibration step

4.5.2 Error factor determination (1/A)

Thermal conductivity of a known media was performed to determine the error factor of the designed set-up (TC-sensor). In addition, several tests were conducted in different media to evaluate reproducibility of the TC (Thermal Conductivity) measure. 2 different sensors (i.e. S4 and S5) were built and proved. The tests with the previous sensors (S1, S2 and S3) were discarded due to instable performance. The result from these tests are shown the graphs below.

4.5.2.2 Tests with the uncoated sensor

- **Tests with pure glycerol**

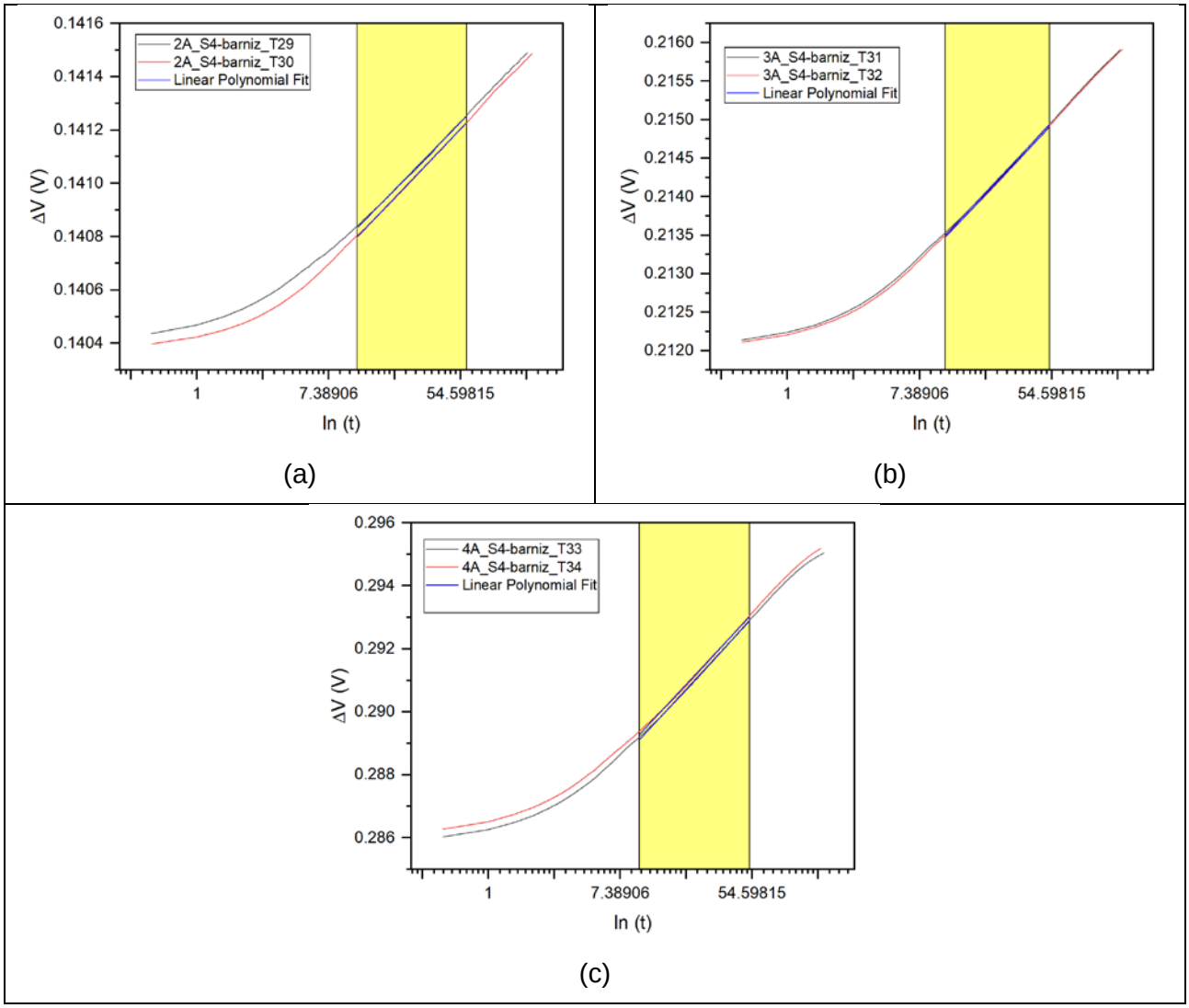

Figure 20. Voltage increase measurements in pure glycerol medium with TC-sensor S4 at different current intensities: (a) I= 1A, (b) I= 3A, (c) I= 4A.

Table 2. Summary of the tests performed with pure glycerol with sensor S4

I - Test	k'	A	k (W/mK)	m	R_0
2A-T29	0.3693	1.2958	0.2850	2.59E-04	0.0698
2A-T30	0.3688		0.2847	2.59E-04	0.0698
3A-T31	0.3580		0.2763	9.08E-04	0.0701
3A-T32	0.3579		0.2762	9.08E-04	0.0702
4A-T33	0.3464		0.2673	2.26E-03	0.0707
4A-T34	0.3500		0.2701	2.24E-03	0.0707

The tests performed with pure glycerol can be found in Figure 20. Voltage against the natural logarithm of time is represented, and the linear part of the graph fitted with a linear regression.

According to the hot wire method described in section 4.2.3, the conductivity obtained will defer from the real one. This difference (i.e. error factor) will, however, be constant and can be obtained with the following equation:

$$k = \frac{1}{A}\frac{I^3 R_0^2 \sigma}{4\pi L}\left(\frac{d\Delta V(t)}{d(lnt)}\right)^{-1}$$

where k is the known conductivity of the medium tested, A is the error factor, I the intensity in the test, L the length of the wire, R_0 the resistance at the beginning of the measurement, σ the temperature coefficient of resistance of the Pt-wire and $\frac{d\Delta V(t)}{d(lnt)}$ the slope of the graph obtained with the linear regression.

The calculations obtained can be seen in Table 2. K' is the conductivity value obtained without correction. It can be seen how the values are quite similar regardless of the intensity used in the test. The error factor obtained was of A = 1.2958.

- **<u>Reproducibility of measurements in glycerol</u>**

The same tests performed with sensor S4 in the previous section were repeated with a different sensor (S5) to verify the reproducibility of the experimental method in the same medium.

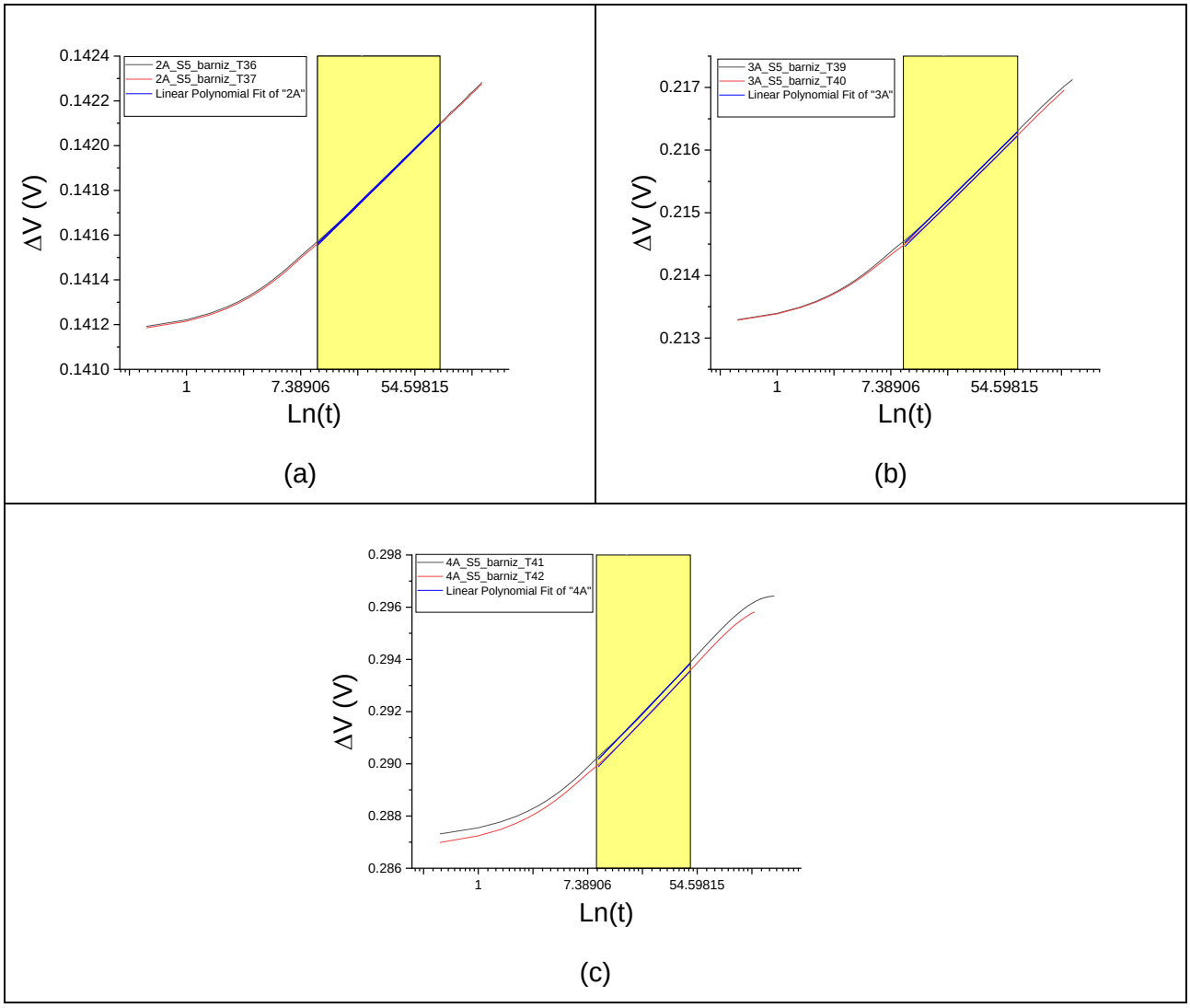

Figure 21. Voltage increase measurements in pure glycerol medium with TC-sensor S5 at different current intensities: (a) I= 2A, (b) I= 3A, (c) I= 4A

Table 3. Summary of the tests performed with pure glycerol with sensor S5

I - Test	k'	A	k (W/mK)	m	R_0
2A-T37	0.387	1.2958	0.299	2.50E-04	0.0702
2A-T38	0.384		0.296	2.52E-04	0.0702
3A-T39	0.372		0.287	8.93E-04	0.0707
3A-T40	0.373		0.287	8.91E-04	0.0707
4A-T41	0.370		0.285	2.18E-03	0.0714
4A-T42	0.369		0.285	2.18E-03	0.0714

It can be seen in Figure 21 and Table 3 how the results are similar to those obtained in the previous subsection.

- **Measurements in methanol**

Thermal conductivity tests in methanol were performed with sensor S5 to validate the data obtained in the tests with glycerol, especially the error factor “A”.

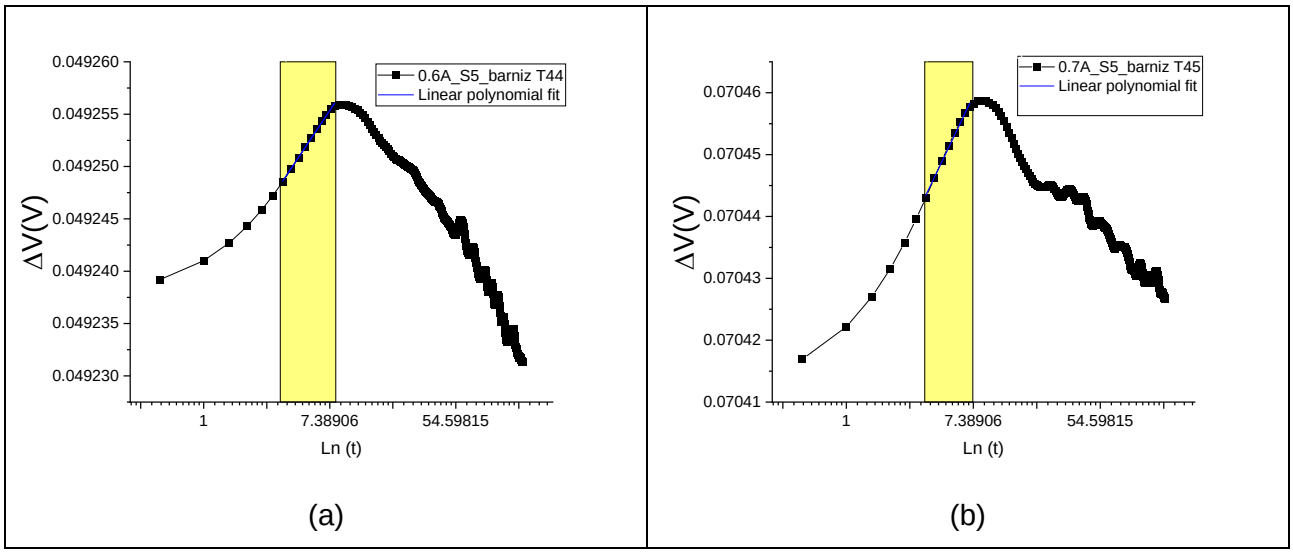

Figure 22. Voltage increase measurements in pure methanol medium with TC-sensor S5 at different current intensities: (a) I= 0.6A, (b) I= 0.7A

Measurements in methanol were challenging due to the low boiling point of the liquid. As it can be seen in Figure 22, the potential difference did not increase constantly against time, but it reached a maximum, after which it starts dropping. This result is due to the fact that the sensor is heated when current flows though it and, at a certain time, the heat in the fluid near the wire is high enough to make convection gradients in the fluid, faking the reading. In any event, some linear areas in the graph could be identified to calculate the thermal conductivity if the energy current was low enough (i.e. 0.6 and 0.7A).

Table 4. Summary of the tests performed with sensor S5 in methanol

I - Test	A	k (W/mK)	m	R_0
0.6A-T37	1.2958	0.222	9.02E-06	0.070109
0.7A-T38		0.235	1.35E-05	0.070042

The calculated thermal conductivity applying the previously calculated correction factor (A=1.2958) was 0.228±0.01 W/mK (see *Table **4***). Despite the fact of the trouble found, this value is quite similar to the thermal conductivity of methanol found in the literature (0.203 W/mK).

4.5.2.3 Tests with the coated sensor

- **<u>Plastik 70 isolation spray</u>**

In order to avoid short-circuits due to the high electrical conductivity of the metal hydride one sensor was coated with Plastik 70 isolation spray. The error factor of this sensor (named S6) was calculated performing conductivity measurements in pure glycerol, following the same methodology developed in section 4.5.2.1.

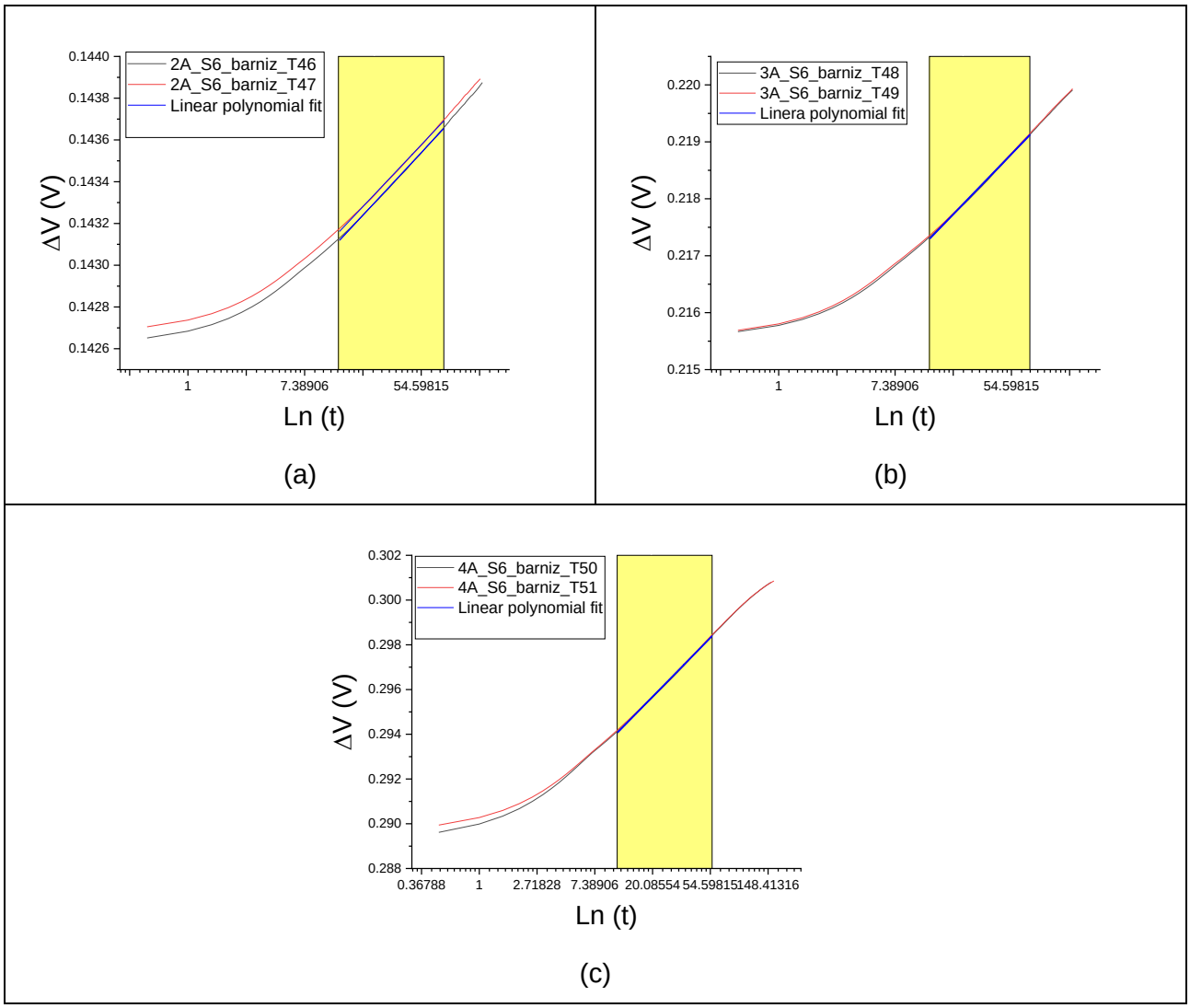

Figure 23. Voltage increase measurements in pure glycerol medium with coated TC-sensor S6 at different current intensities: (a) I= 2A, (b) I= 3A, (c) I= 4A

Table 5. Summary of the tests performed with pure glycerol with sensor S6 coated with Plastik 70 spray

I - Test	k'	A	k (W/mK)	m	R_0
2A-T46	0.329	1.1210	0.294	3.00E-04	0.0710
2A-T47	0.334		0.298	2.96E-04	0.0711
3A-T48	0.320		0.285	1.06E-03	0.0716
3A-T49	0.320		0.285	1.06E-03	0.0716
4A-T50	0.310		0.276	2.64E-03	0.0720
4A-T51	0.311		0.278	2.63E-03	0.0721

As it can be seen, the new correction factor of A=1.1210 shows a clear difference with the factor for the uncoated sensor (A=1.2958), corresponding to 15.5 % difference. This change is due to the isolation layer applied onto the sensor.

- **Kapton film**

The use of Plastik 70 isolation spray was, however, not successful for the isolation of the wire once installed in the tank. The swelling of the hydride during its activation process caused some damage on the coating layer sufficient to lead to short-circuit between wire and the metallic wall of the tank, making the conductivity measurement inside the tank impossible. And alternative coting was then applied using Kapton film as insulation medium (see Figure 24).

Figure 24. Pt-wire insulated with Kapton film

The error factor of this sensor (named S7) was calculated performing conductivity measurements in pure glycerol, following the same methodology developed in the sections above.

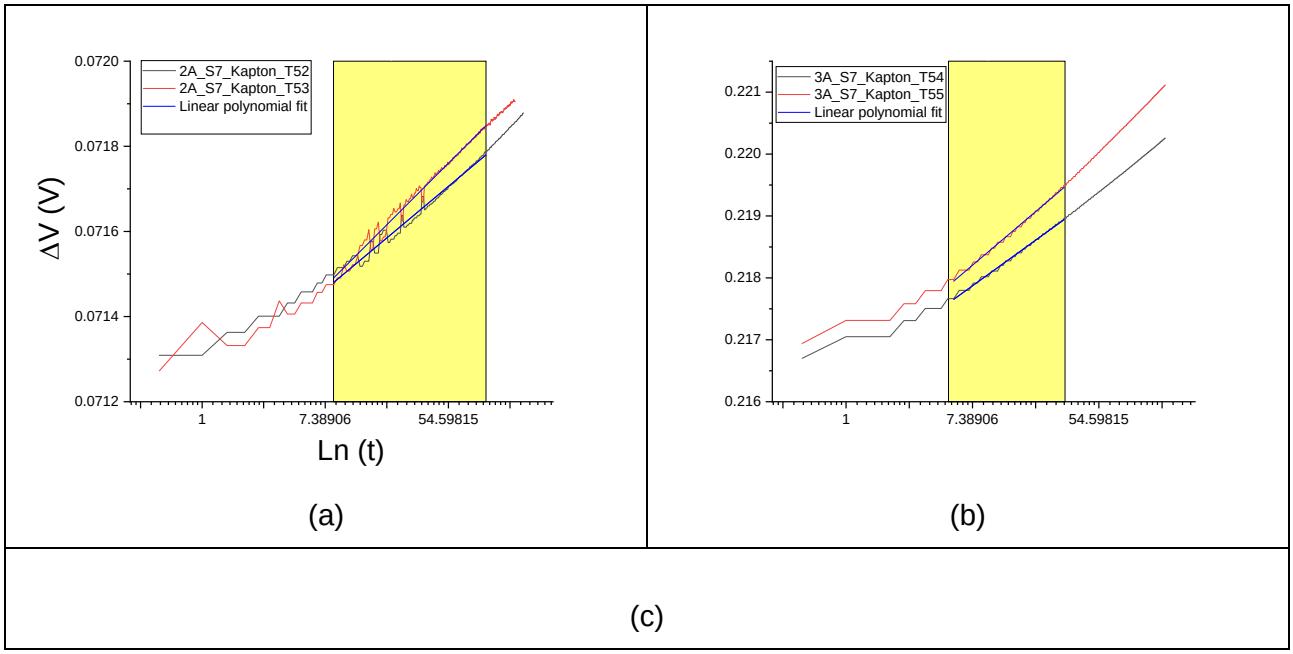

Figure 25. Voltage increases measurements in pure glycerol medium with coated TC-sensor S6 at different current intensities: (a) I= 2A, (b) I= 3A, (c) I= 4A

Table 6. Summary of the tests performed with pure glycerol with sensor S6 coated with Kapton

I - Test	k'	A	k (W/mK)	m	R_0
2A-T52	0.4086	1.315	0.3107	1.45E-04	0.0718
2A-T53	0.4449		0.3383	1.21E-04	0.0712
3A-T54	0.3417		0.2598	9.81E-04	0.2164
3A-T55	0.3867		0.2941	8.67E-04	0.2165
4A-T56	0.3330		0.2532	2.49E-03	0.0731
4A-T57	0.3824		0.2908	2.21E-03	0.0738

The updated correction factor of A=1.315 shows more proximity to the factor for the uncoated sensor (A=1.2958). This way the presence of insulation is less intrusive that that caused by the Pastik 70 coating (A=1.1210). **A=1.315** is the factor to be used for the measurements in the tank during the filling process.

4.6 Thermal conductivity results

Absorption/desorption test were performed with the hydride tank at three different temperatures: 10, 20 and 30 °C following the methodology described in section 4.4. The results are detailed in the following subsections.

4.6.1 Tests at 10 °C without conductivity measurements

*Figure **26*** shows the results of the absorption test performed at 10 °C feeding 100 Nml/min of hydrogen to the tank. The pressure starts from 0 bar and increases continuously until 15 bar is reached. There are two changes of slope during the filling process. The first inflection point corresponds to the moment where the real absorption process begins, while the second inflection point is related to the moment when the hydride is saturated. The flow keeps its maximum value while the hydride is absorbing and drops continuously when it is saturated until reaching its minimum value once the tank is full. Finally, the temperature in the tank increases gradually while the hydride

is absorbing hydrogen, and it starts to decrease once if gets saturated. This behaviour is coherent with the exothermicity of absorption processes.

The desorption process starts in each cycle with a sudden drop in pressure. This behaviour is due to the gas realise in the system until reaching the saturation pressure of the hydride. The pressure decreases then continuously while the discharging flow is constant. At the end of the process, pressure remains basically constant until the tank is empty, showing a gradual decrease in the value of the discharging flow. Conversely to the absorption process, the temperature in the tank decreases during the hydrogen release. Noteworthy desorption in and endothermic process.

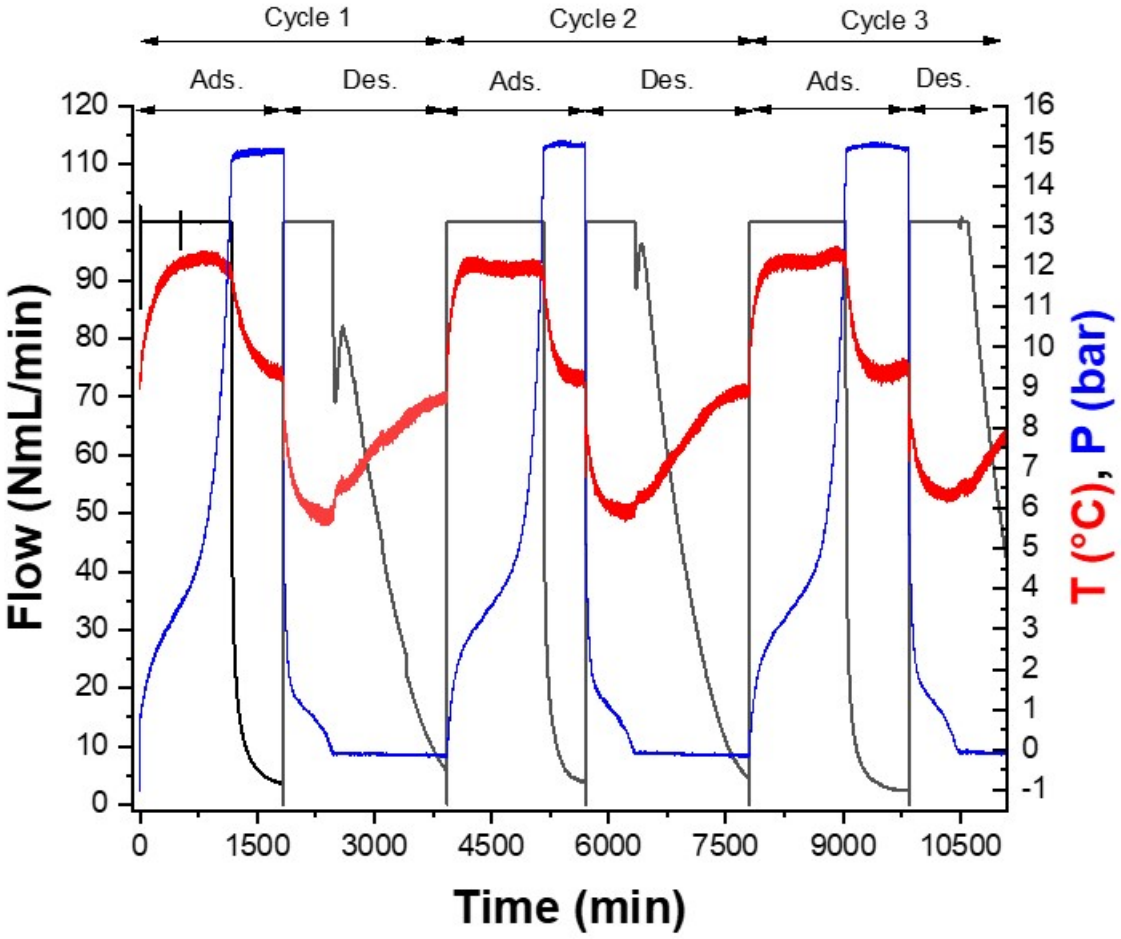

Figure 26. Evolution of flow, temperature and pressure during the absorption/desorption cycles at 10 °C

The volume absorbed by the tank is calculated from the measurements by integrating the flow rate over time and subtracting the calculated dead volume (i.e. 85.90 mL). The volume of hydrogen absorbed and desorbed in each cycle can be seen in Table 7. The absorbed volume is always greater than the desorbed volume due to the fact that the hydride is not able to release all the hydrogen supplied and some part of it remains absorbed.

Table 7. Volume of hydrogen charged and discharged during the absorption/desorption cycles at 10°C

Cycle	Volume (LN)	
	Load	**Unload**
1	123.3	122.2
2	129.1	123.0
3	129.0	123.3

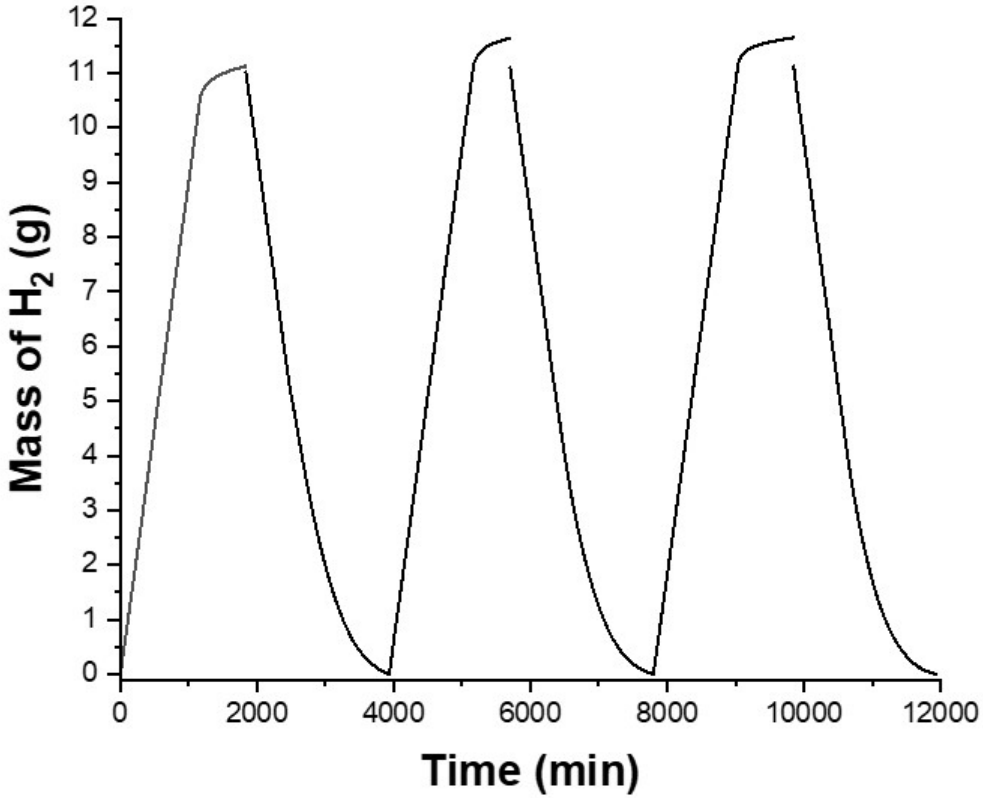

Figure 27. Mass of hydrogen absorbed or liberated during the cycles at 10 °C

Figure 27 shows the evolution of the mass of hydrogen absorbed and desorbed with each cycle. The graphs shows how the hydride is absorbing slightly more hydrogen in each cycle, suggesting that the hydride will reach “full activation” after some hours of operation.

4.6.2 Tests at 20 °C without conductivity measurements

This subsection shows the results of the tests performed with the tank at 20 °C. The methodology followed was the same that in the previous tests at 10 °C and analogous results are shown below.

Figure 28 shows the results of the absorption test performed at 20 °C feeding 100 Nml/min of hydrogen to the tank. Due to a loss of communication between computer and PLC during the third cycle, the data of the absorption step were not registered. Therefore, these data were lost and are not represented in the following graphs. The pressure shows the same tendency as before, with the two inflection points owing to the beginning and end of the absorption process. Flow shows again the contrary tendency to the pressure values. And the evolution of temperature is coherent with an exothermic process for the absorption cycles, and endothermic process of the desorption step.

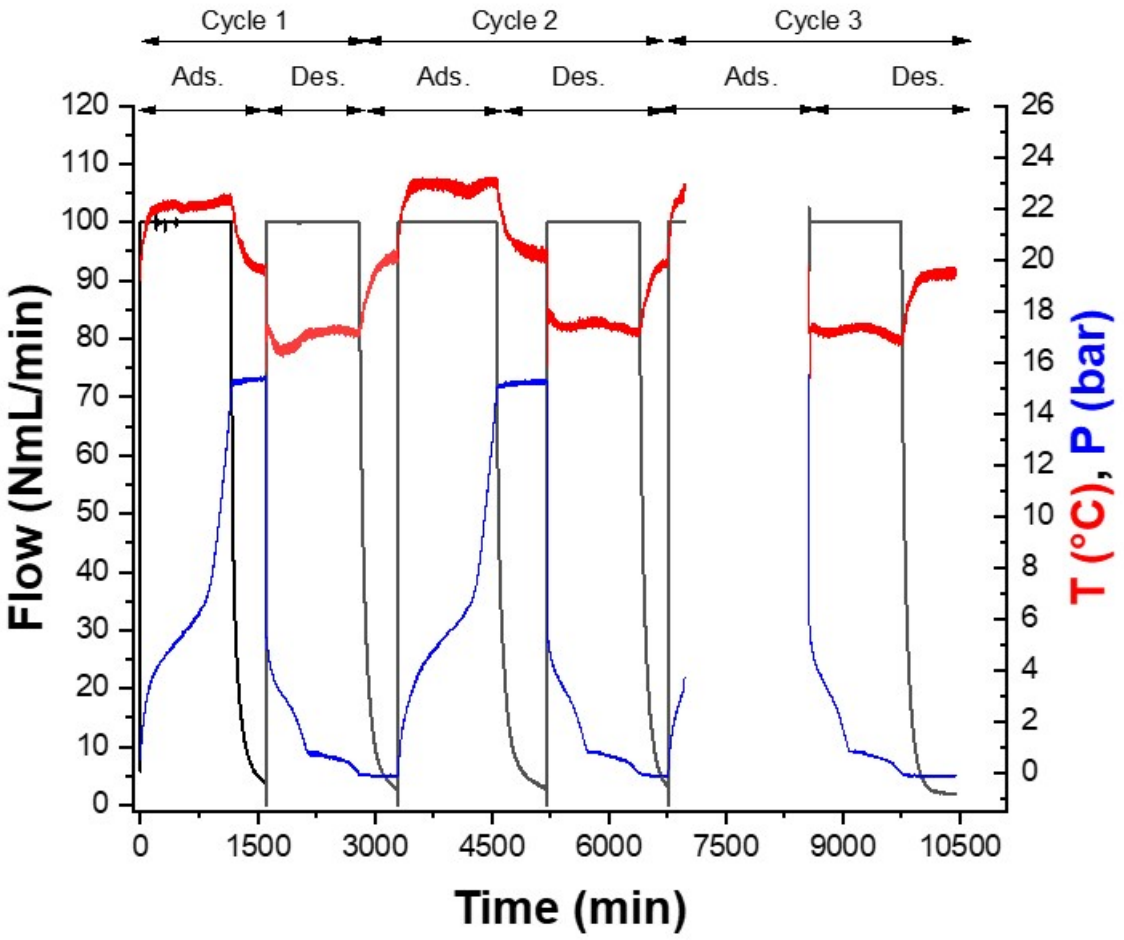

Figure 28. Evolution of flow, temperature and pressure during the absorption/desorption cycles at 20 °C

The volume absorbed by the tank is once again calculated integrating the flow rate over time and subtracting the calculated dead volume (i.e. 85.90 mL). The volume of hydrogen absorbed and desorbed in each cycle can be seen in Table 8. The total volume of hydrogen stored or liberated is always higher that the corresponding values in the test at 10 °C. The absorbed volume is again higher than the desorbed volume due to the fact that the hydride is not able to release all the hydrogen supplied and some part of it remains absorbed.

Table 8. Volume of hydrogen charged and discharged during the absorption/desorption cycles at 20°C

Cycle	**Volume (LN)**	
	Load	**Unload**
1	122.6	127.7
2	134.2	125.3
3	-	125.3

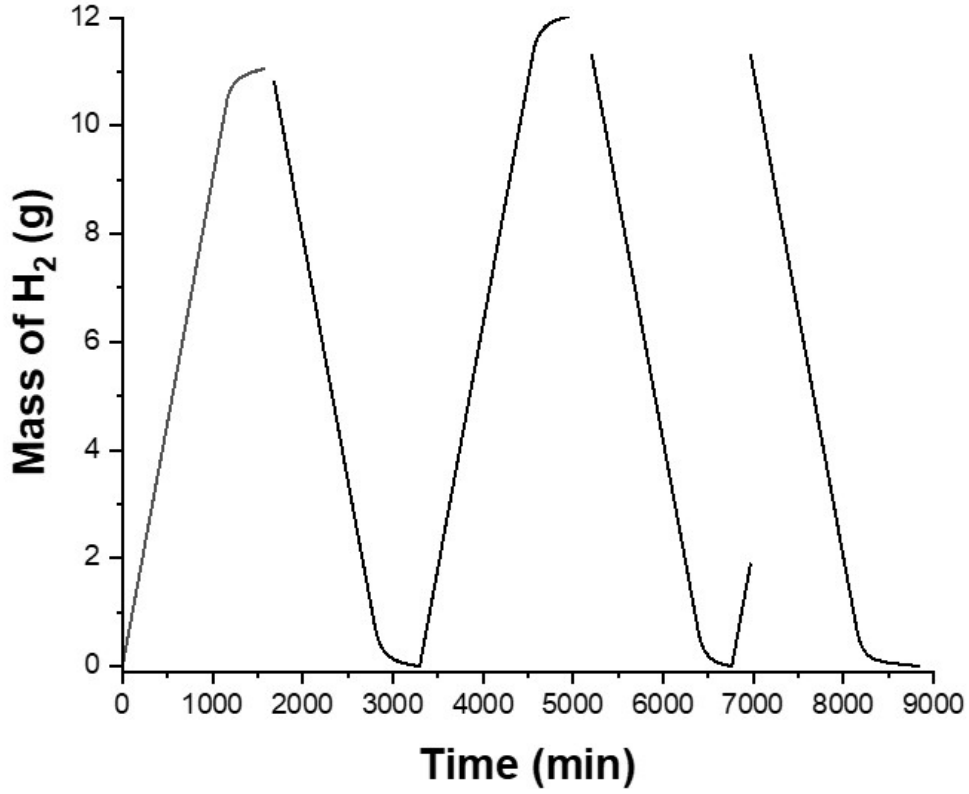

Figure 29. Mass of hydrogen absorbed or liberated during the cycles at 20 °C

Finally, Figure 29 shows the evolution of the mass of hydrogen absorbed and desorbed with each cycle. The graphs shows how the hydride is absorbing slightly more hydrogen in each cycle, suggesting that the hydride will reach “full activation” after some hours of operation.

4.6.3 Tests at 30 °C with conductivity measurements

A final absorption cycle was performed at 30 °C, following the same methodology as in the previous temperatures. This time, the thermal conductivity was measured with the hot wire method using a Kapton-insulated Pt-wire. After the tests at 20 °C, the tank was open and the wire replaced by a new one with the right insulation (i.e. coating film), and the tests at 30 °C were performed.

Figure 30 shows the results of the absorption test performed at 30 °C feeding 100 Nml/min of hydrogen to the tank. The pressure shows the same tendency as before, with the two inflection points owing to the beginning and end of the absorption process. Flow shows again the contrary tendency to the pressure values. And the evolution of temperature is coherent with an exothermic process for the absorption cycles, and endothermic process of the desorption step. The cycles are clearly shorter than those obtained at lower temperatures, indicating that the absorption and desorption of hydrogen occurs faster.

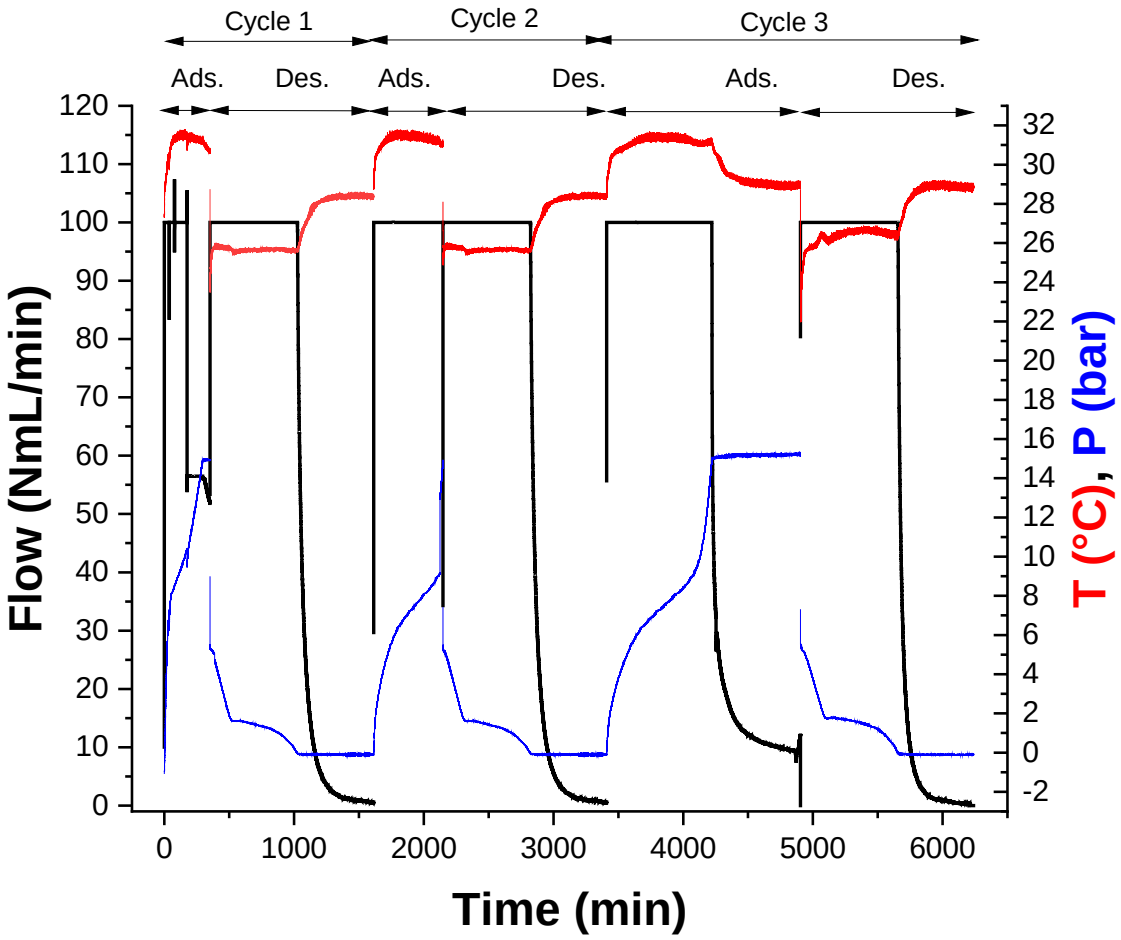

Figure 30. Evolution of flow, temperature and pressure during the absorption/desorption cycles at 30 °C

The volume absorbed by the tank is once again calculated integrating the flow rate over time and subtracting the calculated dead volume (i.e. 85.90 mL). The volume of hydrogen absorbed and desorbed in each cycle can be seen in Table 9. The total volume of hydrogen stored or liberated is considerable lower than the values obtained in the test at 30 °C. The result is logical since the absortion capacity of hydrides decrease as temperature gets higher. As in the previus cycles, the absorbed volume is again higher than the desorbed volume due to the fact that the hydride is not able to release all the hydrogen supplied and some part of it remains absorbed. The evolution of the mass of hydrogen absorbed and desorbed against time is also depicted in Figure 31.

Table 9. Volume of hydrogen charged and discharged during the absorption/desorption cycles at 30°C

Cycle	**Volume (LN)**	
	Load	**Unload**
1	72.6	57.4
2	72.6	53.5
3	91.1	79.0

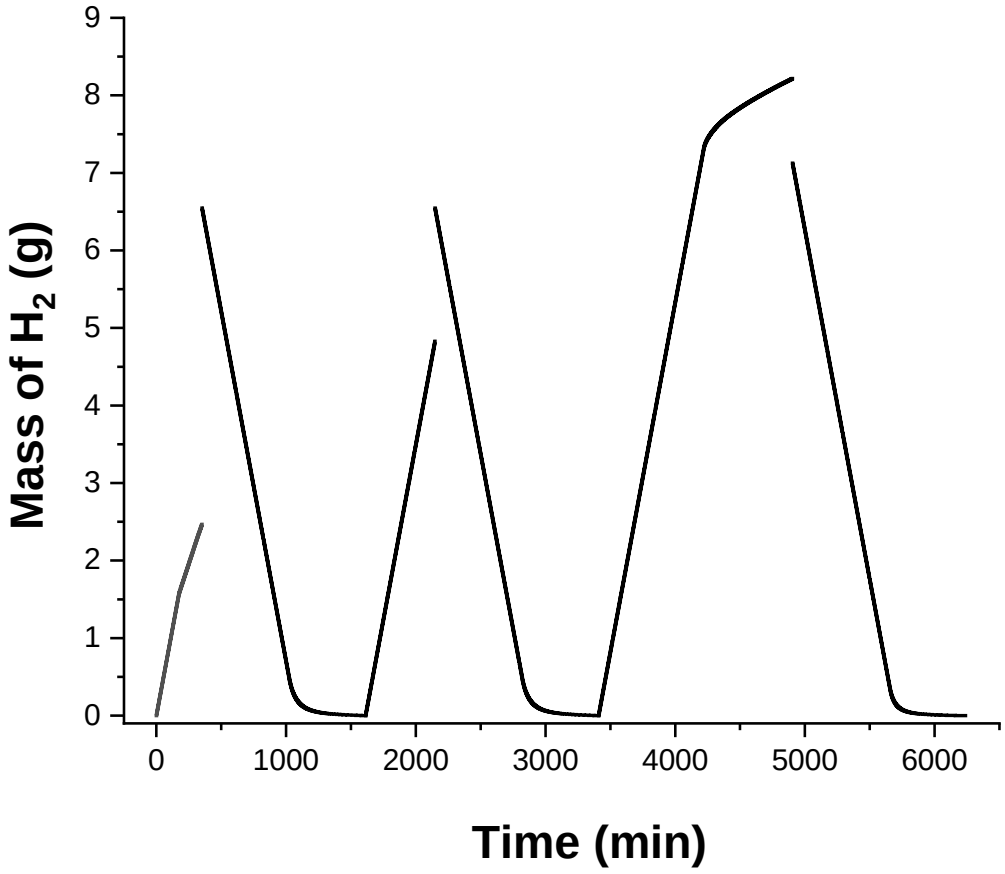

Figure 31. Mass of hydrogen absorbed or liberated during the cycles at 30 °C

The thermal conductivity of the hydride inside the tanks was measured at several steps during the absorbtion and desoption cycle with the hot wire method, following the same methodology as for the conductivity tests in glycerol and methanol of section 4.5. An intensity of 2 A was used for the measurements. The graph representing the voltage against the natural logarithm of time for each one of this steps can be seen in *Figure* ***32***.

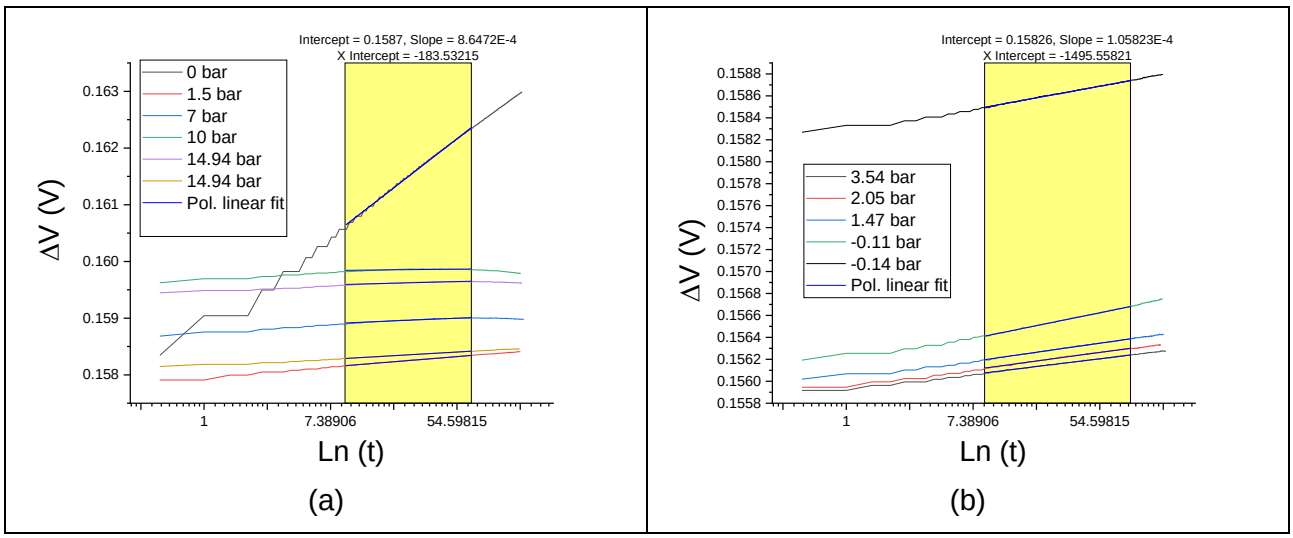

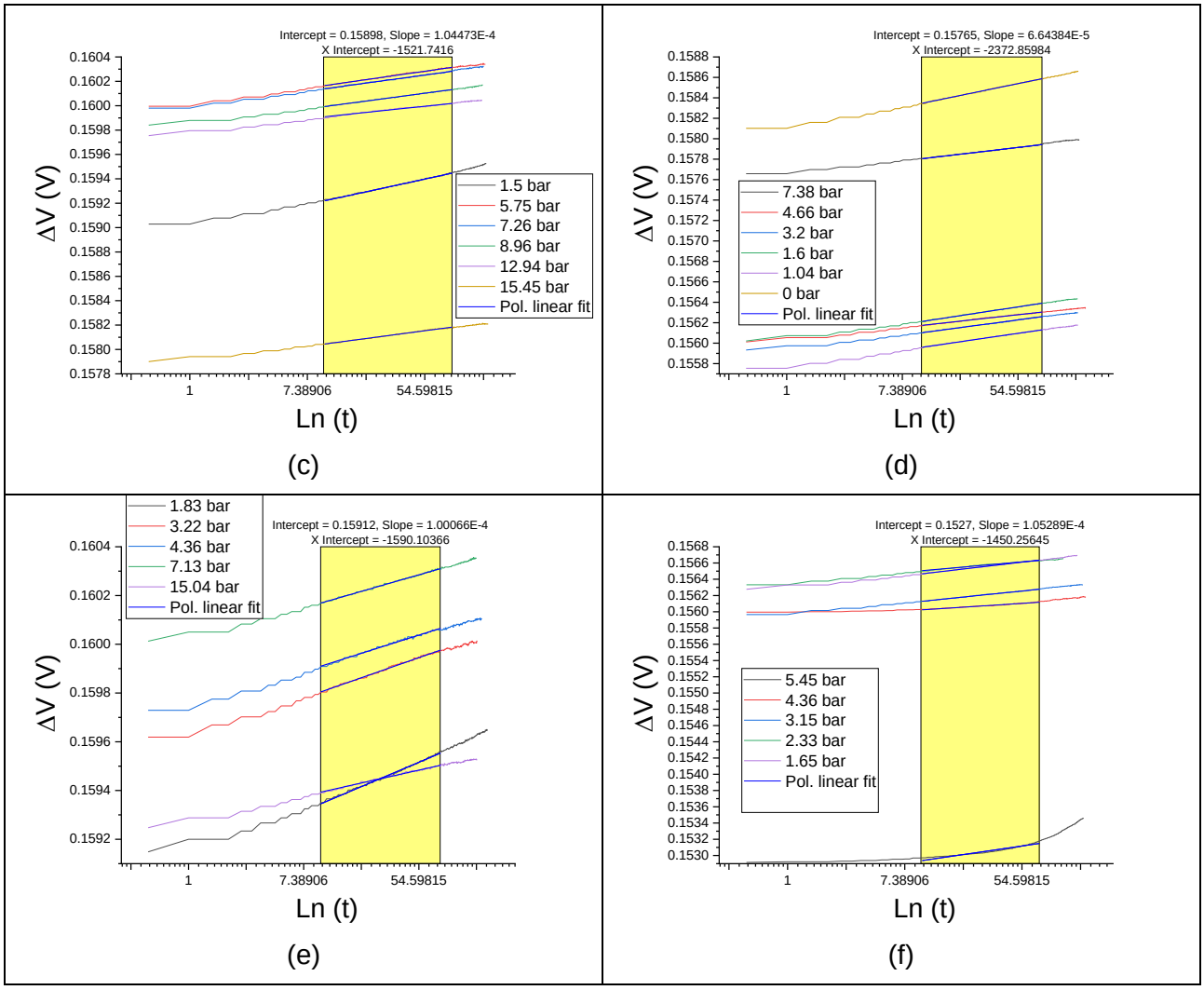

Figure 32. Voltage increase measurements inside the hydride tank with the TC-sensor coated with Kapton at different absorption cycles: (a) cycle 1 absorption, (b) cycle 1 desorption, (c) cycle 2 absorption, (d) cycle 2 desorption, (e) cycle 3 absorption and (f) cycle 3 desorption.

The results of the tests depicted in Figure 32 are summarized in Table 10. It can be seen the pressure in the tank when the masurement was performed, and the slope of the linear regresion of the curve of voltage against the natural logarithm of time, as well as the resistance at the beginning of the measurement. The error factor was determined in section 4.5.2.2, being of A=1.315. With all this information, the thermal conductivity of the hydride can be calculated as follows:

$$k = \frac{1}{A}\frac{I^3 R_0^2 \sigma}{4\pi L}\left(\frac{d\Delta V(t)}{d(lnt)}\right)^{-1}$$

where k is the known conductivity of the medium tested, A is the error factor (1.315), I the intensity in the test, L the length of the wire, R0 the resistance at the beginning of the measurement, σ the temperature coefficient of resistance of the Pt-wire and $\frac{d\Delta V(t)}{d(lnt)}$ the slope of the graph obtained with the linear regression.

Table 10. Summary of results of the conductivity tests at 30 °C

Cycle	Stage	Test number	Pressure (bara)	Intensity (A)	R0 (Ω)	Slope	K (W/mK)
1	Absoption	0	-1.00	2.002	0.079096	8.65E-04	0.107
		1	1.50	2.002	0.078798	9.08E-05	1.009
		2	7.00	2.002	0.079223	4.74E-05	1.953
		3	10.00	2.002	0.0797	5.16E-05	1.818
		4	14.94	2.002	0.079603	5.84E-05	1.601
		5	15.11	2.002	0.078956	6.44E-05	1.428
	Desoption	1	3.54	2.002	0.0778	7.08E-05	1.262
		2	2.05	2.002	0.077856	7.84E-05	1.141
		3	1.47	2.002	0.077815	8.26E-05	1.081
		4	-0.11	2.002	0.077902	1.17E-04	0.763
		5	-0.14	2.002	0.078937	1.06E-04	0.868
2	Absoption	1	1.50	2.002	0.079316	1.04E-04	0.888
		2	5.75	2.002	0.079798	6.89E-05	1.364
		3	7.26	2.002	0.07979	6.60E-05	1.423
		4	8.96	2.002	0.079801	6.41E-05	1.465
		5	12.94	2.002	0.079758	5.03E-05	1.864
		6	15.45	2.002	0.078951	6.38E-05	1.442
	Desoption	1	7.38	2.002	0.078829	6.64E-05	1.380
		2	4.66	2.002	0.077967	6.25E-05	1.434
		3	3.20	2.002	0.077928	7.57E-05	1.183
		4	1.60	2.002	0.077933	8.58E-05	1.043
		5	1.04	2.002	0.077838	8.21E-05	1.088
		6	-0.10	2.002	0.078933	1.16E-04	0.793
3	Absoption	1	1.83	2.002	0.079455	1.00E-04	0.931
		2	3.22	2.002	0.07973	8.25E-05	1.136
		3	4.36	2.002	0.079785	7.48E-05	1.256
		4	7.13	2.002	0.079807	6.80E-05	1.381
		5	15.02	2.002	0.079426	5.30E-05	1.757
	Desorción	1	5.45	2.002	0.077957	4.67E-05	1.917
		2	3.15	2.002	0.077944	7.41E-05	1.210
		3	2.33	2.002	0.078088	6.32E-05	1.423
		4	1.65	2.002	0.077905	8.42E-05	1.063
		5	0.50	2.002	0.076359	1.05E-04	0.817

The calculated thermal conductivity is also shown in Table 10. At the beginning of the test, the initial thermal conductivity of the hydride was 0.107 W/m·K in an atmosphere of vacuum after evacuating the Argon in which the tank was delivered. It can be seen how the thermal conductivity of the hydride increases considerably as it absorbs hydrogen and the pressure inside the tank starts to rise, reaching values of up to 1.9 W/m·K. Once the hydrogen is desorbed, the conductivity decreases again to values of 0.8 W/m·K. The value is higher than the first measurement because of the remaining content of hydrogen that the hydride is not able to release. This evolution of the thermal conductivity with the hydrogen content in the tank is also depicted in Figure 33. It can be seen how

the values obtained are quite similar regardless the absorption cycle. The values obtained are similar to those that can be found in the literature and follow the same trend with hydrogen pressure.[1]

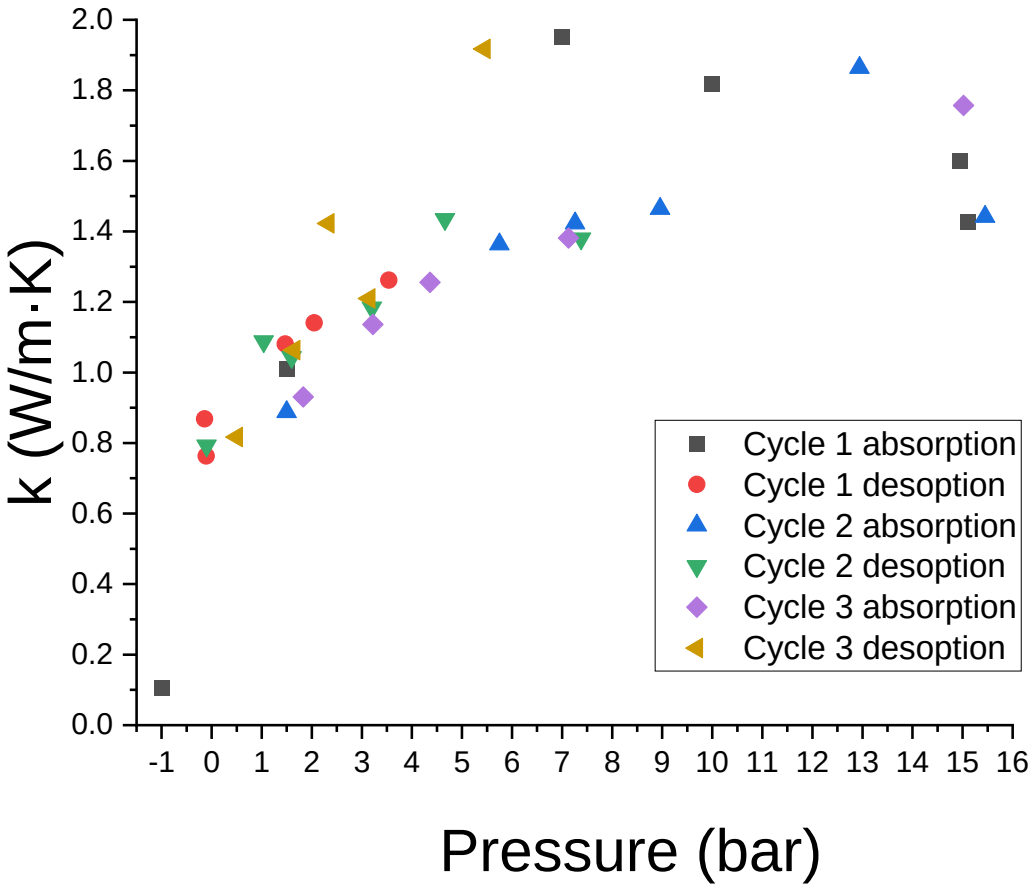

Figure 33. Effect of hydrogen pressure on the thermal conductivity of the hydride at 30 °C

4.6.4 Tests at 10 °C with conductivity measurements

One absorption/desorption cycle was repeated at 10 °C, this time measuring the thermal conductivity of the hydride, to compare the results with those obtained in section 4.7.3.1 and check the effect of the temperature on the evolution of the thermal conductivity against pressure.

[1] Christopher, M. D. (2006). Application of the transient hot-wire technique for measurement of effective thermal conductivity of catalyzed sodium alanate for hydrogen storage (Doctoral dissertation, Virginia Tech).

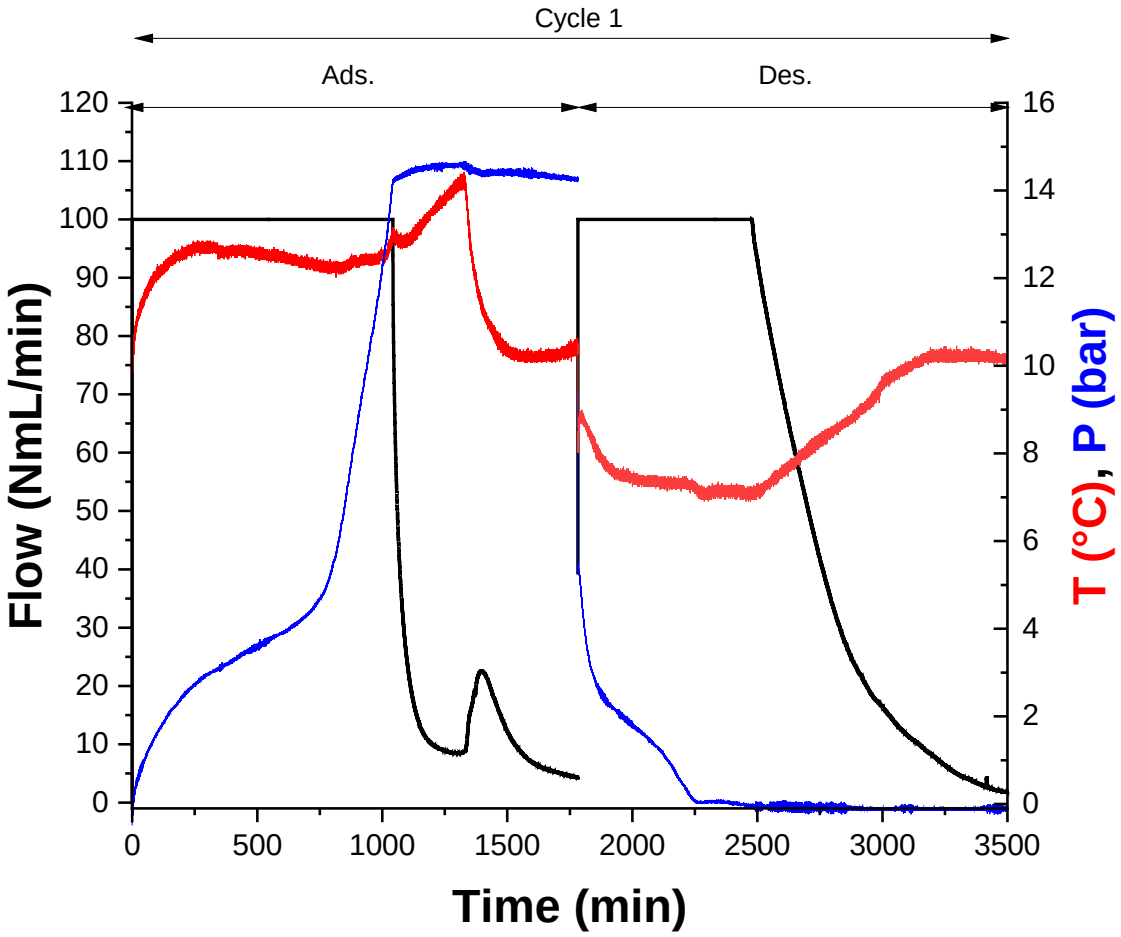

Figure 34. Evolution of flow, temperature and pressure during one absorption/desorption cycle at 10 °C

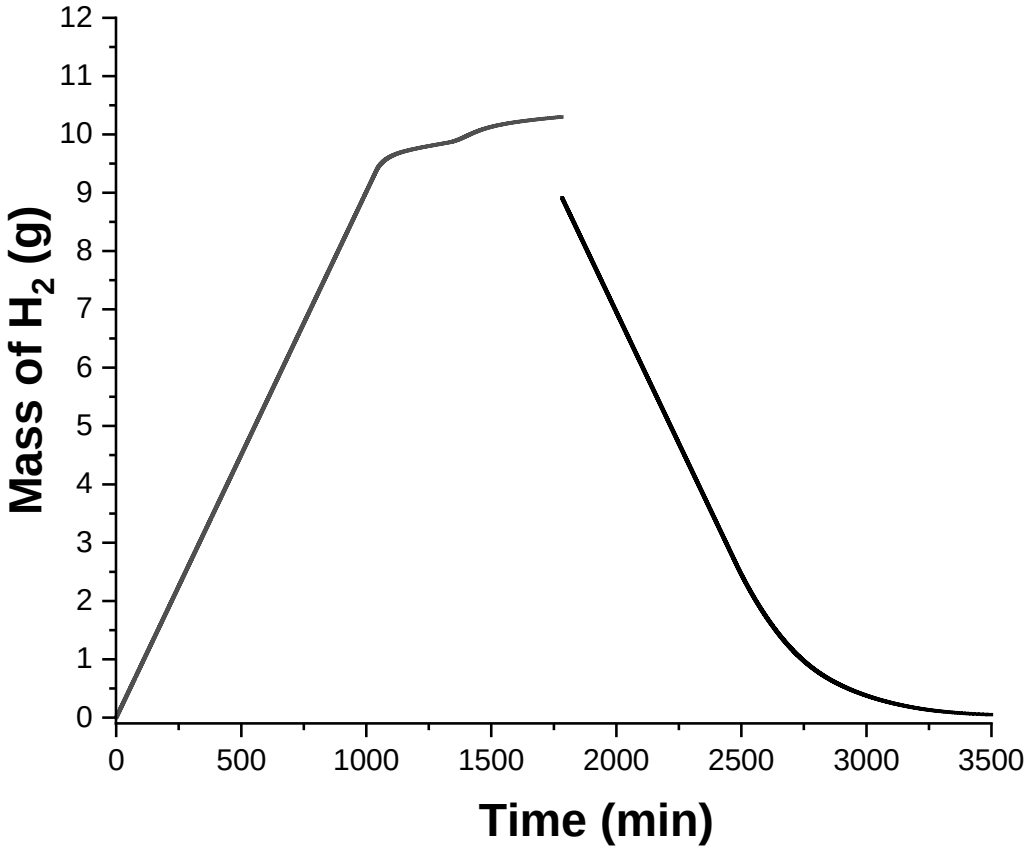

Figure 35. Mass of hydrogen absorbed or liberated during the cycle at 10 °C

Figure 34 shows the results of the absorption test performed at 10 °C feeding 100 Nml/min of hydrogen to the tank. The evolution of flow, pressure and temperature is basically the same as that of the test in section 4.7.3.1. The amount of hydrogen absorbed was 114.2 LN and the amounto of hydrogen desorbed 98.8 LN. An amount slighty smaller to that found in the first test in section 4.7.3.1. The evolution of the mass of hydrogen absorbed and desorbed is depicted in Figure 35, showing the same trend and similar values to those in Figure 27.

The thermal conductivity of the hydride inside the tanks was measured at several steps during the absorbtion and desoption with the hot wire method. An intensity of 2 A was used again for the measurements. The graph representing the voltage against the natural logarithm of time for each one of this steps is depicted in Figure 36, whose results can be seen in Table 11.

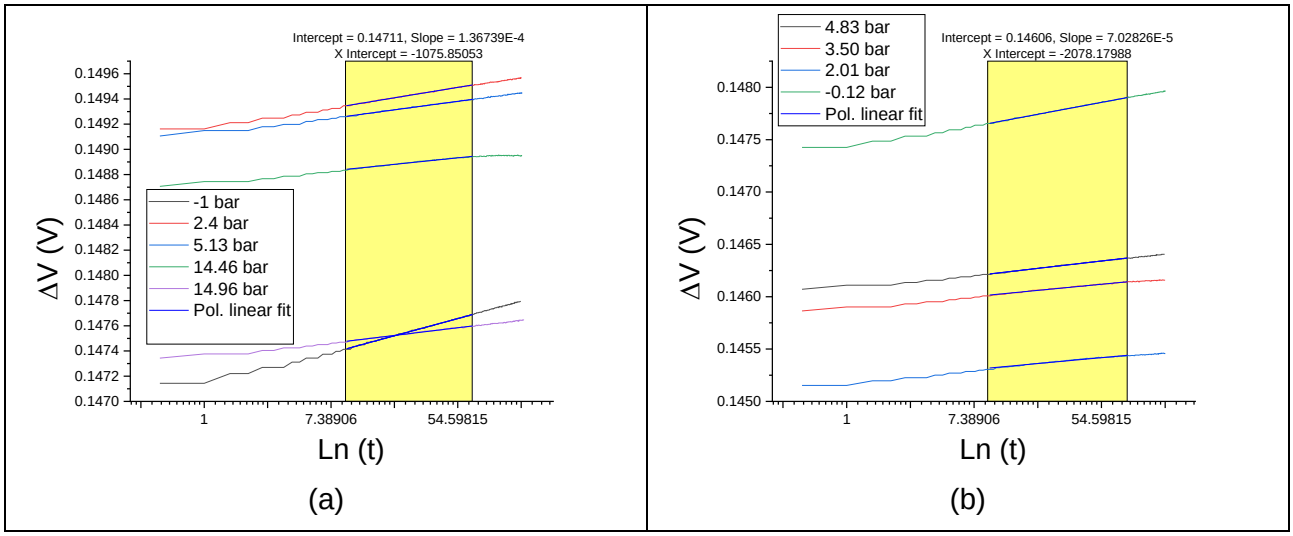

Figure 36. Voltage increases measurements inside the hydride tank with the TC-sensor coated with Kapton at 10 °C

Table 11. Summary of results of the conductivity tests at 10 °C

Cycle	Stage	Test number	Pressure (bara)	Intensity (A)	R0 (Ω)	Slope	K (W/mK)
1	Adsorción	0	-1	2.002	0.073535	1.37E-04	0.583
		1	2.4	2.002	0.074469	8.26E-05	0.990
		2	5.13	2.002	0.074516	6.77E-05	1.211
		3	14.46	2.002	0.0744	5.18E-05	1.575
		4	14.96	2.002	0.073452	6.11E-05	1.303
	Desorción	1	4.83	2.002	0.0728	7.03E-05	1.113
		2	3.5	2.002	0.07275	5.85E-05	1.334
		3	2.01	2.002	0.072432	5.61E-05	1.380
		4	-0.12	2.002	0.073566	1.14E-04	0.701

The calculated thermal conductivity is also shown in Table 11 and the evolution of the thermal conductivity with the hydrogen content in the tank is depicted in Figure 37. The values of thermal conductivity obtained follow the same trend as in the tests at 30 °C. Just small differences can be seen owing to the effect of temperature of the conductivity of the hydride.

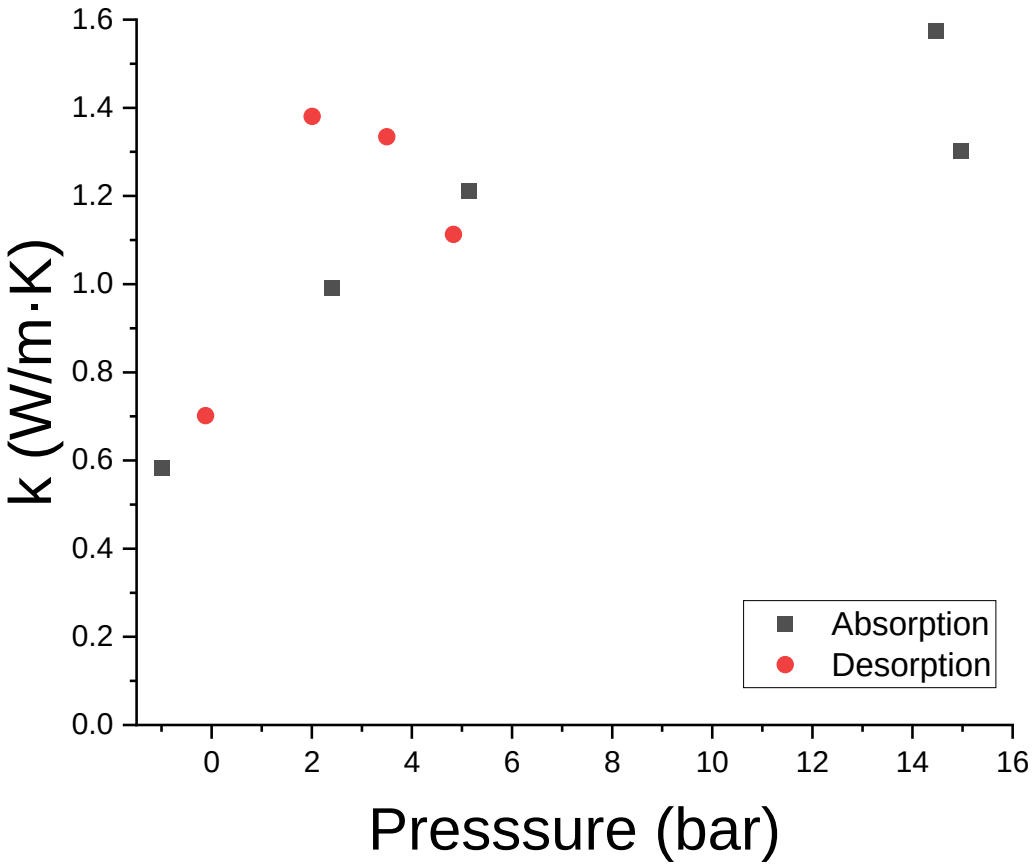

Figure 37. Effect of hydrogen pressure on the thermal conductivity of the hydride at 10 °C

5 Assessing the influence of pollutants in hydrogen gas

5.1 Definition of pollutants (A4.2.1)

MAHYTEC, FHA, BAM and MPG define as pollutants of reference the most common elements of the list of pollutants ISO 14687-2. Based on this, a series of binary reference gas is obtained from a gas supplier with the same concentration of pollutant as indicated as the maximum acceptable for the standard. In order to compare the sensibility of each pollutant, we compare capacity results after 50 charge-discharge cycles with the maximum concentration defined in the standard, and a concentration five times higher.

Table I shows the concentration values retained for each pollutant in relation to ISO 14687-2 (being 1x the maximum allowed concentration according to the standard):

Table 12 - Pollutants elements and concentration

Pollutants	Proportion of pollutant in H_2		
	1x	**5x**	**10x**
N_2	100 µmol/mol 100 ppm	500 µmol/mol 500 ppm	1000 µmol/mol 1000 ppm
CO	0,2 µmol/mol 0,2 ppm	1µmol/mol 1 ppm	
CO2	2 µmol/mol 2 ppm	10 µmol/mol 10 ppm	
O_2	5 µmol/mol 5 ppm	25 µmol/mol 25 ppm	
H_2O	5 µmol/mol 5 ppm	25 µmol/mol 25 ppm	

5.2 Experimental set-up and procedure

In order to set up the experimental protocole, we measured the capacity during the absorption and desorption of each cycle. For this purpose, a gravimetric measurement was the most appropriate. From this, the choice to carry out tests on samples of 100 g of hydride was made, because of MAHYTEC's experience in using this scale, which allows mass measurements to be made to quantify the weight capacity of the hydride. In addition, thermal regulation is necessary to have a better comparability between each cycle and also to reduce the time.

A sufficiently light test tank had to be designed to allow accurate measurement of hydrogen capacity and to allow sufficient heat exchange with the outside. We already had a scale that allowed us to measure precisely to a hundredth of a gram if we did not exceed 750 g. In summary, the design had to meet the following specifications:

- Mass less than 750 g including hydrogen connections and metal hydride
- Facilitate heat exchange between the hydride and the outside thanks to fins and with the smallest possible diameter
- A filtration system of a few µm
- Simple assembly/disassembly system
- To be able to integrate a valve
- Pressure resistance up to 150 bar (for possible testing of 3rd stage hydrides)

Figure 38 - Test tanks for pollutant test

After studying the possibility of making our own mixture by buying pure gas bottles and then mixing with a mixer. It turned out to be more economical and reliable to buy directly from experienced manufacturers.

Below there is the P&ID (piping and instrumentation diagram). There are four independent lines, one for each pollutant proportion. Each line is equipped with its own cylinder with a mixture of hydrogen and pollutant, a regulator that can go up to 34 bar_a. There is a three-way valve to alternate between charge and discharge. A quick coupling allows to easily control the pressure in the pipework.

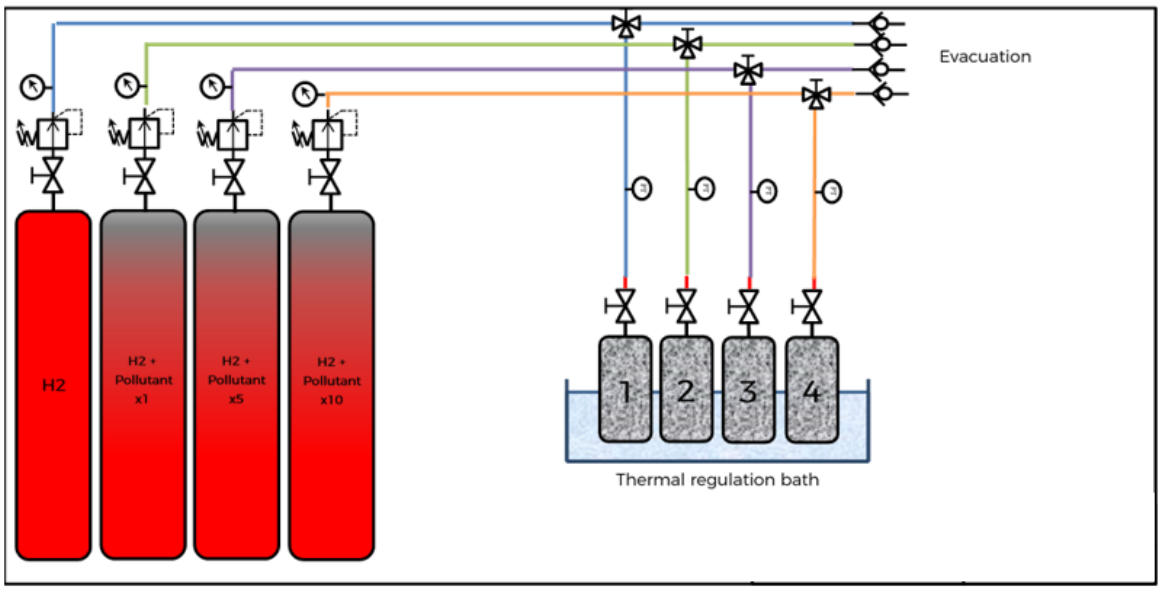

Figure 39 - P&ID of test bench

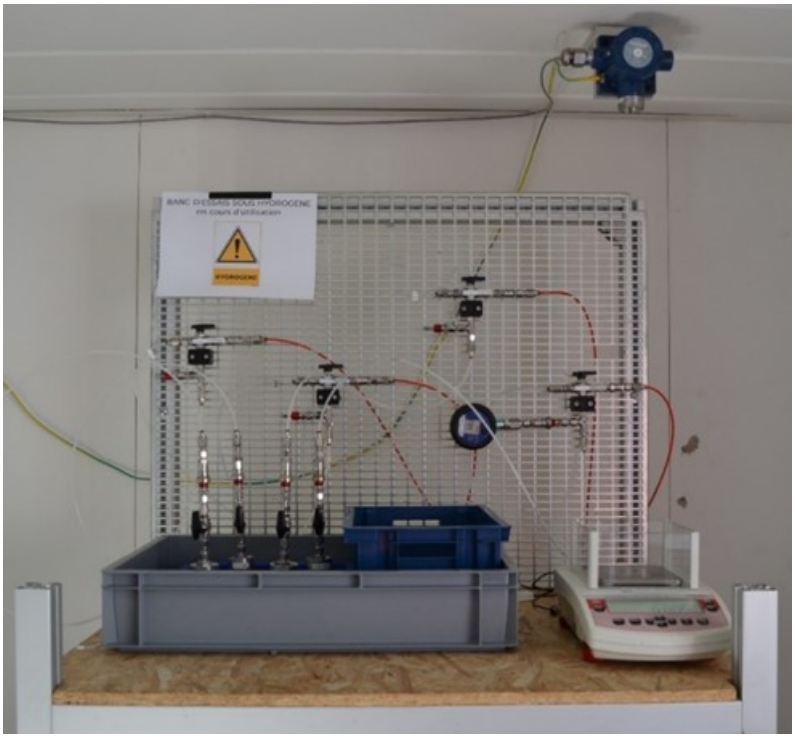

Figure 40 - Bench test photo

The set of tests is separated into 3 distinct campaigns with four samples tested each time:

- A first one with the control sample under hydrogen 4.5 and three with the different nitrogen mixtures.
- A second with the mixtures including carbon monoxide and those with carbon dioxide.
- A third with the mixtures including oxygen and those with water.

Each test campaign consists of 50 absorption/desorption cycles at ambient temperature and PCT curve after cycles 5, 20 & 50 at 8, 22 & 45°C. These tests measure the evolution of:

- The hydrogen capacity during the charge and discharge of each cycle
- The pressures of the absorption and desorption plates
- Absorption and desorption enthalpies

To optimize the cycle time, we were able to achieve a 3-hour charge and discharge. This allows a minimum of 3 cycles per day. PCTs take an average of 3 days per temperature.

5.3 Results about PCT curves using binary reference gas with pollutants

5.3.1 Control sample under hydrogen 4.5

The graph below shows the evolution of the absorption capacity during the charge (Cabs) in normal green, the hydrogen desorption (Cdes) in light green (meaning capacity remaining in the hydride after desorption) and in dark green the reversible capacity (Crev), i.e. the usable hydrogen during a cycle. The evolution of Cabs, Cdes and Crev for each pollutant proportion can be seen in the Annex section.

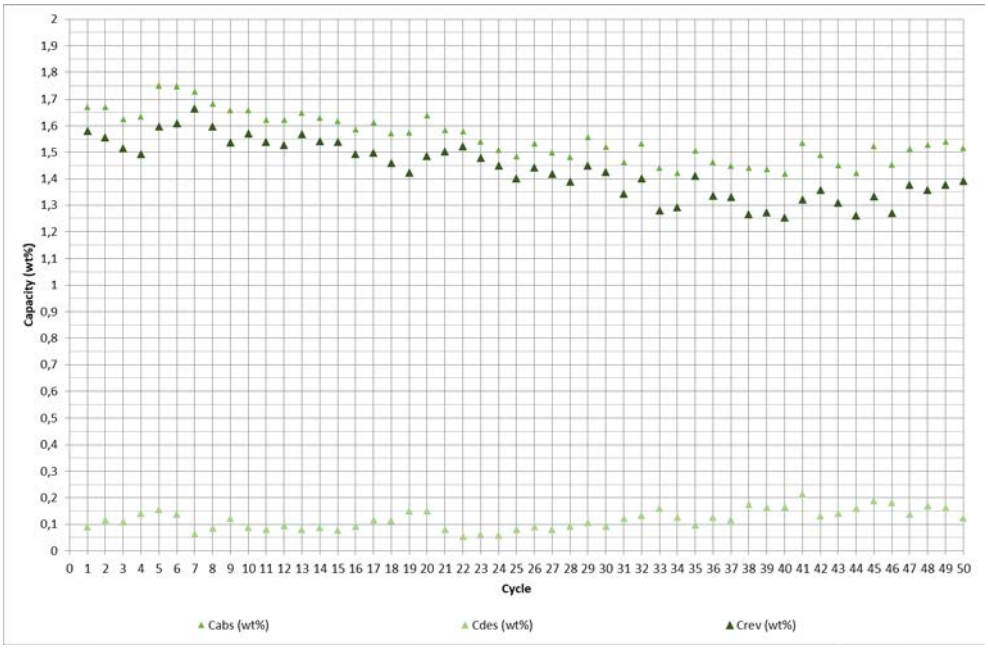

Figure 41 - Capacity evolution under H2 4.5 on 50 cycles at ambient temperature (room temperature)

For the hydrogen 4.5 test, we can observe on the graph above:

- A decrease Cabs until cycle 33 and then a stabilisation until cycle 50
- A stable value of Cdes until cycle 30
- A decrease in Crev, which consists of Cabs-Cdes, until cycle 33 and then a stabilisation until cycle 50

With this result, we can see the hydride have a degradation under an hygrogen 4.5. This degradation reaches each type of capacity, with a decrease of almost 10% on the max capacity and more than 12% on the reversible capacity. Further analysis of this result and of the results of tests using pollutants are presented in the next section.

Now, we will observe the influence of cycling on the PCT curves and on some of their characteristics. We have grouped the curves by temperature for better visibility.

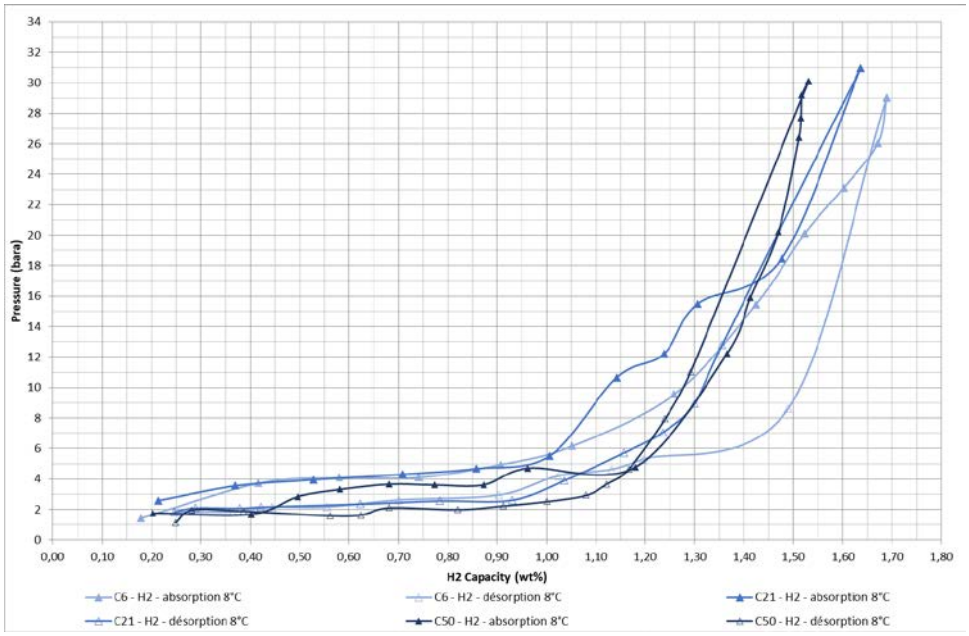

Figure 42 - PCT under H2 4.5 at 8°C after cycles 6, 21 and 50

We begin with the PCT curves at 8°C we can observe:

- A decrease in absorption capacity at 30 bara from 1,69wt% after cycle 6, to 1,64wt% after cycle 21 and 1,53wt% after cycle 50
- A slight decrease of the absorption plateau at cycle 50 from about 4 bara to 3,5 bara
- A slight decrease of the desorption plateau at cycle 50 from about 2,5 bara to 2 bara

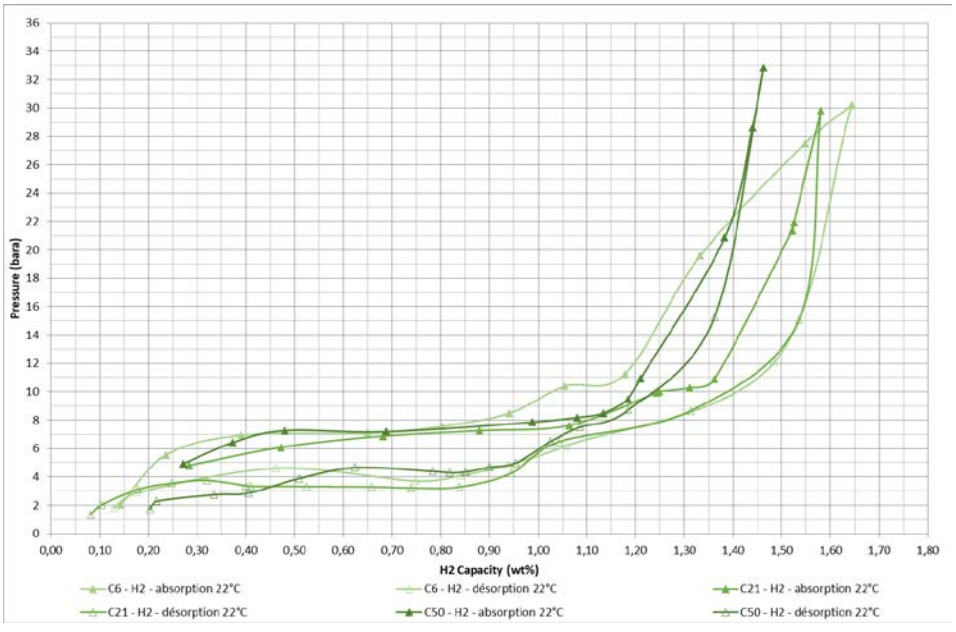

Figure 43 - PCT under H2 4.5 at 22°C after cycles 6, 21 and 50

From these PCT curves above at 22°C we can observe:

- A decrease in absorption capacity at 30 bara from 1,64wt% after cycle 6, to 1,58wt% after cycle 21 and 1,46wt% after cycle 50
- No significant change in absorption plateau.
- A desorption plateau that oscillates between 3 and 5 bara

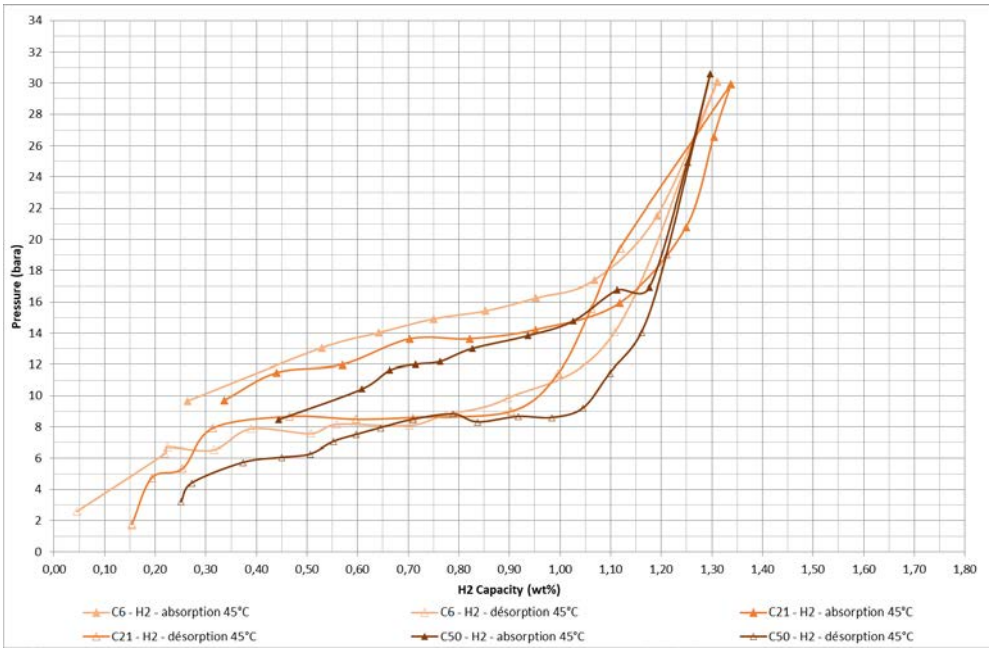

Figure 44 - PCT under H2 4.5 at 45°C after cycles 6, 21 and 50

From these PCT curves above at 45°C we can observe:

- No significant change in absorption capacity at 30 bara
- A decrease of the absorption plateau, from 10-17 bara at cycle 6, to 10-15 bara at cycle 21 and to 8 to 14 bara at cycle 50

From these curves and the Van't Hoff equation we extracted the enthalpy of absorption and desorption at different cycles (6, 21 and 50).

Van't Hoff equation: $\ln\left({P_{eq}}/{P_0}\right) = \frac{\Delta H}{RT} + \frac{\Delta S}{T}$

Table 13 - Evolution of absorption and desorption enthalpy under H2 4.5

		Cycle 6	Cycle 21	Cycle 50	Evolution rate (%)
H_2 4.5	**Absorption enthalpy (KJ/mol)**	25,76	22,95	23,44	-9,00
	Desorption enthalpy (KJ/mol)	22,06	24,5	27,26	+23,57

On the table above, we can observe a decrease for absorption enthalpy and an increase for desorption enthalpy. This result can show a decrease for the kinetic desorption. Indeed, with the same heat input for each cycle, if the calorie requirement increases with each cycle, the hydride cools down faster and therefore the reaction rate at reactor scale decreases. This phenomenon could explain in part the fact that the hydride desorbs less and less as the discharge time is identical for each cycle.

5.3.2 Influence of nitrogen

Nitrogen is a pollutant that is usually considered relatively innocuous to the metal hydride. For more clarity in the results with pollutant, we have kept the evolution of the reversible capacity on the graph below.

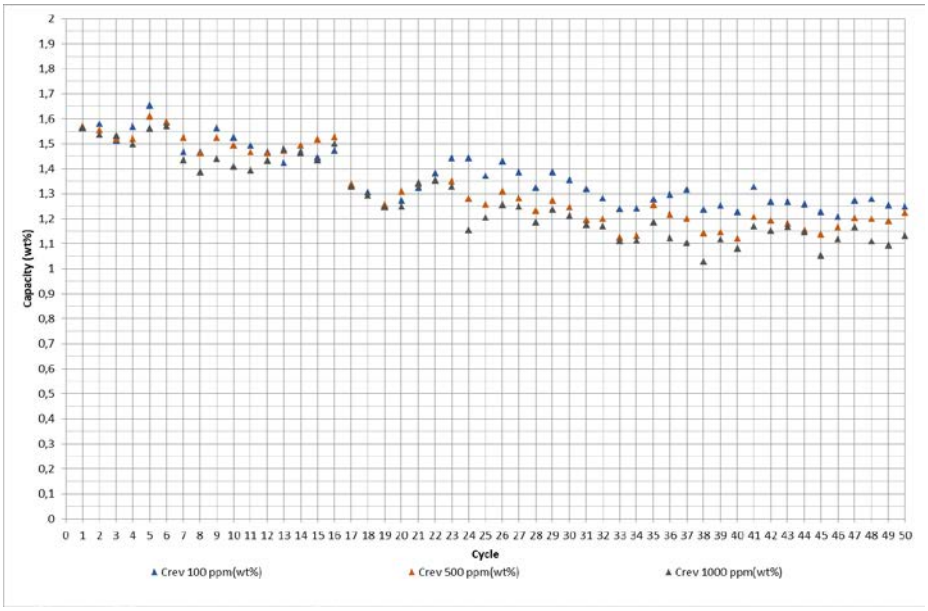

Figure 45 - Reverse capacity under H2 + N2 on 50 cycles – Proportion of N2: 100 ppm, 500 ppm and 1000 ppm

For the N2 test, we can observe on the graph above a decrease Crev during 35 cycles and then a stabilisation until cycle 50.

As for capacity results, for the tests with the pollutants and their different proportions we will just observe the curves at 22°C for more clarity.

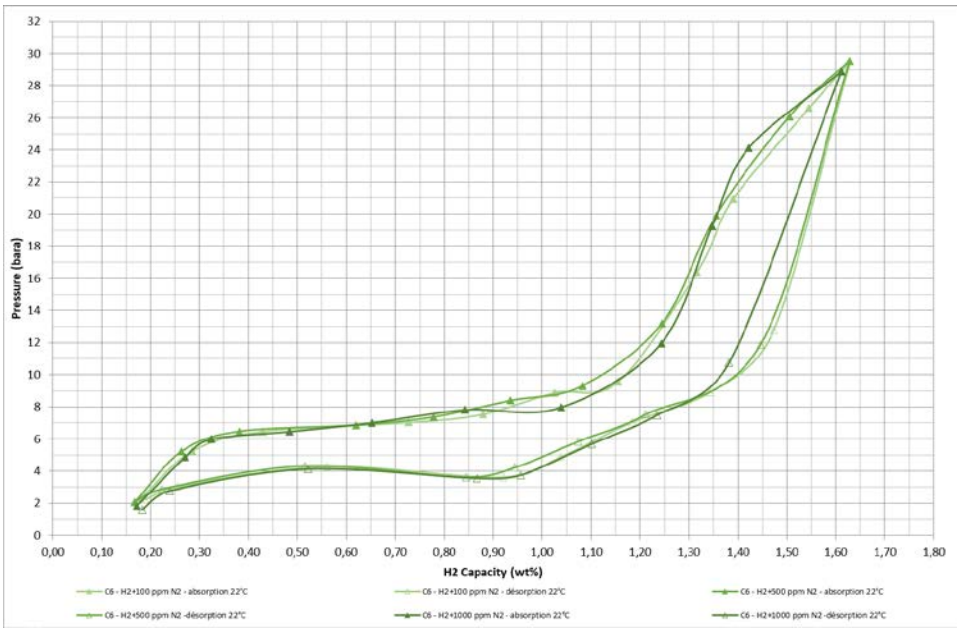

Figure 46 - PCT under H2 + N2 at 22°C after cycles 6

From these PCT curves above we can observe, after 6 cycles, no significant change between each PCT under different proportion of N2. We have a maximal capacity of 1,63wt% at 29 bara, an absorption plateau between 6 and 8 bara and a desorption plateau between 3 and 4 bara.

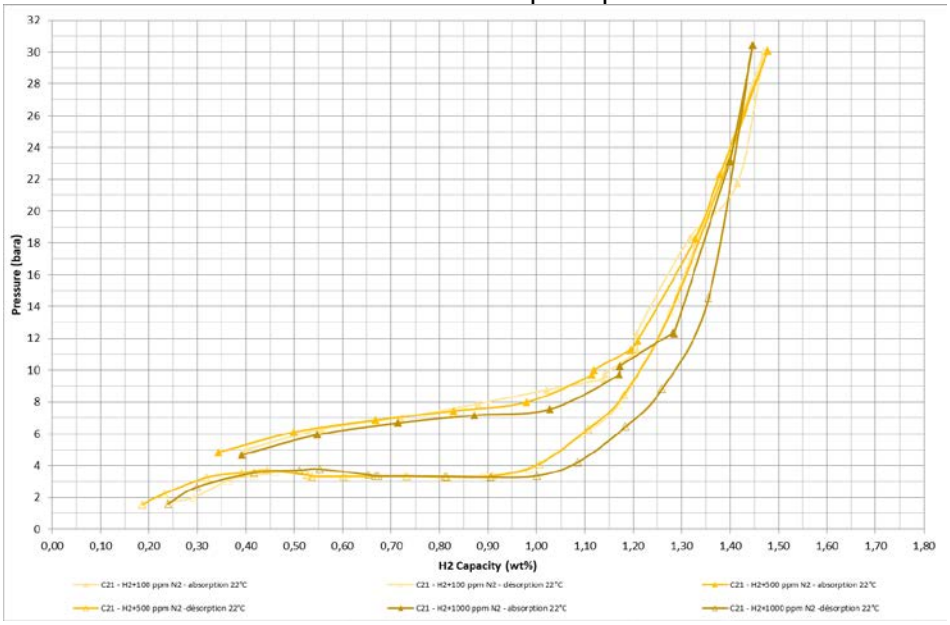

Figure 47 - PCT under H2 + N2 at 22°C after cycles 21

After 21 cycles, from these PCT curves above we also can observe no significant change between each PCT under different proportion of N2. Compared with cycle 6, we have a decrease of the maximal capacity at 1,45wt at 29 bara. The absorption and desorption plateaus are the same.

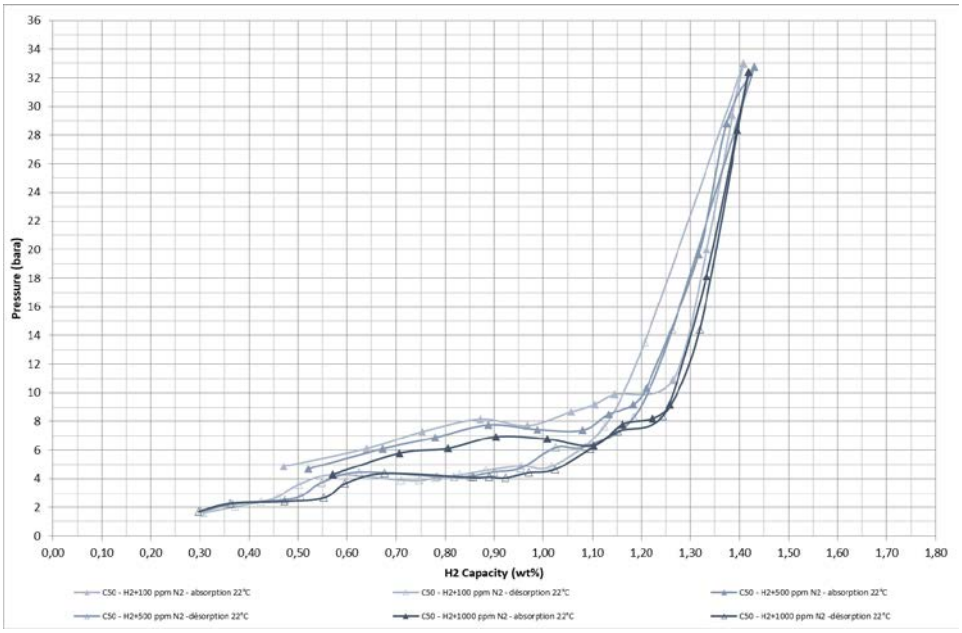

Figure 48 - PCT under H2 + N2 at 22°C after cycles 50

After 50 cycles, from these PCT curves above we also can observe no significant change between each PCT under different proportion of N2 about capacity and desorption plateau. However, we observe a decrease about 2 bara of with absorption plateau. Compared with previous cycles, we

have a decrease of the maximal capacity at 1,38wt at 29 bara. The desorption plateaus are the same.

On the table below, the enthalpy of absorption and desorption at different cycles (6, 21 and 50). During the test, we had a problem with the bottle with mixture H2 + 500 ppm N2, which have a leak on a manometer. So, we need to replace them, and to avoid lost so much time we decide to didn't make the PCT curve at 8 and 45°C for cycles 6. So, we can't obtain enthalpy result for cyles 6.

Table 14 - Evolution of absorption and desorption enthalpy under H2 + N2

		Cycle 6	Cycle 21	Cycle 50	Evolution rate (%)
N_2: 100 ppm	**Absorption enthalpy (KJ/mol)**	25,21	22,04	23,51	-6,74
	Desorption enthalpy (KJ/mol)	-27,27	-25,77	-27,78	+1,87
N_2: 500 ppm	**Absorption enthalpy (KJ/mol)**	N.A.	22,07	21,83	-1.09
	Desorption enthalpy (KJ/mol)	N.A.	-24,85	-27,22	+9,53
N_2: 1000 ppm	**Absorption enthalpy (KJ/mol)**	25,49	23,14	26,53	+4,08
	Desorption enthalpy (KJ/mol)	-26,96	-25,23	-26,96	+0,00

We can observe different evolution of enthalpies. But it is difficult to see any significant behaviour because of the experimental dispersion.

5.3.3 Influence of carbon monoxide

Carbon monoxide is a pollutant that is usually considered to have an impact on capacity and kinetic to the metal hydride characteristic. The evolution of the reversible capacity on the graph below.

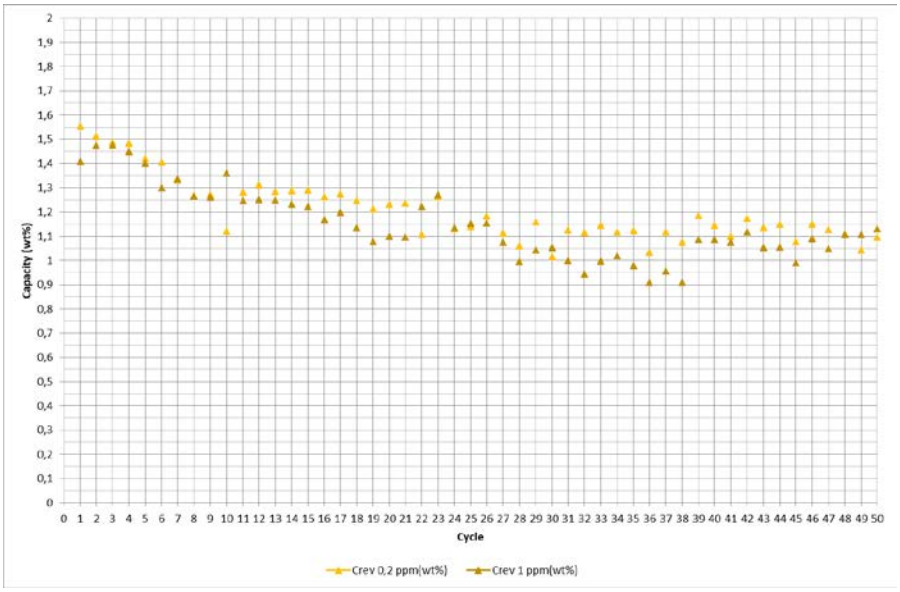

Figure 49 - Reverse capacity under H2 + CO on 50 cycles – Proportion of CO: 0,2 ppm and 1 ppm

For the CO test, we can observe on the graph above a decrease Cabs until cycle 30 and then a stabilisation until cycle 50.

We can be seen that there is a degradation between the first cycle and the last 50 cycles. The augmentation of CO proportion seems have no more effect on this. The evolution rates are equivalent for absorption capacity and the reversible capacity.

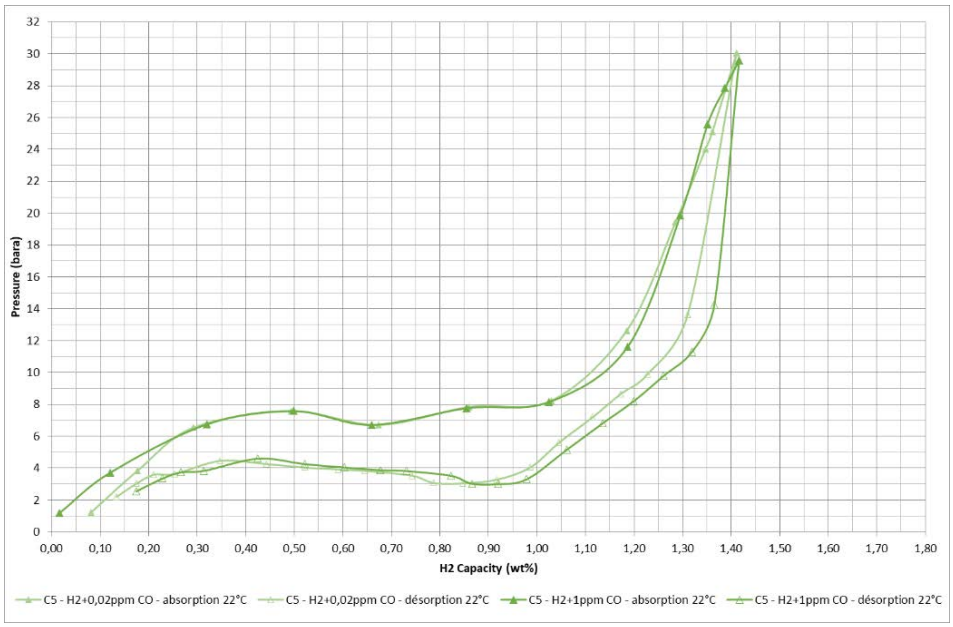

Figure 50 - PCT under H2 + CO at 22°C after cycles 5

From these PCT curves above we can observe, after 5 cycles, no significant change between each PCT under different proportion of CO. We have a maximal capacity of 1,42wt% at 30 bara, an absorption plateau between 6 and 8 bara and a desorption plateau between 3 and 4 bara.

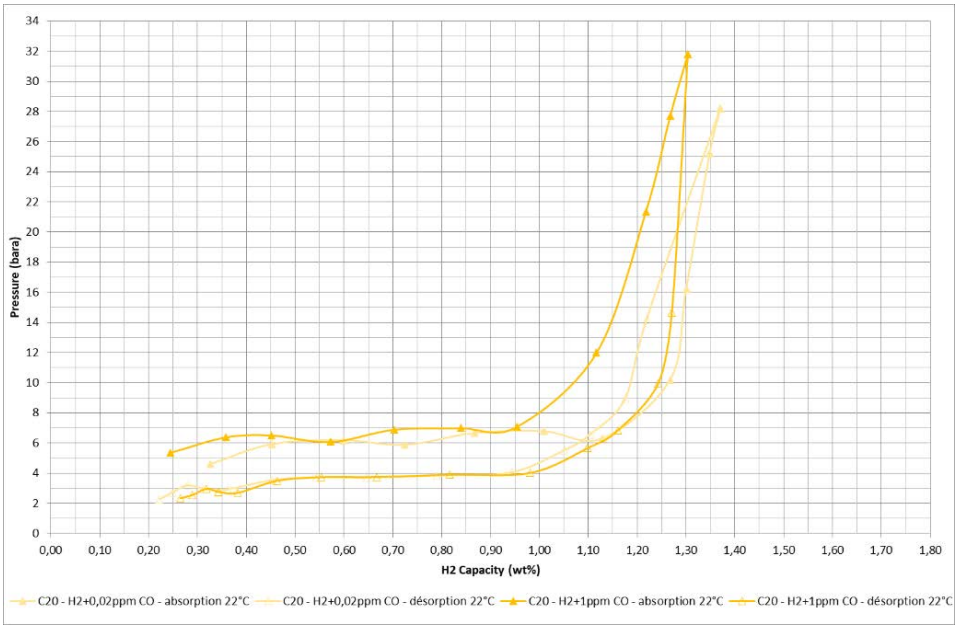

Figure 51 - PCT under H2 + CO at 22°C after cycles 20

From these PCT curves above we can observe, after 20 cycles, significant change between each PCT under different proportion of CO. We have a maximal capacity 28 bara of 1,37wt% with 0,2 ppm of CO and 1,28wt% 1 ppm of CO. Little change for absorption plateau, it is between 6 and 7 bara (8 bara for cycles 5) and no change for desorption plateau always between 3 and 4 bara.

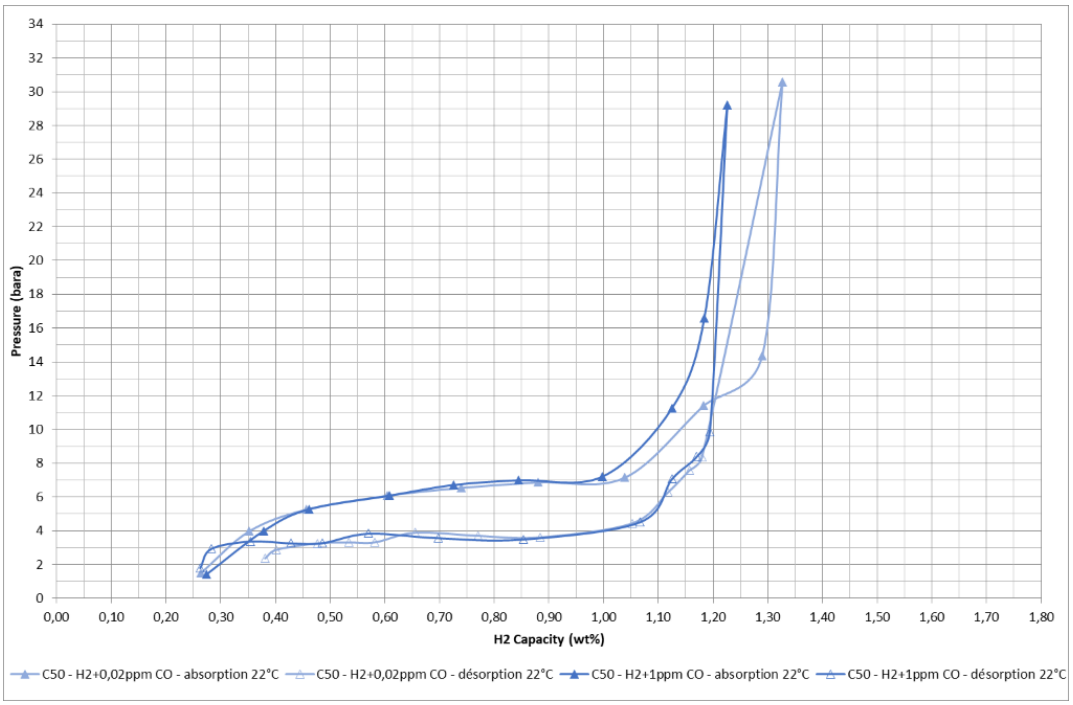

Figure 52 - PCT under H2 + CO at 22°C after cycles 50

From these PCT curves above we can observe, after 50 cycles, significant change between each PCT under different proportion of CO. We have a maximal capacity 29 bara of 1,31wt% with 0,2 ppm of CO and 1,23wt% 1 ppm of CO. It is lower than cycle 20. No change for absorption plateau, for desorption plateau with cycle 20.

Table 15 - Evolution of absorption and desorption enthalpy under H2 + CO

		Cycle 5	Cycle 20	Cycle 50	Evolution rate (%)
CO: 0,2 ppm	**Absorption enthalpy (KJ/mol)**	22,62	23,81	24,92	+10,17
	Desorption enthalpy (KJ/mol)	-28,75	-27,30	-28,89	+0,49
CO: 1 ppm	**Absorption enthalpy (KJ/mol)**	23,19	23,76	24,77	+6,81
	Desorption enthalpy (KJ/mol)	-28,20	-27,30	-29,03	+2,94

5.3.4 Influence of carbon dioxide

The evolution of the reversible capacity for carbon dioxide tests is shown in the graph below.

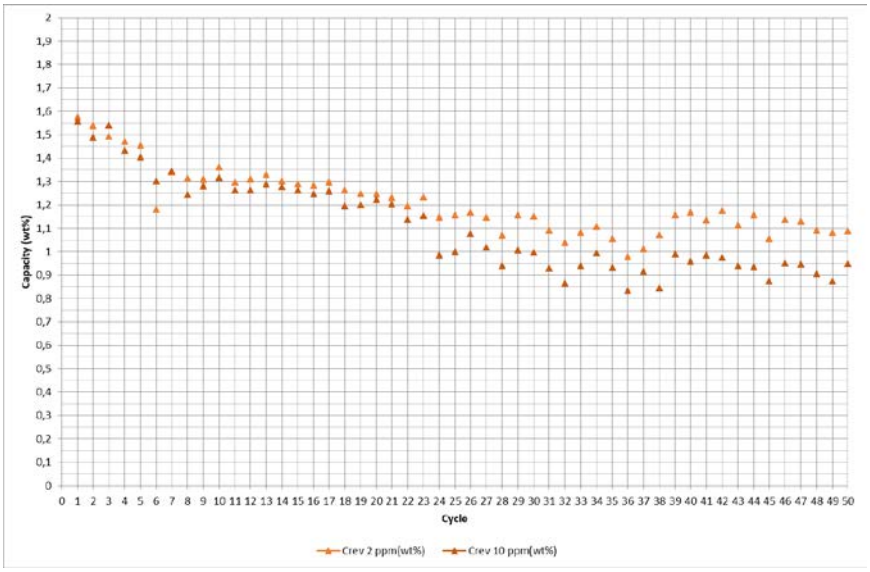

Figure 53 - Reverse capacity under H2 + CO2 on 50 cycles – Proportion of N2: 0,2 ppm, 1 ppm

For the CO2 test, we can observe on the graph above a decrease Cabs until cycle 23 and then a stabilisation until cycle 50. The evolution rates are equivalent for absorption capacity than for CO but more important with the reverse capacity. At the end we keep for the only 73% with 2 ppm of CO2 and even 62% of reverse capacity with 10 ppm of CO2.

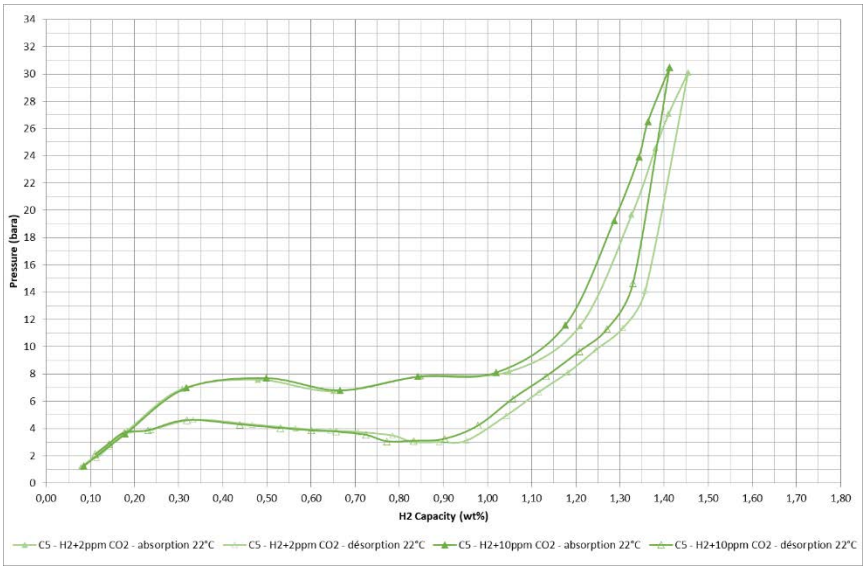

Figure 54 - PCT under H2 + CO2 at 22°C after cycle 5

From these PCT curves above we can observe, after 5 cycles, no significant change on the absorption and desorption plateau between each PCT under different proportion of CO2. However, there are already a difference about the capacity. We have a maximal capacity at 30 bara of 1,46wt% for 2 ppm of CO2, and 1,42wt% for 10 ppm of CO2.

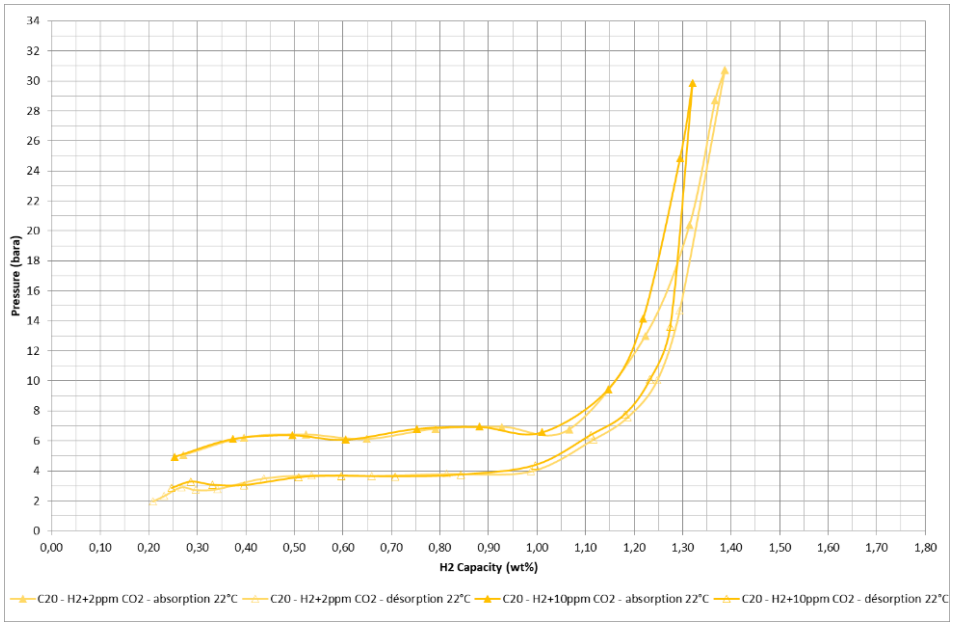

Figure 55 - PCT under H2 + CO2 at 22°C after cycles 20

From these PCT curves above we can observe, after 20 cycles, always no significant change on the absorption and desorption plateau between each PCT under different proportion of CO2. And, always a difference about the capacity. We have a maximal capacity at 30 bara of 1,39wt% for 2 ppm of CO2, and 1,32wt% for 10 ppm of CO2.

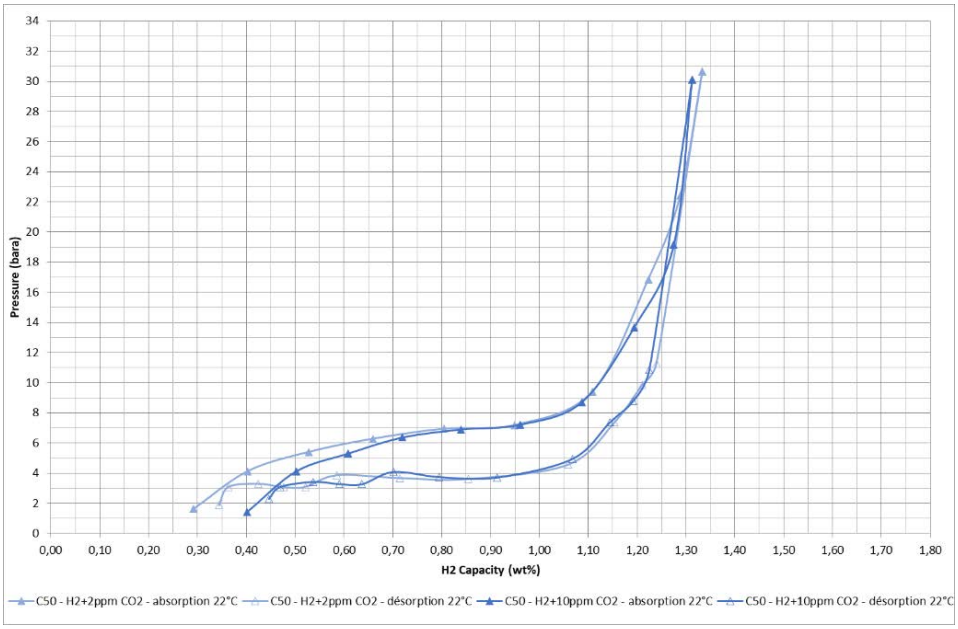

Figure 56 - PCT under H2 + CO2 at 22°C after cycles 50

From these PCT curves above we can observe, after 50 cycles, always no significant change on the absorption and desorption plateau between each PCT under different proportion of CO2. We have a maximal capacity at 30 bara of 1,32wt% for 2 ppm of CO2, and 1,31wt% for 10 ppm of CO2.

Table 16 - Evolution of absorption and desorption enthalpy under H2 + CO2

		Cycle 5	Cycle 20	Cycle 50	Evolution rate (%)
CO2: 2 ppm	**Absorption enthalpy (KJ/mol)**	23,65	24,65	24,61	+4,06
	Desorption enthalpy (KJ/mol)	-28,25	-26,74	-26,71	-5,45
CO2: 10 ppm	**Absorption enthalpy (KJ/mol)**	24,54	24,97	23,99	-2.24
	Desorption enthalpy (KJ/mol)	-27,08	-27,62	-28,09	+3,73

5.3.5 Influence of oxygen

For the O2 test, we can observe on the graph above a decrease Cabs until cycle 36 and then a stabilisation until cycle 50. We can see that there is a degradation between the first cycle and the last 50 cycles. The augmentation of O2 proportion seems have more effect on this, especially on reverse capacity. The evolution rates are equivalent for absorption capacity than for CO but more important with the reverse capacity. At the end we keep for the only 75% with 5 ppm of O2 and even 64% of reverse capacity with 25 ppm of O2.

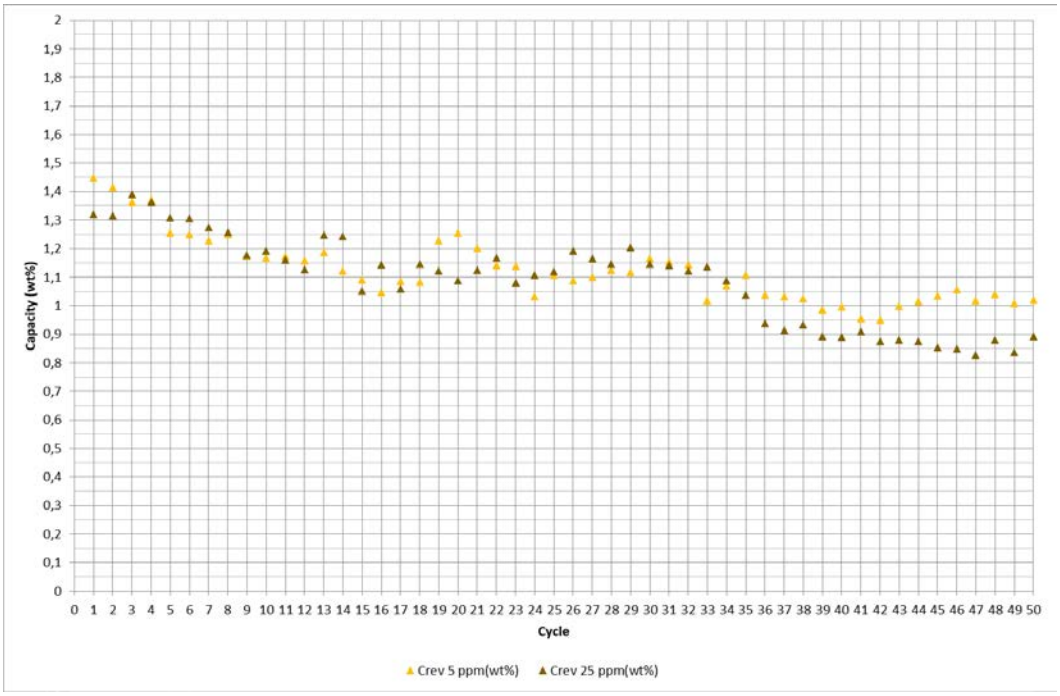

Figure 57 - Reverse capacity under H2 + O2 on 50 cycles – Proportion of O2: 5 ppm, 25 ppm

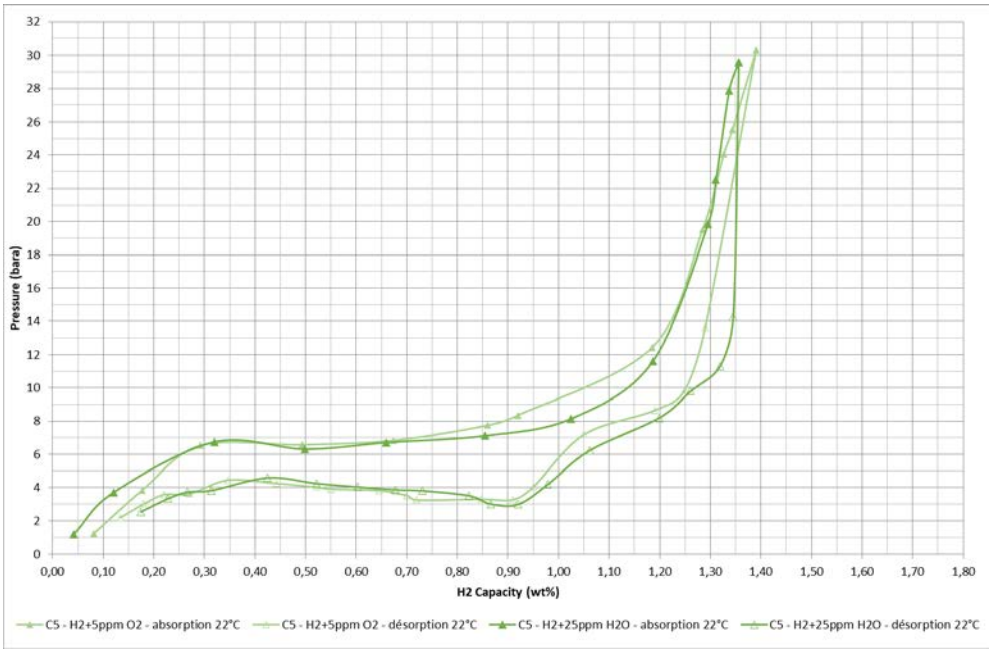

Figure 58 - PCT under H2 + O2 at 22°C after cycles 5

From these PCT curves above we can observe, after 5 cycles, no significant change on the absorption and desorption plateau between each PCT under different proportion of O2. However, there are already a difference about the capacity. We have a maximal capacity at 30 bara of 1,39wt% for 5 ppm of O2, and 1,36wt% for 25 ppm of O2.

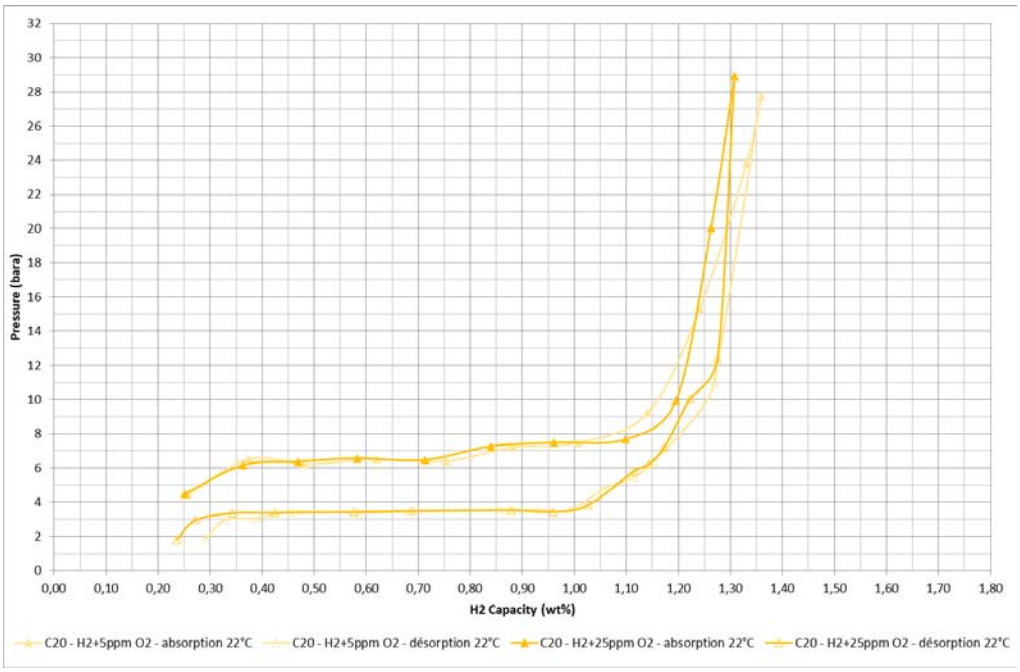

Figure 59 - PCT under H2 + O2 at 22°C after cycles 20

From these PCT curves above we can observe, after 20 cycles, always no significant change on the absorption and desorption plateau between each PCT under different proportion of O2. We have a maximal capacity at 28 bara of 1,37wt% for 5 ppm of O2, and 1,31wt% for 25 ppm of O2.

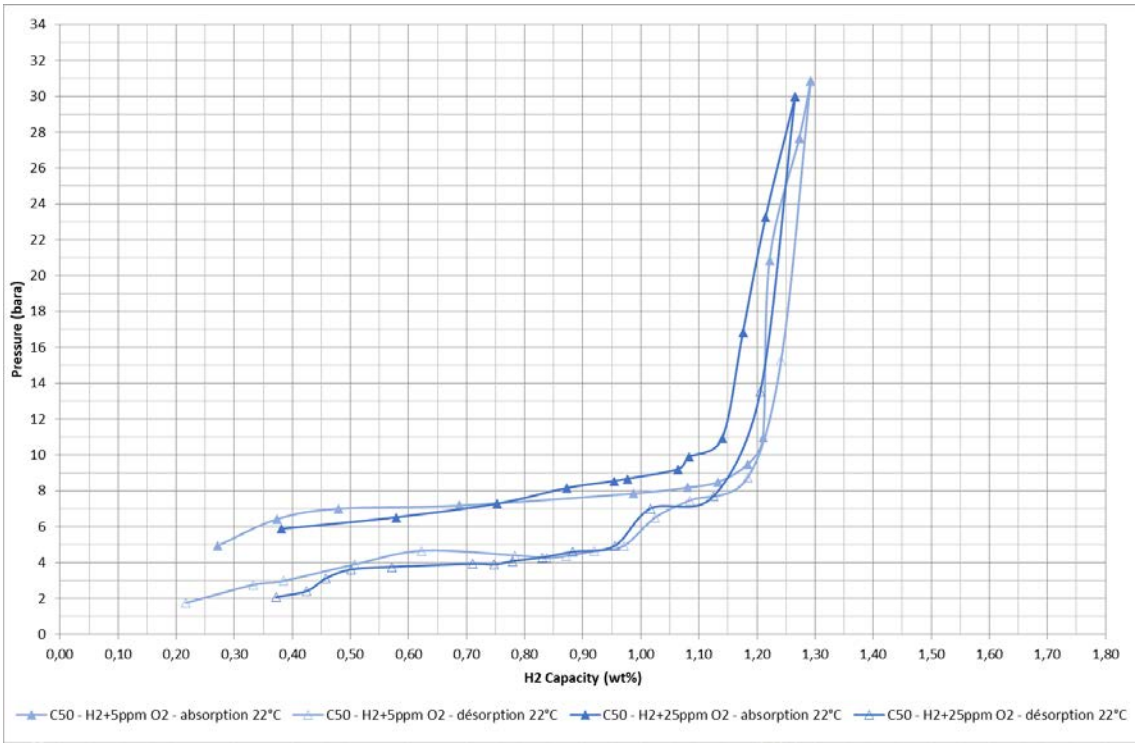

Figure 60 - PCT under H2 + O2 at 22°C after cycles 50

From these PCT curves above we can observe, after 50 cycles, always no significant change on the absorption and desorption plateau between each PCT under different proportion of O2. We have a maximal capacity at 30 bara of 1,29wt% for 5 ppm of O2, and 1,27wt% for 25 ppm of O2.

Table 17 - Evolution of absorption and desorption enthalpy under H2 + O2

		Cycle 5	Cycle 20	Cycle 50	Evolution rate (%)
O_2: 5 ppm	**Absorption enthalpy (KJ/mol)**	23,29	23,50	25,09	+7,73
	Desorption enthalpy (KJ/mol)	-27,67	-28,88	-28,56	+3,22
O_2: 25 ppm	**Absorption enthalpy (KJ/mol)**	25,53	24,23	26,18	+2,55
	Desorption enthalpy (KJ/mol)	-27,95	-28,58	-29,48	+5,47

There is an overall increase in enthalpy whatever the proportion of O_2. This has an impact on both absorption and desorption. And should therefore increase on the energy needed during the loading and compression of hydrogen.

5.3.6 Influence of H_2O

For the H_2O test, we can observe on the graph above a decrease Cabs until cycle 27-28 and then a stabilisation until cycle 50. It is faster than with O_2.

It can be seen that there is a degradation between the first cycle and the last 50 cycles. The increase in the proportion of H_2O has more effect on this parameter of capacity. At the end, we keep for the only 68% with 5 ppm H_2O and even 64% of the reverse capacity with 25 ppm H_2O. CO2

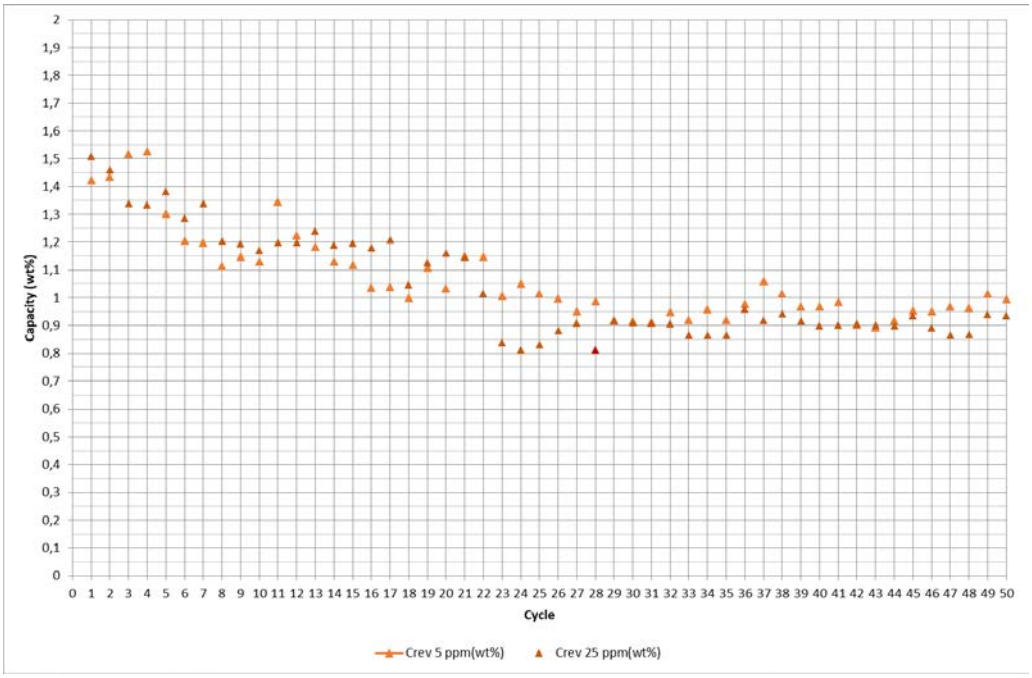

Figure 61 - Reverse capacity under H2 + H2O on 50 cycles – Proportion of H2O: 5 ppm, 25 ppm

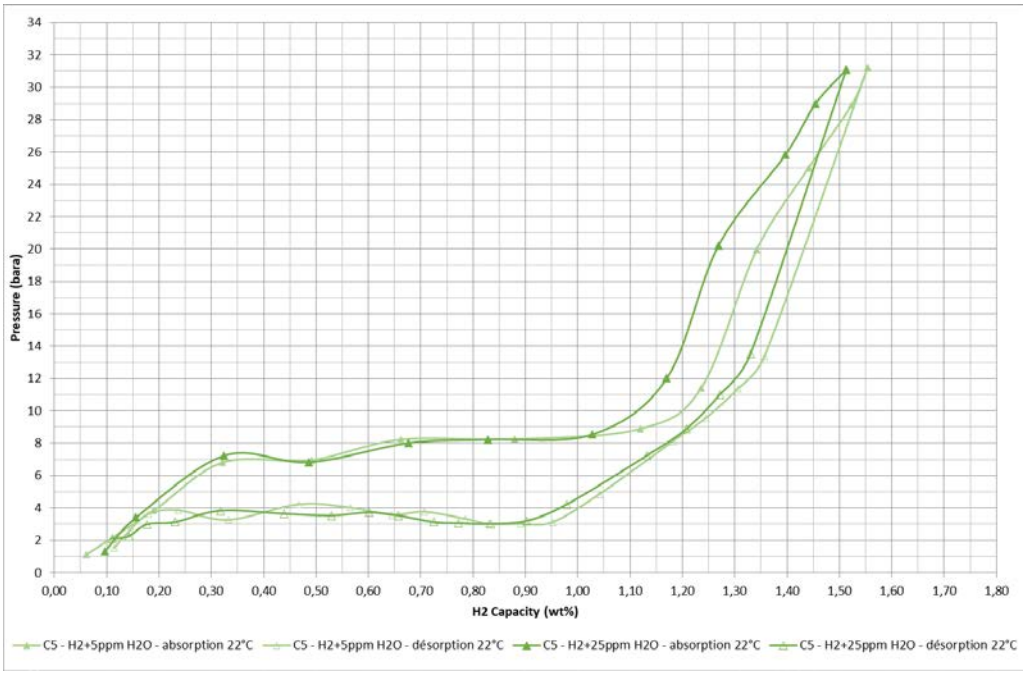

Figure 62 - PCT under H2 + H2O at 22°C after cycles 5

From these PCT curves above we can observe, after 5 cycles, no significant change on the absorption and desorption plateau between each PCT under different proportion of H2O. However, there are already a difference about the capacity. We have a maximal capacity at 30 bara of 1,55wt% for 5 ppm of H2O, and 1,51wt% for 25 ppm of H2O.

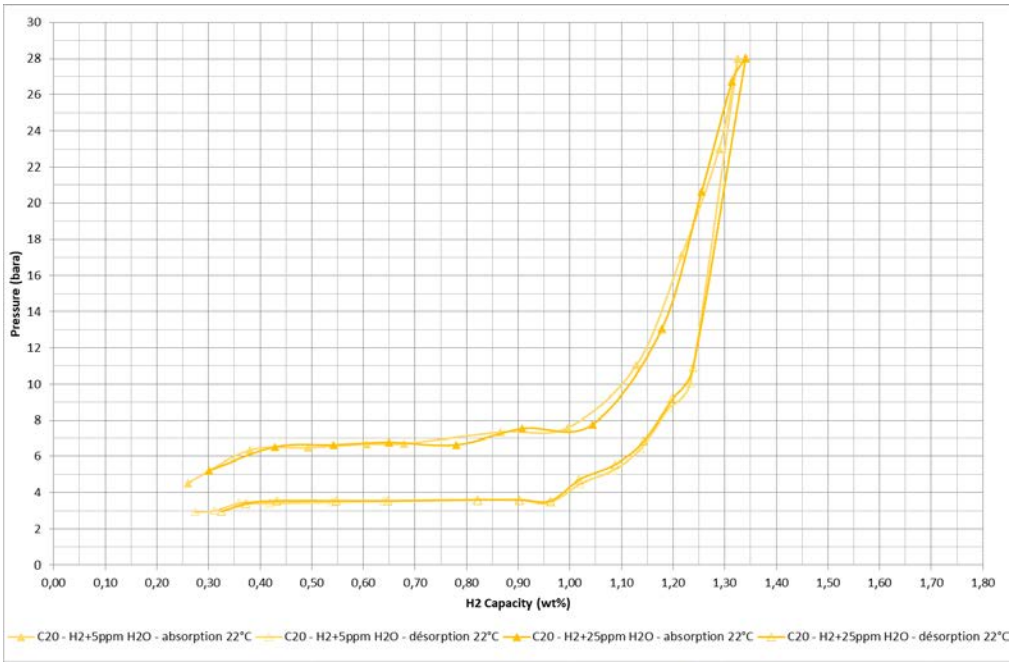

Figure 63 - PCT under H2 + H2O at 22°C after cycles 20

From these PCT curves above we can observe, after 20 cycles, always no significant change on the absorption and desorption plateau between each PCT under different proportion of H2O. We have a maximal capacity at 30 bara of 1,34wt% for 5 ppm of H2O, and 1,33wt% for 25 ppm of H2O.

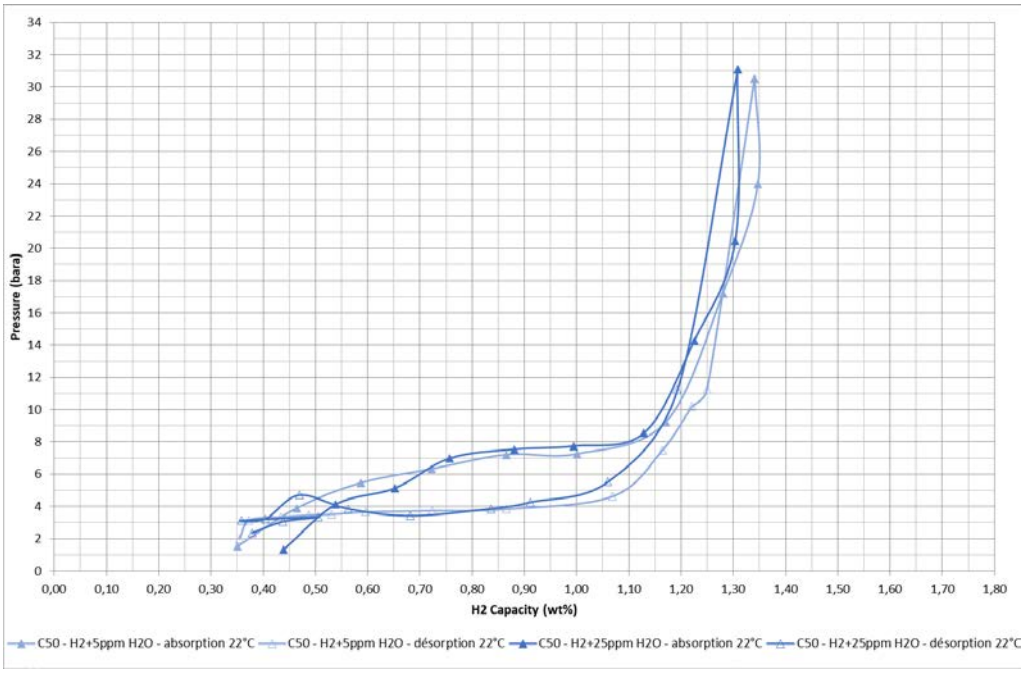

Figure 64 - PCT under H2 + H2O at 22°C after cycles 50

From these PCT curves above we can observe, after 50 cycles, always no significant change on the absorption and desorption plateau between each PCT under different proportion of H2O. We have a maximal capacity at 30 bara of 1,34wt% for 5 ppm of H2O, and 1,31wt% for 25 ppm of H2O.

Table 18 - Evolution of absorption and desorption enthalpy under H2 + H2O

		Cycle 5	Cycle 20	Cycle 50	Evolution rate (%)
H_2O : 5 ppm	**Absorption enthalpy (KJ/mol)**	-24,86	-24,31	-25,43	+2,29
	Desorption enthalpy (KJ/mol)	-27,64	-28,06	-28,22	+2,10
H_2O : 25 ppm	**Absorption enthalpy (KJ/mol)**	24,60	25,21	25,45	+3,82
	Desorption enthalpy (KJ/mol)	-27,24	-26,52	-30,29	+11,20

As with O_2, there is an overall increase in enthalpy whatever the proportion of H_2O. This has an impact on both absorption and desorption. And should therefore increase on the energy needed during the loading and compression of hydrogen.

5.4 Analyse of results

From the results of previous section, we made a statistic analysis in order to reduce the impact of experimental dispersion. We made fitting regression exponential equations, except in two cases where linear fitting was more accurate.

The following figure shows an example of fittings for CO pollutant (see in the Annex section the fitting results for the other pollutants)

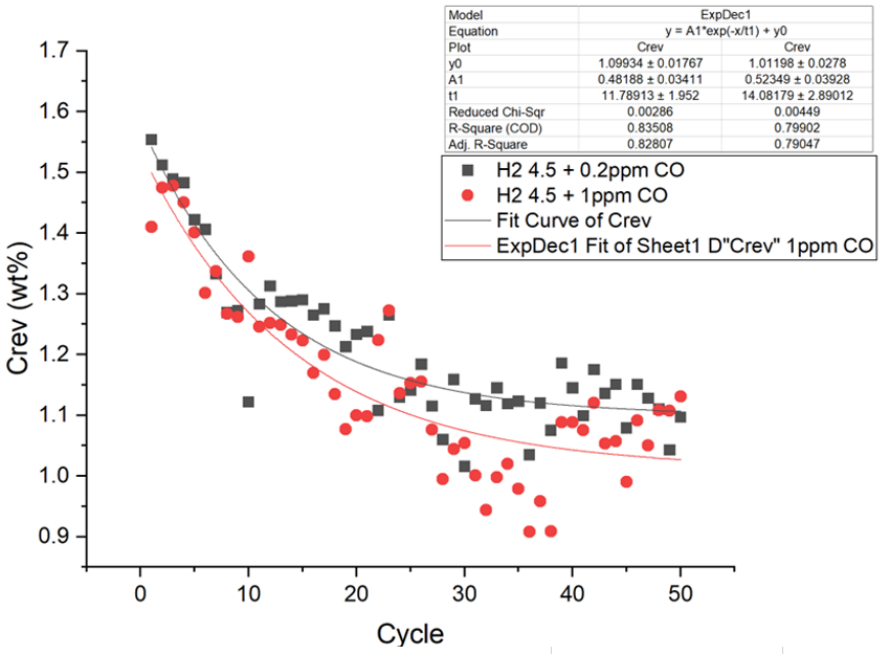

Figure 65 - Exponential fitting for CO capacity evolution

We also made a fitting of the base case with no additional pollutant, meaning the evolution of hydrogen storage capacity using 4.5 hydrogen gas (meaning with about 5ppm indetermined inpurities). The next figure shows this result and its fitting:

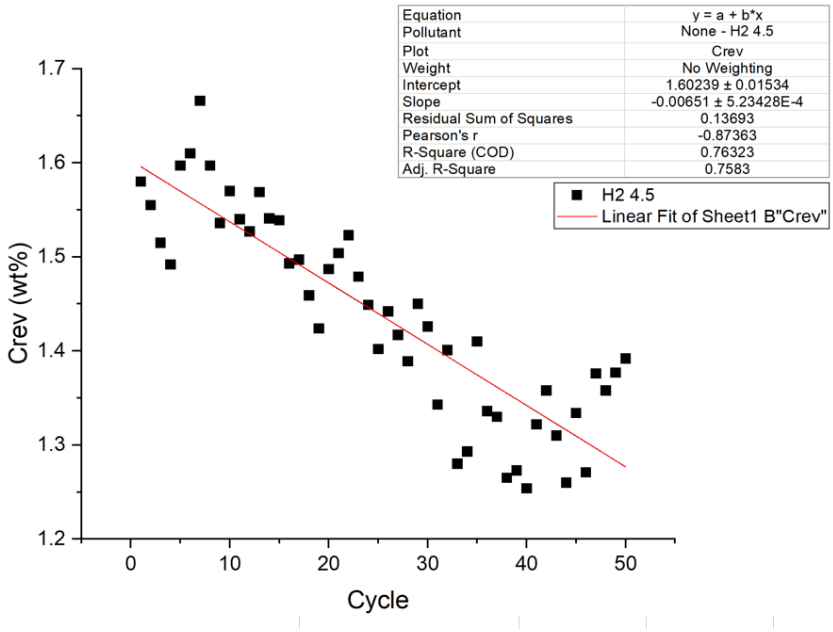

Figure 66 - Capacity evolution of hydride under H2 4.5

With these elements we made a chart with allow us to estimate the expected capacity at cycles 1 and 50 according to the fittings. Then we can quantify the loss of capacity after 50 cycles (named “Capacity reduction”), and also the effect of the pollutant after 50 cycles, by subtracting the loss of capacity of the base case (named “Pollutant reduction”). Note that the fitting parameters correspond to the equation inserted in the previous figures for the linear and exponential fitting.

Table 19 – Summary of pollutants influence on capacity after 50 cycles

Gas (ppm)		Fitting parameter					Cycle capacity (wt%)		Capacity reduction	Pollutant reduction
		a	b	A1	t1	y0	1	50		
H2 4.5		1,60239	-0,00651				1,60	1,28	25%	NA
N2	100			0,451	27,08337	1,17056	1,61	1,24	29%	4%
	500			0,62545	30,805	1,1743	1,78	1,30	37%	12%
	1000			0,68672	34,01988	0,9227	1,59	1,08	47%	22%
CO	0.2			0,48188	11,78913	1,09934	1,54	1,11	39%	14%
	1			0,52349	14,08179	1,01198	1,50	1,03	46%	21%
CO2	2			0,49801	15,59615	1,0666	1,53	1,09	41%	16%
	10			0,78687	24,77729	0,77844	1,53	0,88	74%	49%
O2	5			0,40829	13,62137	1,02133	1,40	1,03	36%	11%
	25	1,34211	-0,00984				1,33	0,85	57%	32%
H2O	5			0,60254	11,48312	0,94076	1,49	0,95	57%	32%
	25			0,70058	15,80521	0,83778	1,50	0,87	72%	47%

We plot the last column in the following figure in order to stress the sensibility of different pollutants after 50 cycles at the maximal concentration allowed by ISO 14678 (blue columns) and the effect of increasing five times this concentration (orange columns). This analysis suggests that an excess of CO2, O2 and H2O pollutants will have a stronger effect than an excess of N2 or CO.

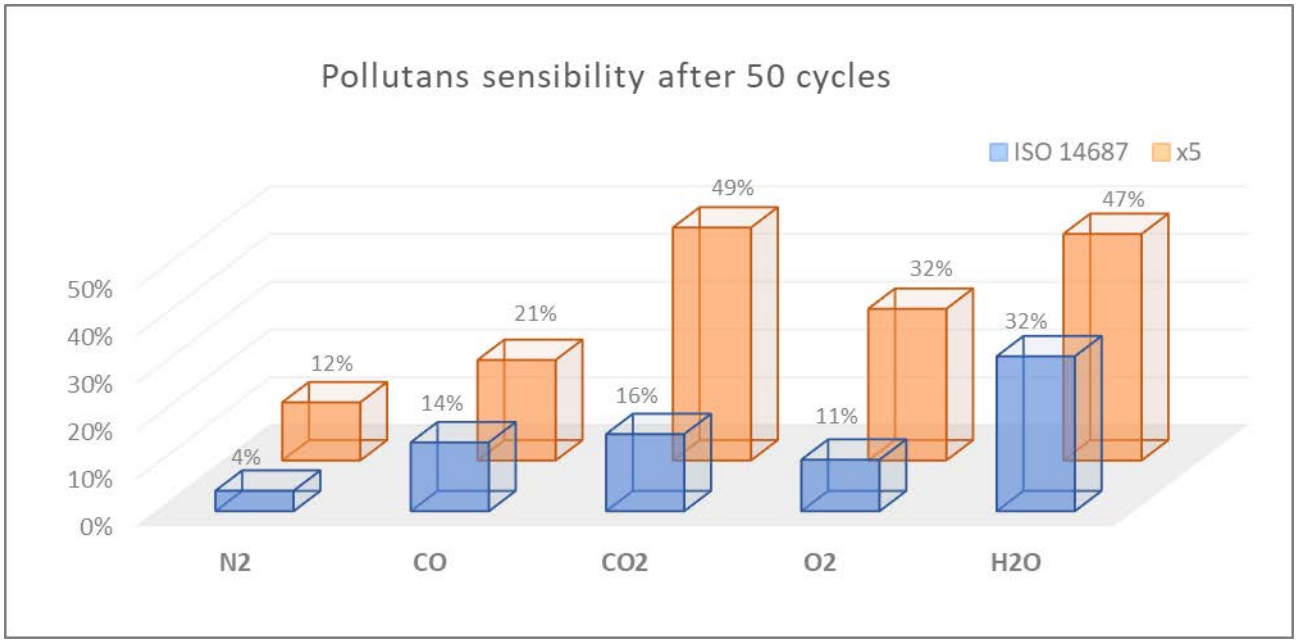

Figure 67 - Graphical impact of pollutants for 1X and x5 the concentration of ISO 14867

6 Reference materials for ab/adsorption uptake and thermal properties

6.1 Harmonise methods using adsorbents

The first step of this task was to set the necessity of a reference material for the community. A survey was distributed among expert participants in the measurement of the hydrogen uptake of porous materials by physical adsorption at cryogenic temperature (cryoadsorption). The questions focussed on the used materials, the measurement of hydrogen uptake and heat conductivity, and the necessity of reference materials among the specific scientific community:

Materials

- Which materials are you mainly using?
- Do you characterize your adsorbent materials before/after hydrogen adsorption analyses by your own?

Hydrogen uptake

- Which method are you using, volumetric (Sieverts) or gravimetric?
- At which temperatures and pressures do you measure?
- What is the used hydrogen gas purity?
- What is the normally used activation procedure?
- Testing cyclability/repeat measurement?
- Do you use “known” hydrogen storage materials as reference/calibration?

Thermal properties

- Do you calculate/measure the heat of adsorption?
- Do you measure thermal conductivity or capacity of your adsorbents?
- Conditions for measuring the thermal conductivity/capacity?

Reference material

- Would a reference material with known properties and hydrogen uptake be useful?
- Amount of used material (g/year)
- Best form for handling?
- Do you have any suggestion for a good reference material?

Eighteen expert participants replied the survey (*Figure **68***). Among them, carbon materials and metal-organic frameworks are the most used, remarking the importance of the control of the crystalline and porous properties of the materials as the most relevant for a reference material.

*Figure **69*** shows that participants measure the hydrogen uptake mainly by volumetric (Sieverts) and gravimetric methods. Volumetric methods are more used due to simplicity. Experiments are usually performed at the temperature of boiling gases (nitrogen at 77 K or argon at 87 K), but a 60 % of participants reported using a temperature controller. All the participants use high pure hydrogen for analysis, and activate the materials mostly by heating at dynamic vacuum. Repeating the measurements is a common practice among participants. About thermal properties, 60 % of participants reported measuring the isosteric heat of adsorption (*Figure **70***) by running isotherms at different temperatures and applying the Clausius-Clapeyron equation and only 11 % the thermal conductivity.

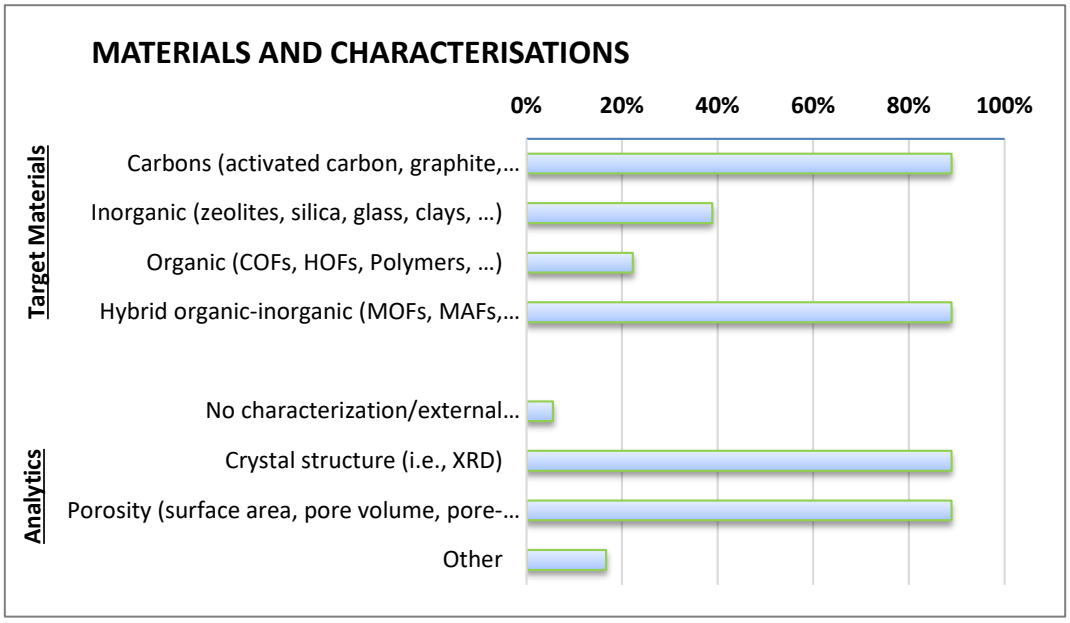

Figure 68 – Results of the survey about the used materials and relevant properties.

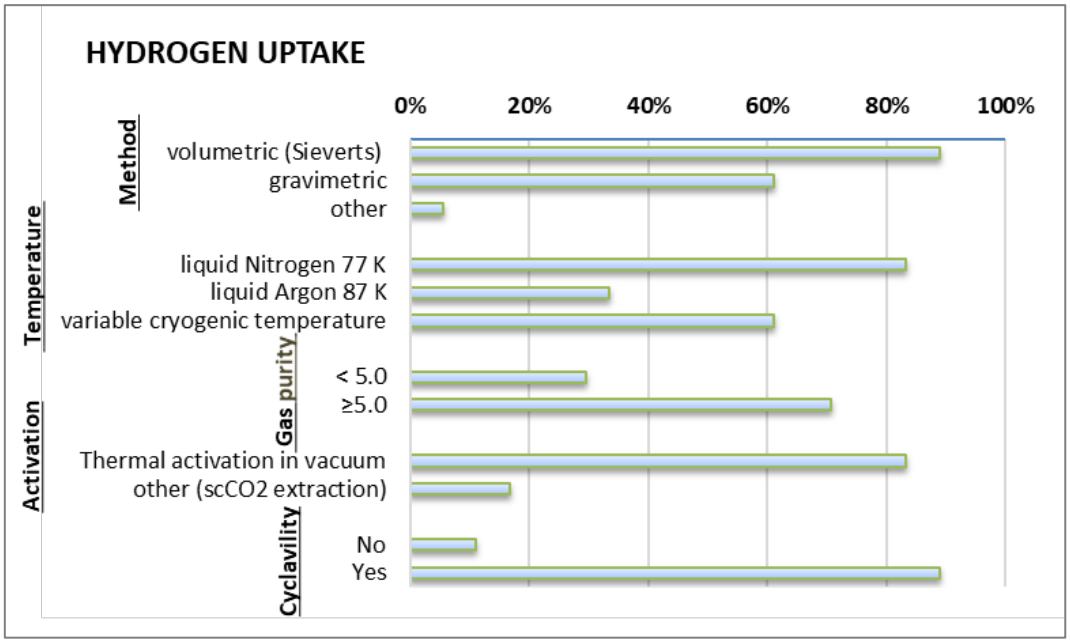

Figure 69 – Results of the survey about the used methods to measure the hydrogen uptake.

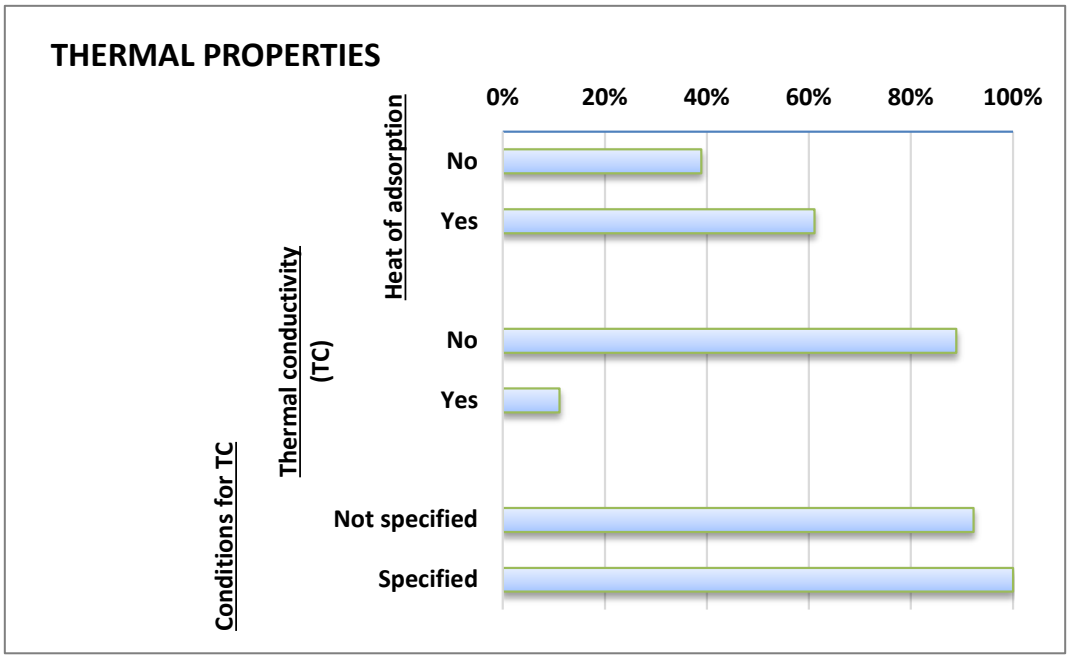

Figure 70 – Results of the survey about the used methods to measure the thermal properties.

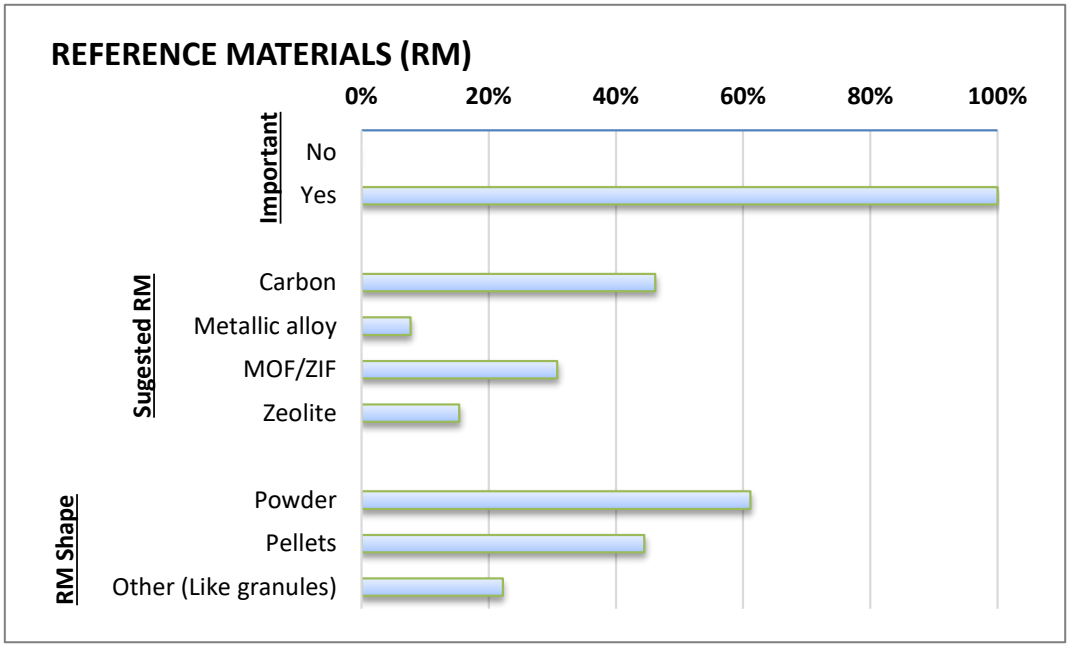

Figure 71 – Results of the survey about the necessity of reference materials for hydrogen cryoadsorption.

6.2 Necessity of a reference material for cryoadsorption of hydrogen

Solid-state hydrogen storage is an alternative under development to reach technical storage densities involving lower storage pressures, by means of chemical bonds in metal-hydrides or by physical adsorption (physisorption) on the surface of porous materials.[1] Among solid-state methods, physisorption shows faster kinetics for charging and discharging and complete reversibility.[2] Using adsorbents for hydrogen storage requires cryogenic temperatures (cryoadsorption), typically around the boiling point of liquid nitrogen, i.e., 77 K, to achieve practical gravimetric and volumetric capacities comparable to high-pressure or liquid hydrogen tanks.[3–7] For the development of cryoadsorption hydrogen storage systems on a technological level, reliable

data are required for the H_2 uptake at low temperature for each material. However, even for established adsorbents, as activated carbons, the reported H_2 uptake shows sometimes large discrepancies between different laboratories.[8–10] An interlaboratory analysis of amorphous porous carbon materials conducted in 2009 found significant deviations and finally recommended regularly and carefully calibrate the devices, including sensors, volumes, and effects of thermal gradients; reduce gas leaks, control the experiment conditions carefully, repeat the isotherms, and post-analyse the data, if necessary.[11] Following these recommendations, the variability of the results was reduced in a subsequent interlaboratory study.[12] Even for a specific adsorbent, the hydrogen uptake can vary depending on the synthesis method, handling and activation conditions, which may affect their structural and/or porous properties.[8,9] To the best of our knowledge, no material has been defined as a standard or reference to assure the reliability of hydrogen adsorption measurements. Therefore, one of the goals of the project MefHySto was to suggest a reference material for physisorption at cryogenic temperature.

In general, the hydrogen uptake at 77K is proportional to the surface area, ca. 1 wt. % at 20 bar each 500m^2/g of BET area (Chahine´s Rule).[13] However, the composition of the material, the pores structure and size, and the pore volume determine not the uptake, but the relationship between the uptake and the pressure, i.e. heat of adsorption, specially at lower pressure than the saturation of the surface.[14] For these reasons, the textural properties, pore size and distribution, phase purity and activation degree must be perfectly characterized in a reference material used for cryoadsorption. To ensure the control of these properties, crystalline structures are more suitable as reference materials than amorphous solids because of the easy assessment of the sample quality by using powder X-ray diffraction (PXRD) to identify the crystalline phase (related to pores size, distribution, and geometry) combined with the calculation of the BET area and pore volume (related to phase purity and activation degree). For this reasons, metal-organic framework materials (MOFs) are more suitable than zeolites as reference materials for hydrogen cryoadsorption because they are also crystalline with well-defined pore-size distribution but also showing generally larger surface areas.

6.3 Candidate to reference material

We selected the material ZIF-8 (Zeolitic Imidazolate Framework-8), made from tetrahedrally coordinated zinc by 2-methylimidazole (meIm), because it possesses strong Zn-C-N coordination bonds providing high thermal and mechanical stability and reducing degradation during handling and activation.[15] This high mechanical strength allows easily pelletizing the powders,[16] reducing the analysis volume, facilitating handling and weighting, and avoiding loss of material during measurements. Furthermore, the high hydrophobicity of ZIF-8 compared to zeolites reduces the adsorption of humidity during the weighting procedure and facilitates the sample preparation and transfer without using inert or dry atmosphere.

Pellets of ZIF-8 were synthesized and pelletized by MOF-Technologies (currently Nuada). The studied material was synthesized in five batch of 10 g each as powders and a large batch of 50 g of pellets. Previously to shipping, the materials were evacuated and kept in vacuum in an airtight plastic bag. The material was characterized by PXRD and N_2 adsorption-desorption experiments at 77 K prior to the interlaboratory experiment and the results are published.[23] X-ray diffraction experiments in powder (PXRD) confirms that the powders and pellets are composed completely of ZIF-8 crystalline phase (*Figure **72***-left). The diffractograms are composed of sharp peaks at 2 theta diffraction angles ca. 7°, 11°, 13°, 15°, 17°, and 18°. In all cases, the peaks correspond to the simulated pattern from the theoretical crystalline phase (ZIF-8_calc.). Additional signals at 13.5°, 17.2°, and 19.1° were also observed for all materials investigated, which can be related to additives used in the synthesis. The pellets maintain the ZIF-8 phase with high crystallinity and a lower relative intensity of corresponding reflections to the additive, potentially ascribed to the post-processing step. N_2 adsorption-desorption experiments at 77 K on powder and pelletized ZIF-8 (*Figure **72***-right) show

type I(a) adsorption isotherms according to the IUPAC classification corresponding to ultramicroporous materials.[16] The isotherms show hysteresis during desorption, which was attributed to framework flexibility due to a gate-opening effect involving the linker molecules. The pellets show higher uptake at P/P_0 values ca. 0.01 compared to powder, indicating a slightly higher BET area (see *Table **20***).

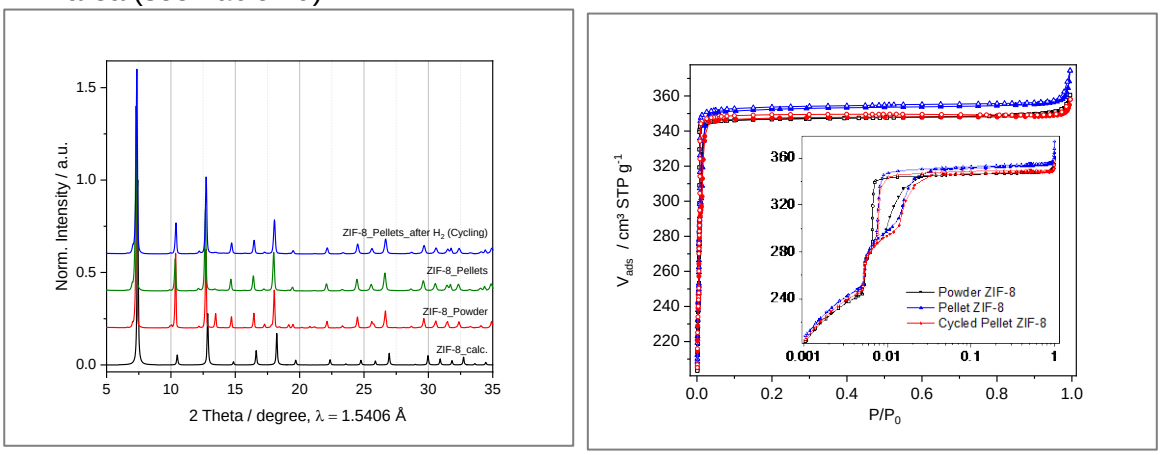

Figure 72 – Left: PXRD of the powder and pelletized ZIF-8 samples before and after the adsorption/desorption experiments of H_2. Right: N_2-adsorption/desorption isotherms at 77 K of powder and pelletized ZIF-8 samples.

Table 20 – Textural properties of the ZIF-8 material as powder, pellets and after cycling experiments.

Sample	**A_{BET} / m² g^{-1}**	**Vp* / cm³ g^{-1}**	**C**
ZIF-8 Powder	1115	0.54	3634
ZIF-8 Pellets	1142	0.55	3550
Cycled ZIF-8 Pellets	1128	0.54	3553

*Total pore volume at $P/P_0 = 0.9$

*Figure **73***-left shows the adsorption isotherms of H_2 at 77 K of the ZIF-8 material as powders and as pellets, collected by three different analysers in BAM and MPG. In general, the higher the pressure, the higher the excess uptake, reaching a maximum uptake called saturation at a pressure value of about 35 bar. From this maximum, a further increase in pressure results in a negative increment of the excess uptake because the density of the gas phase increases with pressure but the adsorbed phase, at supercritical temperature, behaves as an incompressible fluid.[18] The analysed materials adsorb 2.64 – 2.82 wt.% at 25 bar in line with Chahine's Rule. The relative standard deviation (RSD = SD/$\bar{X}$) evaluates the overall deviation of the measurements with respect to the average value, is 2 % at 25 bar among measurements of powder and pellets among the three different devices. These results indicate a good reproducibility of the measurements between the different analysers, and also, a good homogeneity of the adsorption uptake of the different fractions of analysed samples. In addition, the stability of the material to hydrogen adsorption-desorption was tested by cycling test from 10 to 86 bar covering 47 experiments on the packed material. The storage performance near 100 % respect to the stored amount of the first cycle demonstrates that material´s uptake does not change along with the cycling experiment. This due to the high stability of the material to the adsorption-desorption operation, according to the stability of the crystalline phase (*Figure **72***-left) the maintenance of the N_2 adsorption uptake (*Figure **72***-left) and porous properties (*Table **20***) after cycling experiments (Cycled ZIF-8 Pellets). Due to this stability to operation, this material demonstrates potential either as storage media for hydrogen or as a reference material for cryoadsorption.

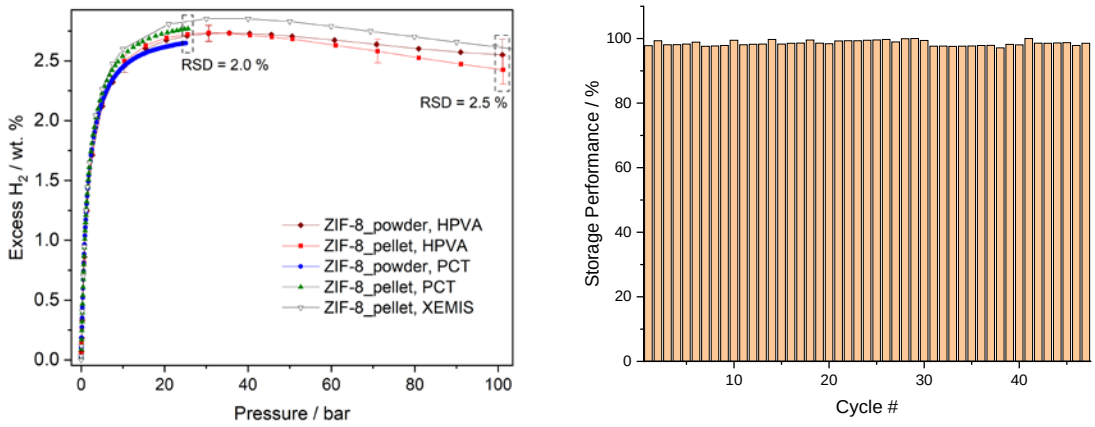

Figure 73 – Left: H_2 adsorption uptake of powders and pellets of ZIF-8 measured with three different devices from BAM (HPVA) and MPG (PCT& XEMIS). Right: H_2 storage performance (% of the gas uptake of the first cycle) during adsorption-desorption cycling of pellets of material ZIF-8 at 77 K.

6.4 Interlaboratory analysis procedure

We distributed pellets of ZIF-8 materials among nine expert laboratories in hydrogen cryoadsorption measurements worldwide. These laboratories used in total 15 different experimental setups to measure the H_2 uptake of different fractions of ZIF-8 as pellets. Each participating laboratory received a closed glass vial containing ca. 2 g of pellets in air. The isotherms were measured up to 100 bar in those devices allowing to operate up to such a high-pressure value by following the provided instructions (*Table **21***). A data sheet was provided for reporting details on the experimental setup and the analysis conditions for each participant (see Annex 8.4.1). The experimental setups were numbered and the information is provided maintaining the anonymity of the participants. A description of each experimental setup is provided in Annex 8.4.1.

Table 21 – Used conditions during the analyses of cryoadsorption on the pelletized ZIF-8 material.

Variable	Value	Unit
Mass of material	1 (volumetric); 0.1 (gravimetric)	g
Outgas time	6 (minimum)	h
Outgas temperature	120	°C
Outgas base pressure	10^{-5} – 10^{-7}	mbar
Min. hydrogen purity	99.999	vol.%
Min. Helium purity	99.9999	vol.%
Analysis temperature	77 (liquid nitrogen)	K
Temperature control	Recommended Liquid Nitrogen	n. a.
Pressure steps (required)	1, 2, 4, 6, 8, 10, 12, 14, 16, 18, 20, 25, 30, 35, 40, 45, 50, 60, 70, 80, 90, 100	bar
Adsorption Equilibration time	10	min/step
Free-space (sample volume) measurements	10 repetitions (10 steps up to max. pressure in gravimetric)	times

6.5 Results of the interlaboratory analysis

*Figure **73***-left shows the H_2 adsorption at 77 K for the 15 setups used by the nine participants. For each setup, the average of the measurements with different masses is taken (see the individual isotherms reported for each setup and analysed mass Annex 8.4.2). Data have been interpolated

for specific pressure points (see *Table* ***21***). The majority of the results are close to each other with only 3 setups showing systematically either higher or lower uptake than most of data. *Figure* ***73***-right shows a boxplot representing the measurements deviation for each interpolated pressure. For better readability, the considered pressure points are evenly spread along with the x-axis. The size of the boxes represents the dispersion of data within percentiles Q1 and Q3 (known as IQR, containing 50 % of data). Boxes are smaller for pressures under 25 bar. For higher pressures, the boxes cover a wider excess region, as well as the range 1.5*IQR that contains data from minimum to maximum uptakes within the calculated distribution. Adsorption uptakes measured out of this region (1.5*IQR) are considered outliers, and they correspond to data from setups 5, 8, and 9.

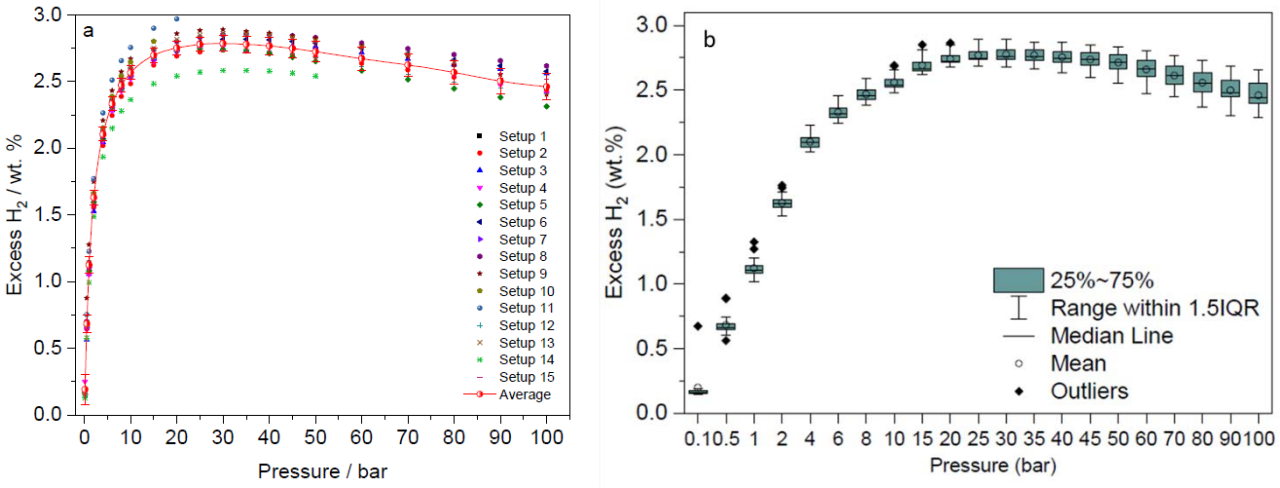

Figure 74 – Left: Comparison of the average H_2 adsorption isotherms at 77 K from each experimental setup up to 100 bar. Right: Deviation box-plot of measurements for interpolated pressure values, removing the outliers.

An RSD of 3 – 4 % among the data from participants (***Figure 75***) demonstrates the high reproducibility of the adsorption results for pressures from 10 to 100 bar. The RSD of the results in the present study are compared to other data from a recent international laboratory H_2 cryoadsorption comparison study on two different porous carbon materials, NORIT R0.8 mm (sample 1, red) and MSP-20 (sample 2, blue).[12] The RSD of the ZIF-8 pellets is lower than that for sample 1 of the previous study, especially between 10 and 60 bar, and only slightly higher (ca. 1 %) than that for sample 2. Overall, our ZIF-8 pellets yield highly reproducible H_2 adsorption isotherms and RSD values comparable to the previous state-of-the-art interlaboratory tests. Compared to sample 2 (MSP-20), which is a powdery, fluffy, amorphous carbon with 2,400 m^2/g BET area,[28] our pellets can be handled easily and the quality of crystalline material can be checked by PXRD.

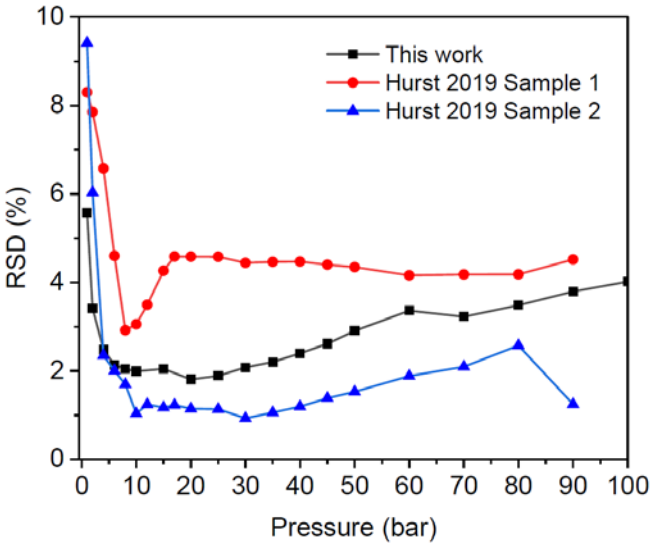

Figure 75 – Relative standard deviation of the measurements performed in this work compared to those in Ref [16] as a function of pressure.

This high reproducibility of the adsorption results also demonstrates the high homogeneity of the synthesized material and its structural/porous properties as well as its structural stability to storage, transport and handling. It is worth mentioning that reported wet- and dry-masses of the analysed materials were similar, corroborating that the hydrophobic material, once successfully activated, adsorbs negligible amounts of moisture from the atmosphere improving the reproducibility of the weighting procedure.

6.6 Conclusion

As summary, we selected the crystalline metal-organic framework material ZIF-8 due to its structural properties and composition of the material, which provides a significant hydrogen uptake, density, and mechanical stability. This mechanical stability allows a high degree of packing and excellent cyclability, which results in repeatable adsorption and desorption amounts of hydrogen during its lifetime. Besides, its hydrophobicity helps to reduce water adsorption during preparation and weighting, also increasing the accuracy of measurements and facilitating an easy, reliable activation. Overall, the high reproducibility of H_2 uptake measured by 15 different experimental setups indicates clearly the high stability and easiness of both the handling and activation process of the ZIF-8 pellets. Furthermore, it demonstrates the high homogeneity of the batch of ZIF-8 pellets prepared by reactive extrusion. Therefore, we suggest the ZIF-8 material used in this study as a reference material for hydrogen cryoadsorption measurements which will help to further develop this hydrogen storage technology.

6.7 References

1. Nazir, A. Rehrnan, S. Hussain, S. Aftab, K. Heo, M. Ikrarn, S.A. Patil, M. Aizaz Du Din, Advanced Sustainable Systems 2022, 6, 2200276.
2. M. Hirscher, V.A. Yartys, M. Baricco, J.B. von Colbe, D. Blanchard, R.C. Bowrnan, D.P. Broorn, C.E. Buckley, F. Chang, P. Chen, Y.W. Cho, J.C. Crivello, F. Cuevas, W.I.F. David, P.E. de Jongh, R.V. Denys, M. Dornheirn, M. Felderhoff, Y. Filinchuk, G.E. Froudakis, D.M. Grant, E.M. Gray, B.C. Hauback, T. He, T.D. Hurnphries, T.R. Jensen, S. Kirn, Y. Kojirna, M. Latroche, H.W. Li, M.V. Lototskyy, J.W. Makepeace, K.T. Moller, L. Naheed, P. Ngene, D. Noreus, M.M. Nygard, S.I. Orirno, M. Paskevicius, L. Pasquini, D.B. Ravnsbaek, M.V. Sofianos, T.J. Udovic, T. Vegge, G.S. Walker, C.J. Webb, C. Weidenthaler, C. Zlotea, J. Alloys Compd. 2020, 827, 153548.
3. Z.J. Chen, K.O. Kirlikovali, K.B. Idrees, M.C. Wasson, O.K. Farha, Chem 2022, 8, 693.

4. O.K. Farha, A.O. Yazaydin, I. Eryazici, C.D. Malliakas, B.G. Hauser, M.G. Kanatzidis, S.T. Nguyen, R.Q. Snurr, J.T. Hupp, Nat. Chem. 2010, 2, 944.
5. R. Balderas-Xicohtencatl, M. Schlichtenrnayer, M. Hirscher, Energy Technol. 2018, 6, 578.
6. L. Zhang, M.D. Allendorf, R. Balderas-Xicohtencatl, D.P. Broorn, G.S. Fanourgakis, G.E. Froudakis, T. Genett, K. Hurst, S. Ling, C. Milanese, Progress in Energy 2022.
7. M. Hirscher, Angew. Chem. Int. Ed. 2011, 50, 581.
8. D.P. Broorn, M. Hirscher, Energy Environ. Sci. 2016, 9, 3368.
9. D.P. Broorn, M. Hirscher, ChemPhysChem 2021, 22, 2141.
10. D.P. Broorn, C.J. Webb, G.S. Fanourgakis, G.E. Froudakis, P.N. Trikalitis, M. Hirscher, Int. J. Hydrogen Energy 2019, 44, 7768.
11. C. Zlotea, P. Moretto, T. Steriotis, Int. J. Hydrogen Energy 2009, 34, 3044.
12. K.E. Hurst, T. Gennett, J. Adarns, M.D. Allendorf, R. Balderas-Xicohtencatl, M. Bielewski, B. Edwards, L. Espinal, B. Fultz, M. Hirscher, M.S.L. Hudson, Z. Hulvey, M. Latroche, D.J. Liu, M. Kapelewski, E. Napolitano, Z.T. Perry, J. Purewal, V. Stavila, M. Veenstra, J.L. White, Y. Yuan, H.C. Zhou, C. Zlotea, P. Parilla, ChemPhysChem 2019, 20, 1997.
13. M. Schlichtenrnayer, M. Hirscher, J. Mater. Chem. 2012, 22, 10134.
14. M. Hirscher, B. Panella, B. Schrnitz, Microporous Mesoporous Mater. 2010, 129, 335.
15. K.S. Park, Z. Ni, A.P. Cote, J.Y. Choi, R. Huang, F.J. Uribe-Rorno, H.K. Chae, M. O'Keeffe, O.M. Yaghi, Proc. Natl. Acad. Sci. USA 2006, 103, 10186.
16. R. Balderas-Xicohtencatl, J.A. Villajos, J. Casaban, D. Wong, M. Maiwald, M. Hirscher, ACS Appl. Energ. Mater. 2023, 6, 9145.
17. M. Thommes, K. Kaneko, A.V. Neimark, J.P. Olivier, F. Rodriguez-Reinoso, J. Rouquerol, K.S.W. Sing, Pure Appl Chem 2015, 87 (9-10), 1051-1069.
18. E. Poirier, A. Dailly, Langmuir 2009, 25 (20), 12169-12176.
19. G. Sdanghi, S. Schaefer, G. Maranzana, A. Celzard, V. Fierro, Int. J. Hydrogen Energy 2020, 45, 25912.

7 Annex

7.1 Global results with Nitrogen

7.1.1 Capacities evolution on 50 cycles

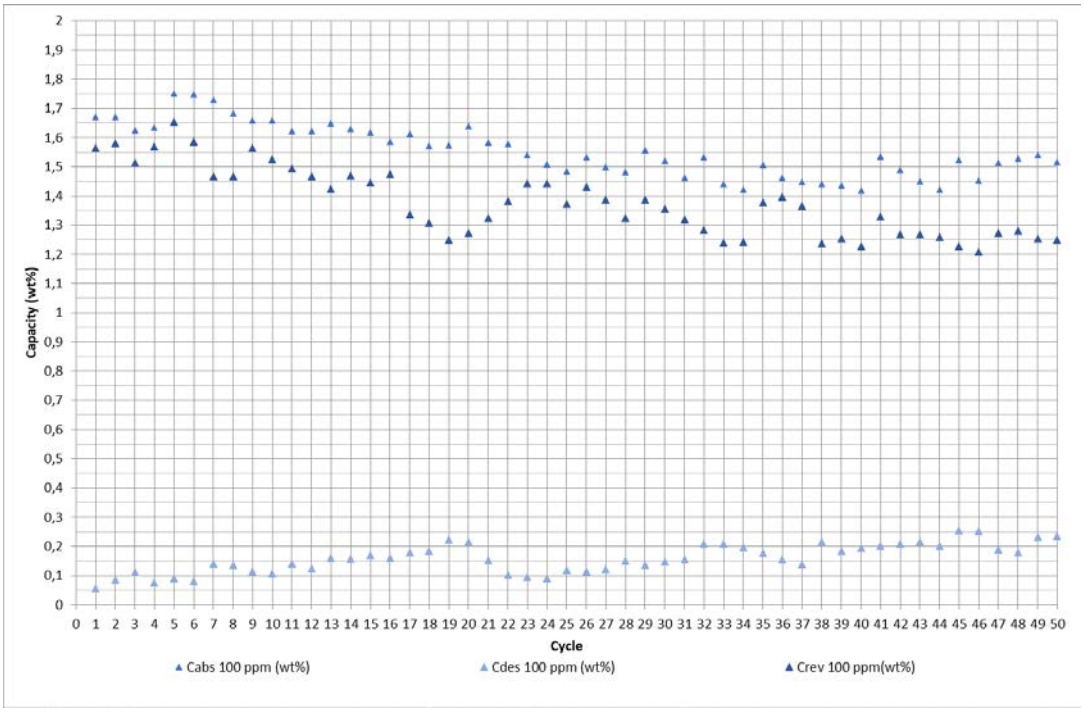

Figure 76 : Capacity under H2 + N2 on 50 cycles – Proportion of N2: 100 ppm

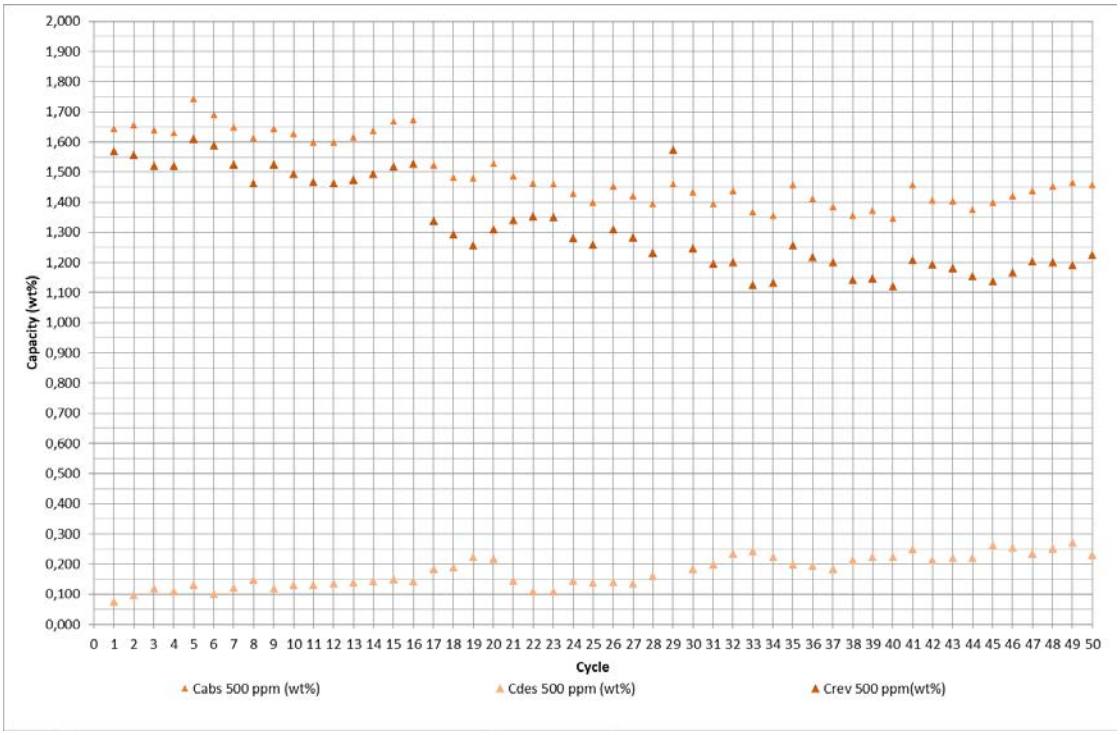

Figure 77 : Capacity under H2 + N2 on 50 cycles – Proportion of N2: 500 ppm

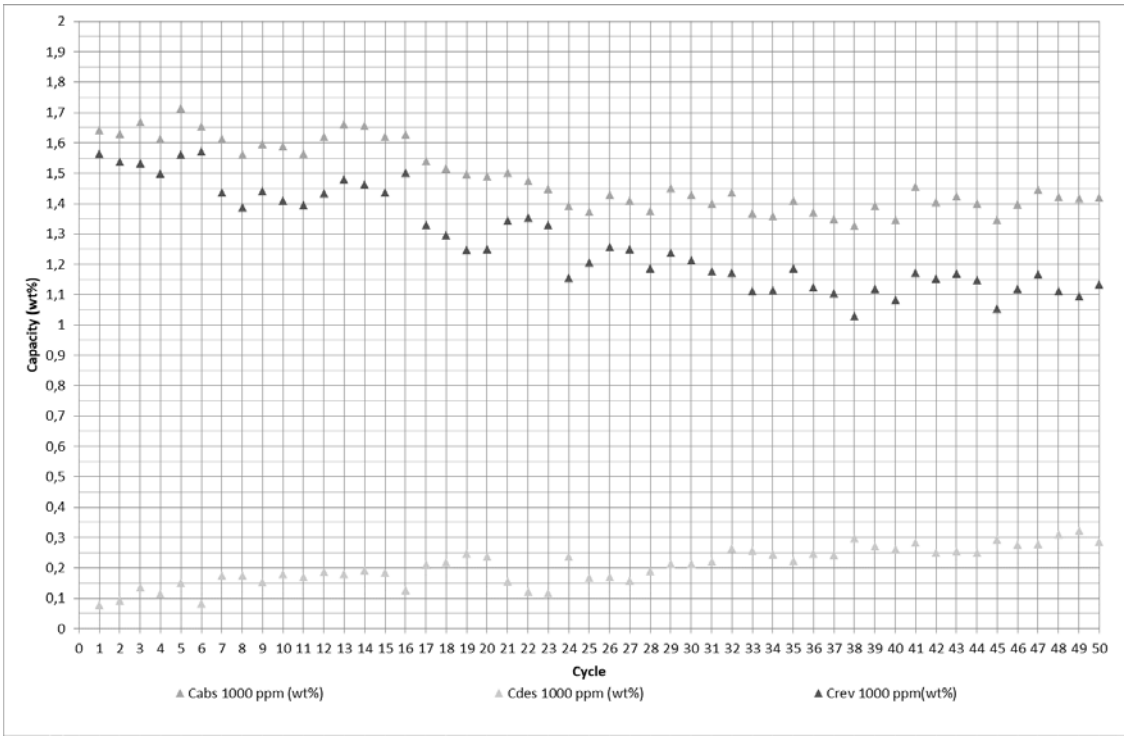

Figure 78 : Capacity under H2 + N2 on 50 cycles – Proportion of N2: 1000 ppm

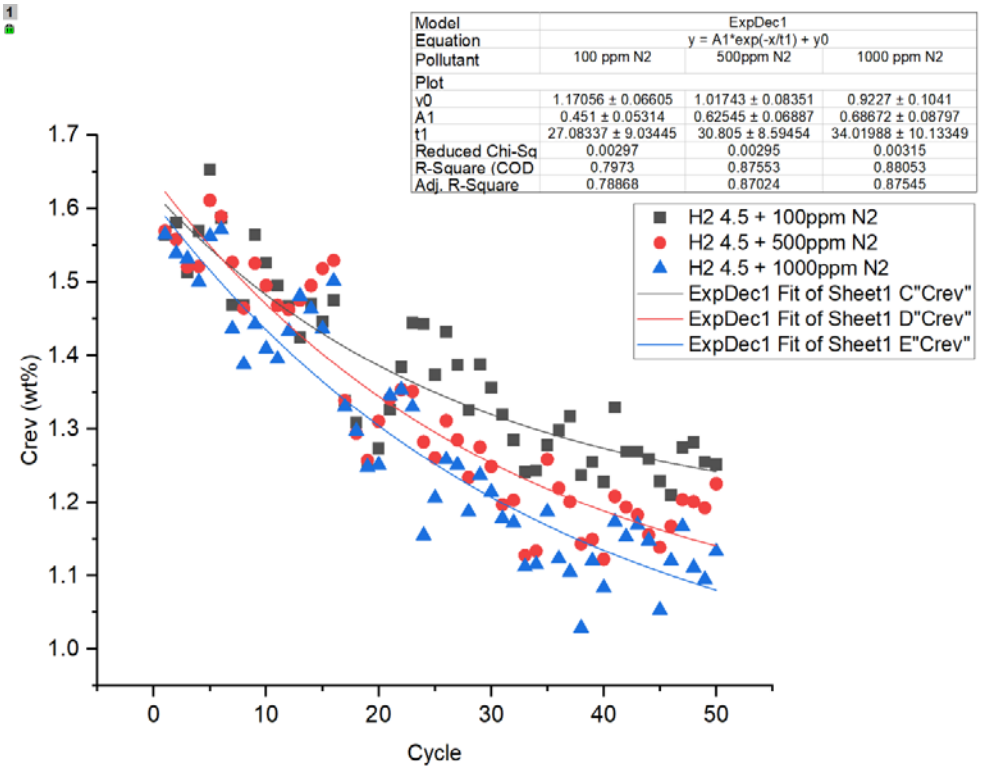

Figure 79 - Fitting of N2 results

7.1.2 PCT curves at different cycle and different temperature

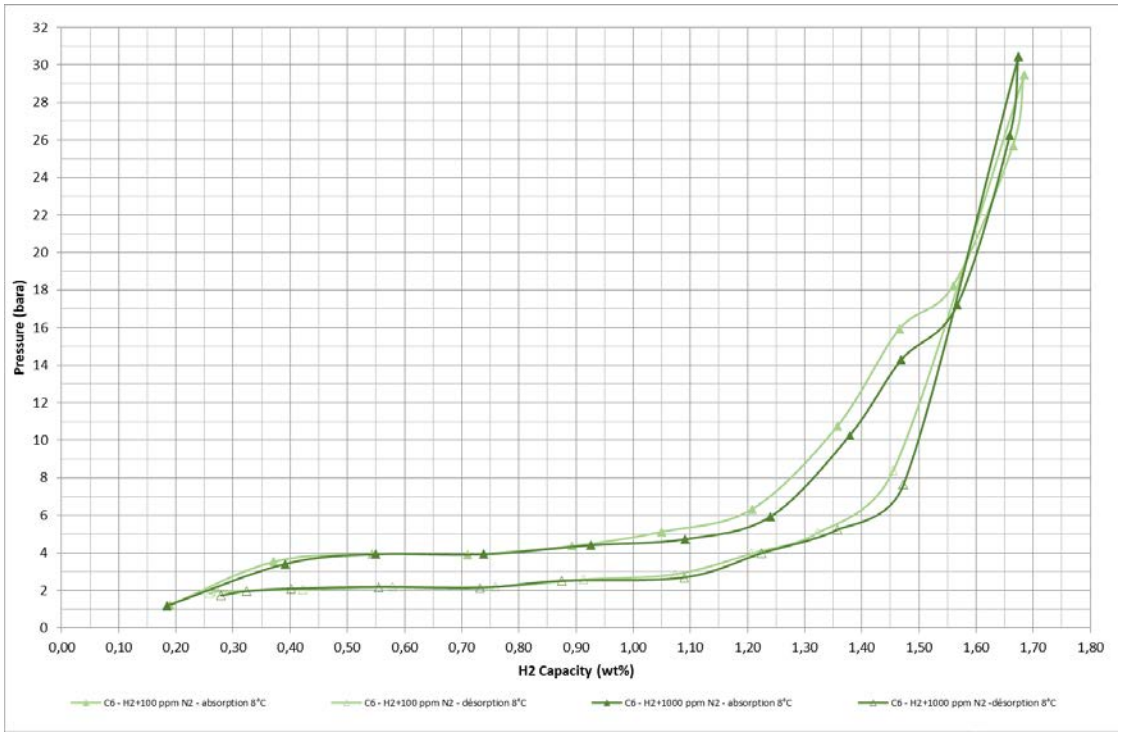

Figure 80 : PCT under H2 + N2 at 8°C after cycles 6

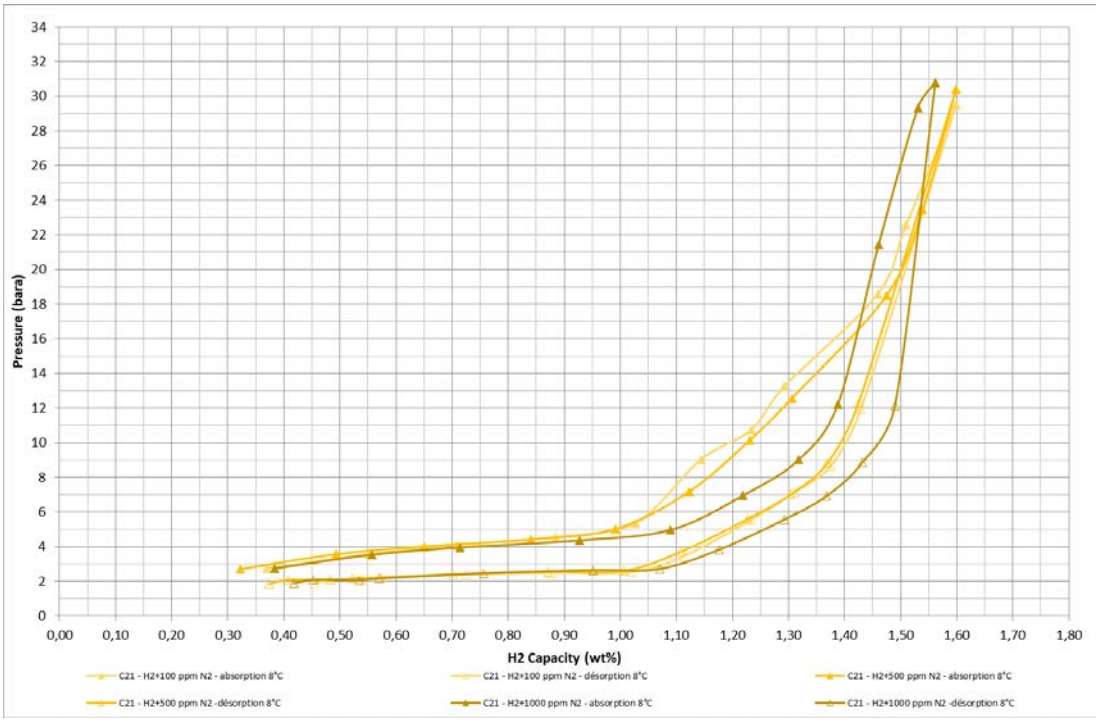

Figure 81 : PCT under H2 + N2 at 8°C after cycles 21

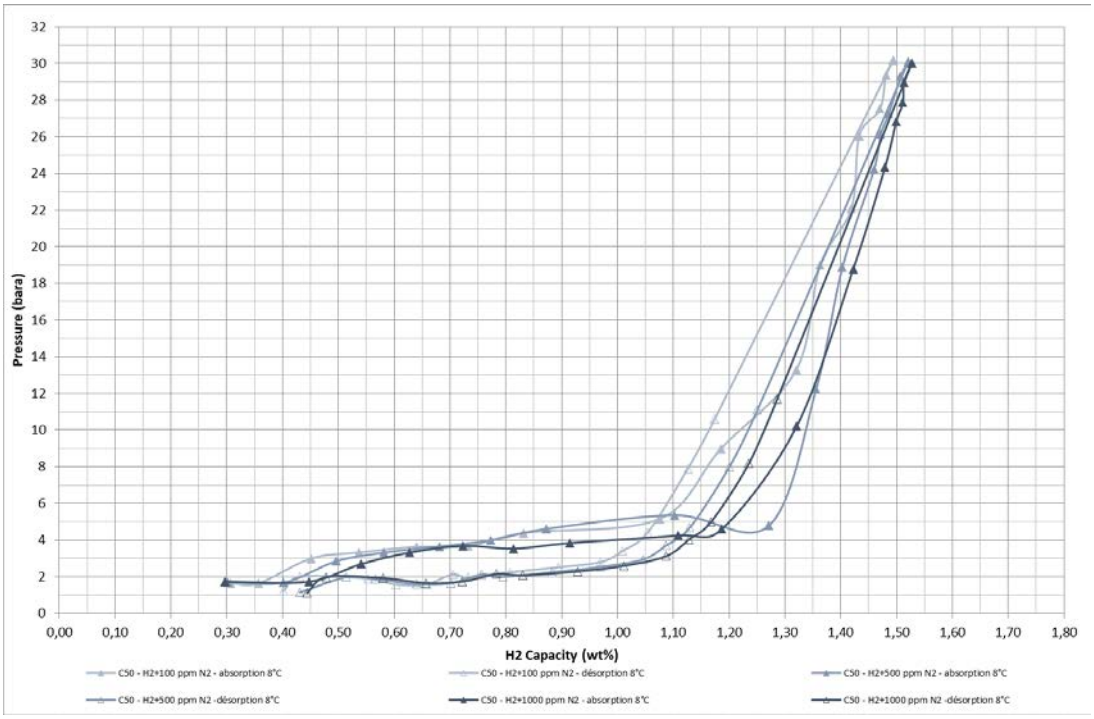

Figure 82 : PCT under H2 + N2 at 8°C after cycles 50

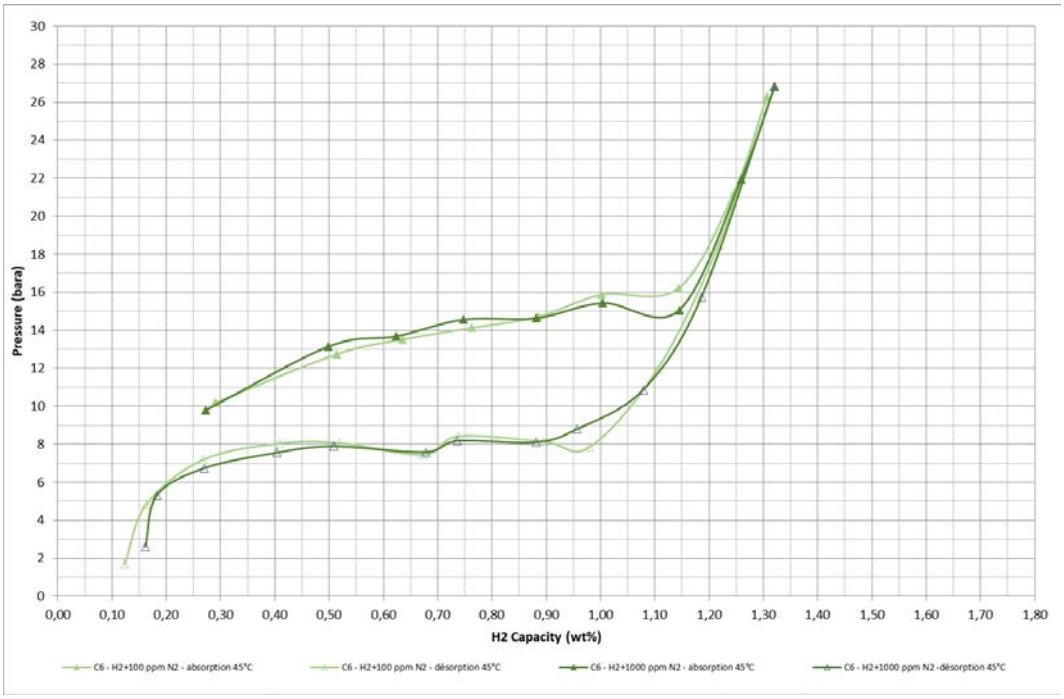

Figure 83 : PCT under H2 + N2 at 45°C after cycles 6

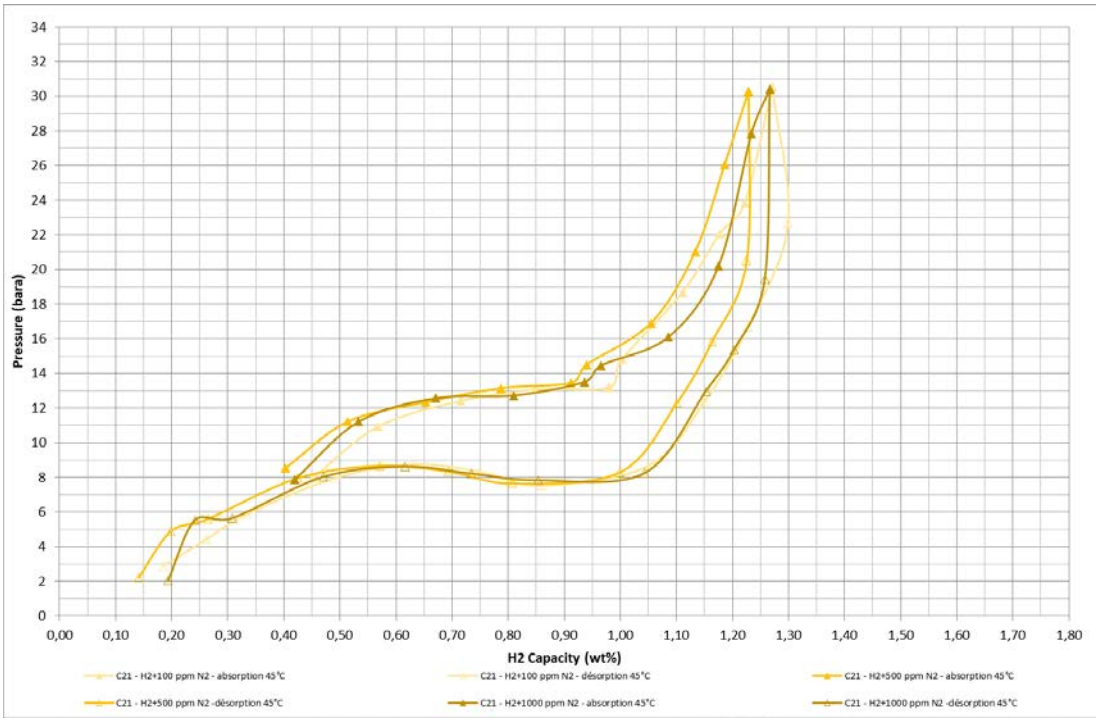

Figure 84 : PCT under H2 + N2 at 45°C after cycles 21

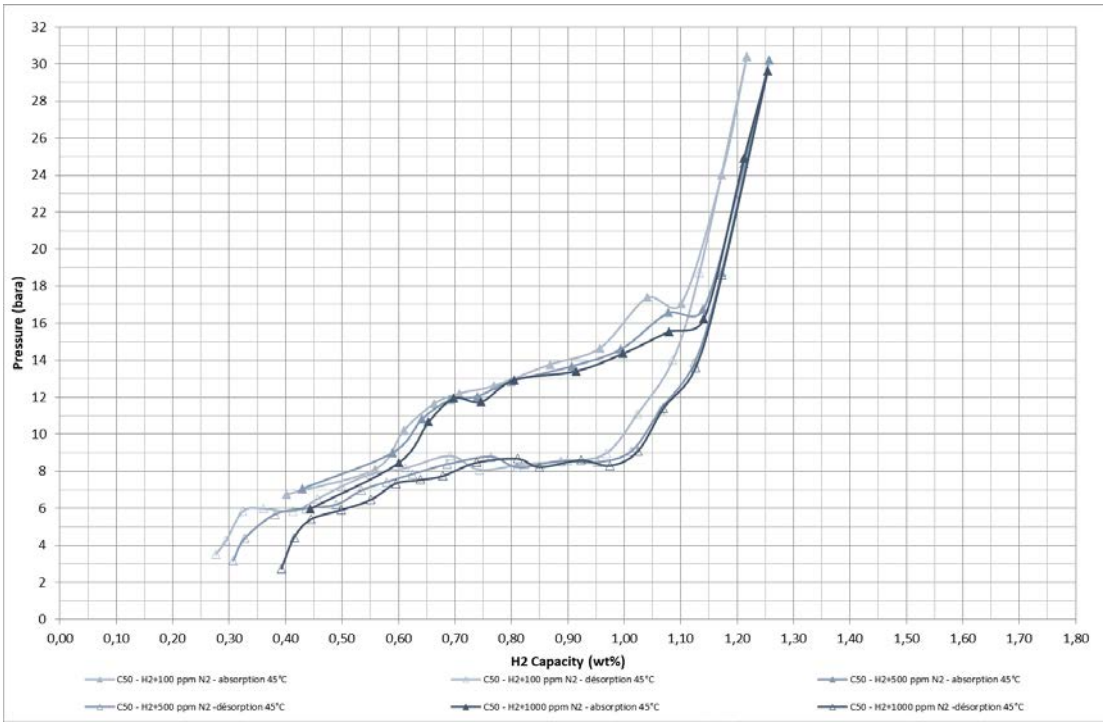

Figure 85 : PCT under H2 + N2 at 45°C after cycles 50

7.2 Global results with carbon monoxide

7.2.1 Capacities evolution on 50 cycles

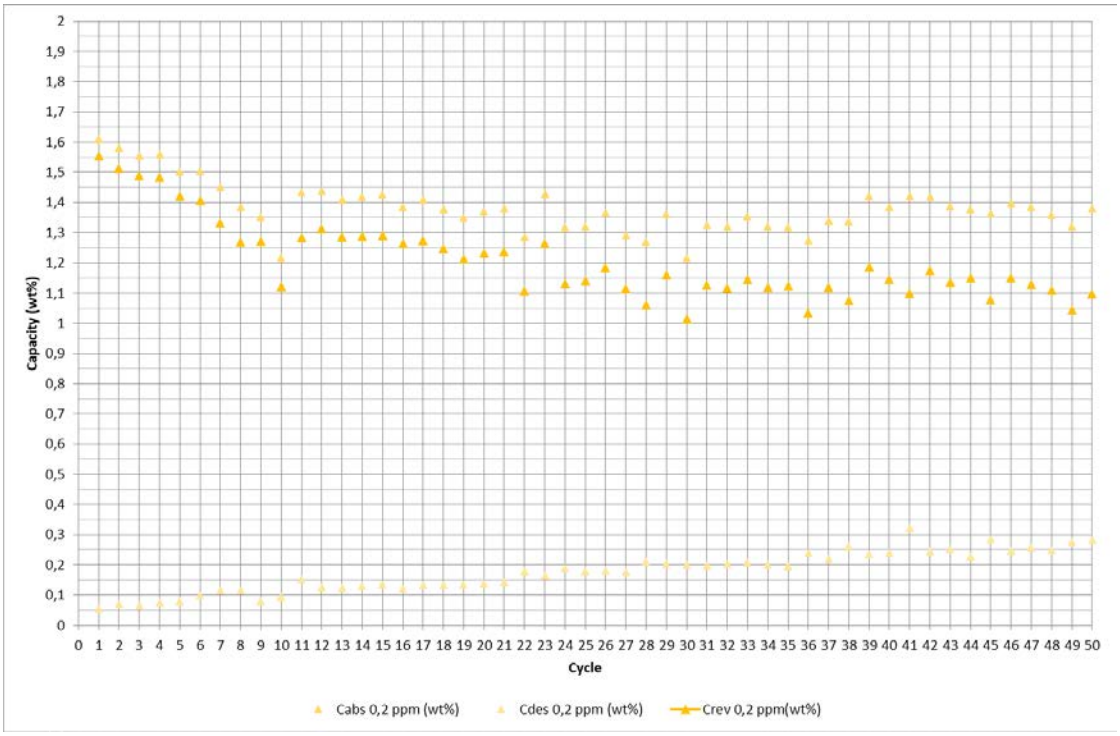

Figure 86 : Capacity under H2 + CO on 50 cycles – Proportion of CO: 0,2 ppm

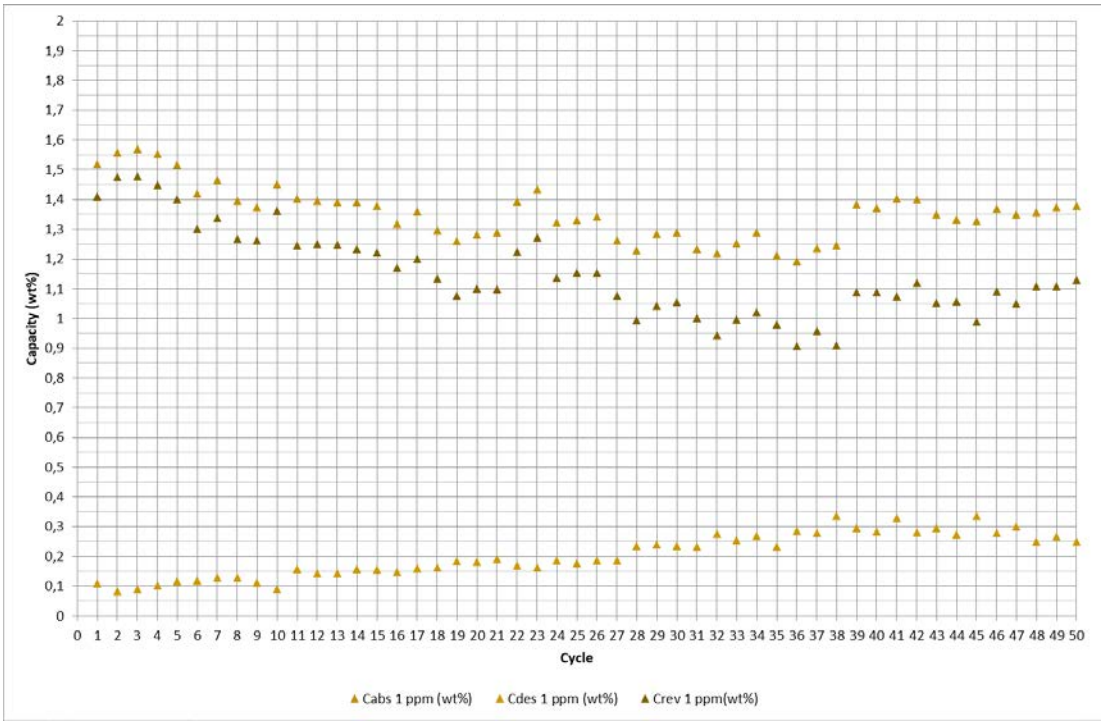

Figure 87 : Capacity under H2 + CO on 50 cycles – Proportion of CO: 1 ppm

7.2.2 PCT curves at different cycle and different temperature

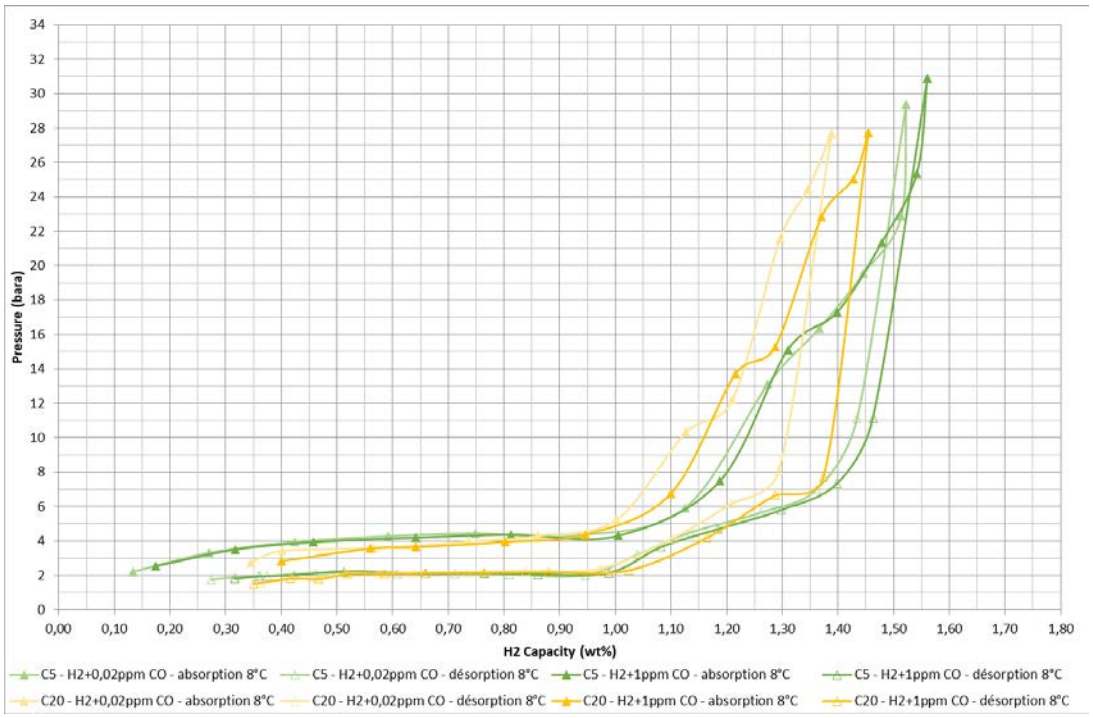

Figure 88 : PCT under H2 + CO at 8°C after cycles 5 and 20

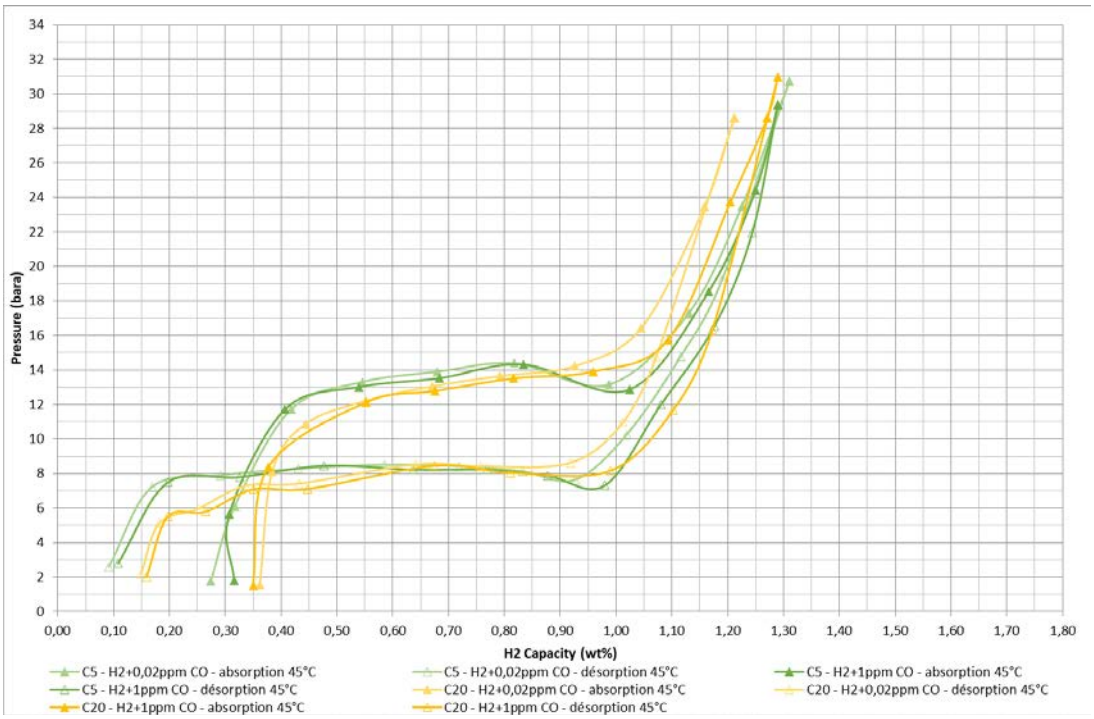

Figure 89 : PCT under H2 + CO at 45°C after cycles 5 and 20

7.3 Global results with carbon dioxide

7.3.1 Capacities evolution on 50 cycles

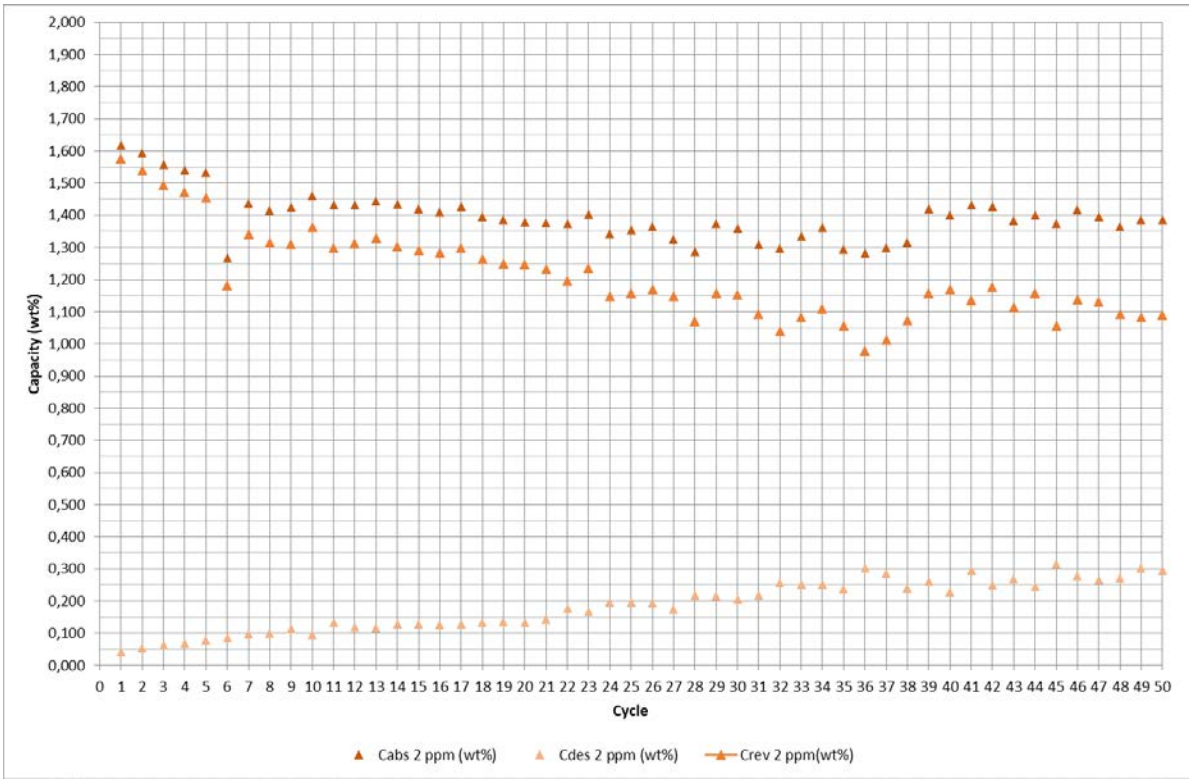

Figure 90 : Capacity under H2 + CO on 50 cycles – Proportion of CO2: 2 ppm

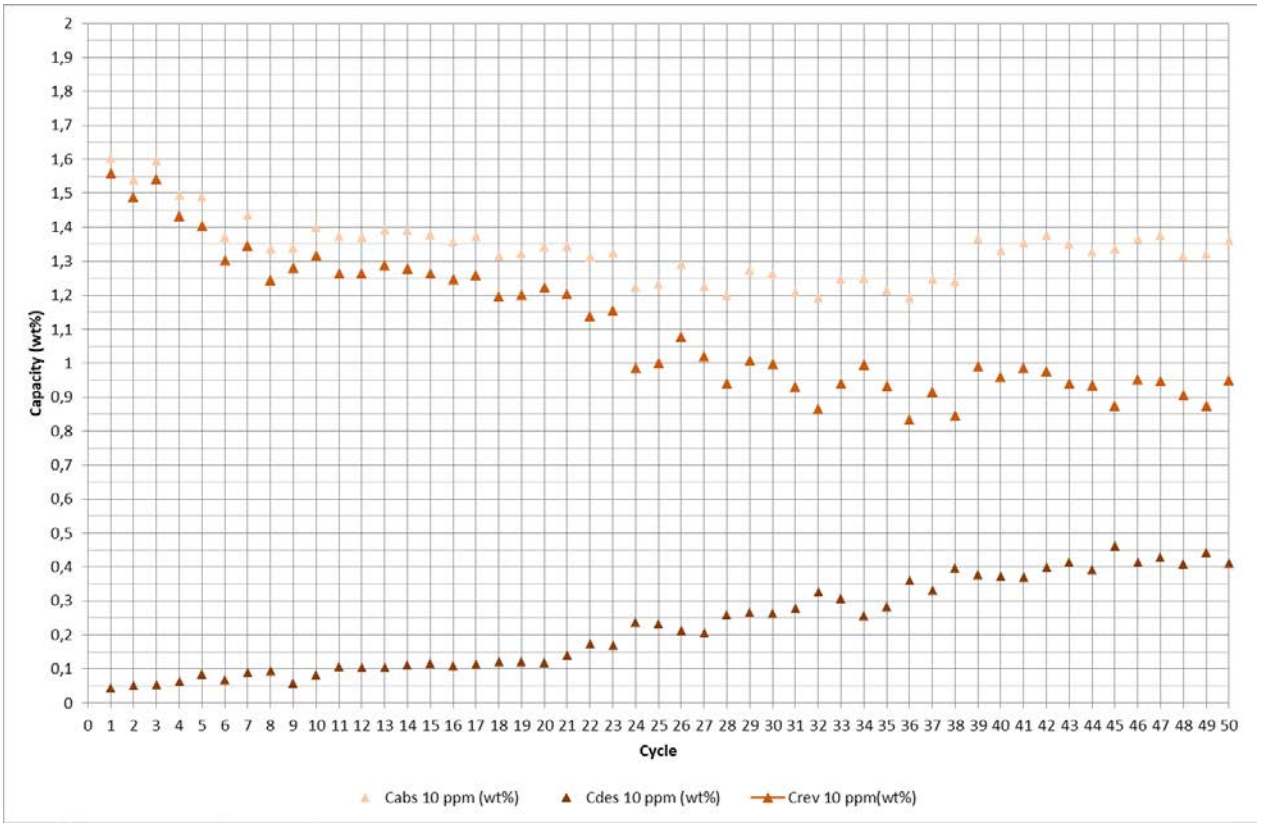

Figure 91 : Capacity under H2 + CO on 50 cycles – Proportion of CO2: 10 ppm

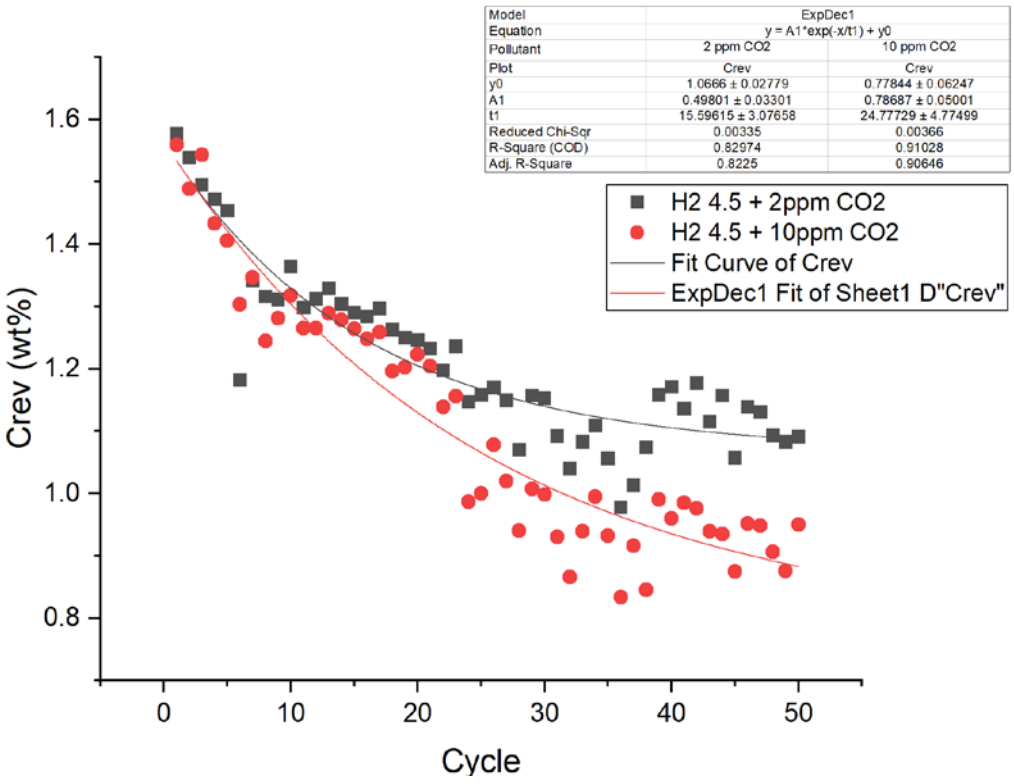

Figure 92 - Fitting of CO2 results

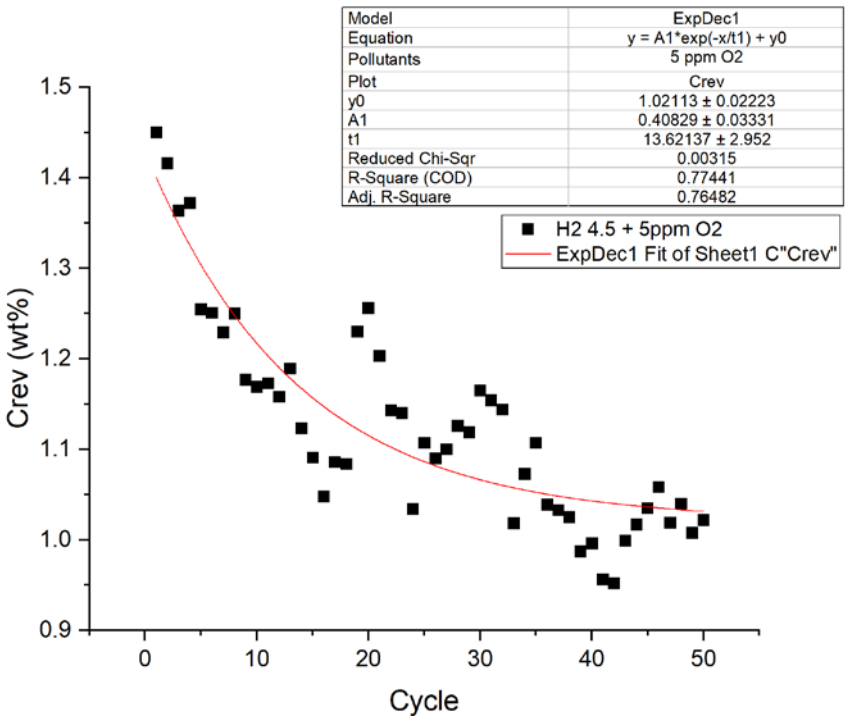

Figure 93- - Fitting of O2 results

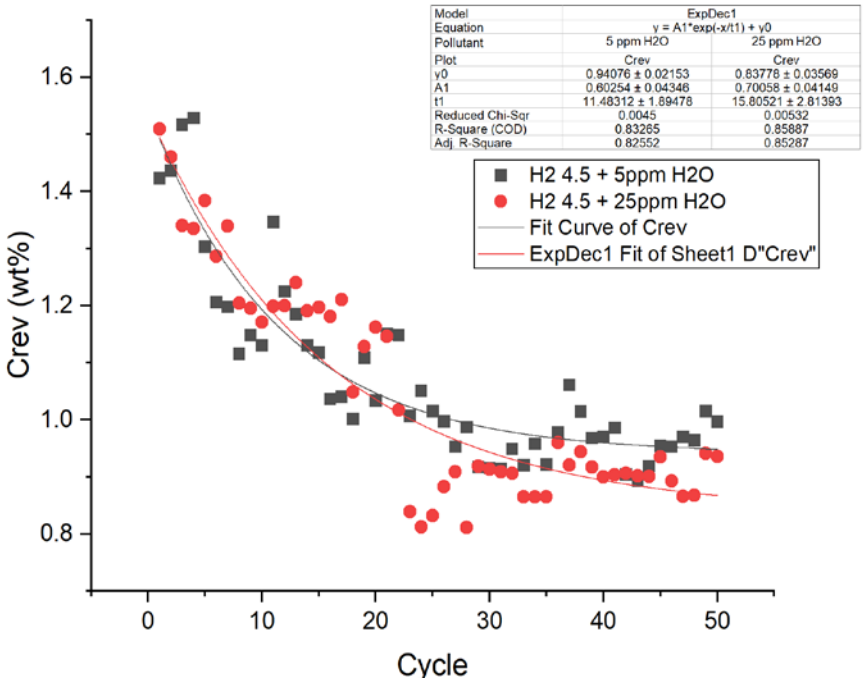

Figure 94 - Fitting of H2O results

7.4 Interlaboratory analysis of cryoadsorption of hydrogen on the candidate as reference material

7.4.1 Sample preparation sheets

Table 22 – Preparation of the sample for measurement from laboratory 2.

SAMPLE PREPARATION						
Run Number (same as "Experiment Result"):						
SAMPLE MASS						
Initial mass: 1.0068	±0.4	mg	Date:	06/12/2022		
After degass (optional):	±	mg	Date:			
Final mass: 1.0049	±0.8	mg	Date:	07/12/2022		
SAMPLE DEGASS	Begin date/time: 06/12/2022 19:00 h		End date/time:	07/12/2022 7:30 h		
Base Vacuum pressure : 5 10^{-6}	units: mbar					
Degas protocol:	☑ Degas protocol Followed	☐ Degas protocol exception (Explain):			☐ Analysis repetition	
Degass explanation: heating from RT to 120°C in 20 min. Dewel time: overnight (ca.11 h)						
Was sample exposed to air after degas and prior to measurement?	☑ No	☐ Yes (explain):				
Air exposure explanation:						

MEASUREMENT INFORMATION					
Measurement method	☐ Gravimetric	☑ Volumetric	☐ Other:	☑ Static	Dynamic
Measurement temperature control	☑ Liquid nitrogen	☐ Other (specify):		If dynamic, flow rate:	
	Hydrogen purity: 99.9999%		Additional purifier used?	☐ Yes	☑ No
	Base Vacuum pressure:	5 10^{-6} mbar	Units:	mbar	
	Sequence order:	☐ He calibration done first	☐ H_2 measurement done first		☑ No He calibration
	Equilibration time/step:	> 10 min	Total time for measurement:	410 min (PCI absorption)	
	Temperature stability 77K	Standard deviation: not meas	Pressure Sensor Accuracy:	☑ 0.04 % of FS:	☐ % of reading:
	Equation of State:	☐ Ideal	☑ Real: Model:	GASPAK V3.32 (Cryodata, Inc.)	

CALIBRATION				
Helium Adsorption correction?	☐ Yes ☑ No	**Supplied adsorption data has no correction.**		
		If other, explain:		
Skeletal Density	☑ Not Measured	☐ Measured:	g/cm³	Method used:

Table 23 – Preparation of the sample for measurement from laboratory 2.

SAMPLE PREPARATION						
Run Number (same as "Experiment Result"):						
SAMPLE MASS						
Initial mass: 1.6030	±0.2	mg	Date:	#########		
After degass (optional):	±	mg	Date:			
Final mass: 1.6001	±0.4	mg	Date:	#########		
SAMPLE DEGASS	Begin date/time: 08/12/2022 18:00 h		End date/time:	09/12/2022 8:00 h		
Base Vacuum pressure : 5 10^{-6}	units: mbar					
Degas protocol:	☑ Degas protocol Followed	☐ Degas protocol exception (Explain):			☐ Analysis repetition	
Degass explanation: heating from RT to 120°C in 20 min. Dewel time: overnight (ca.14 h)						
Was sample exposed to air after degas and prior to measurement?	☑ No	☐ Yes (explain):				
Air exposure explanation:						

MEASUREMENT INFORMATION					
Measurement method	☐ Gravimetric	☑ Volumetric	☐ Other:	☑ Static	Dynamic
Measurement temperature control	☑ Liquid nitrogen	☐ Other (specify):		If dynamic, flow rate:	
	Hydrogen purity: 99.9999%		Additional purifier used?	☐ Yes	☑ No
	Base Vacuum pressure:	5 10^{-6} mbar	Units:	mbar	
	Sequence order:	☐ He calibration done first	☐ H_2 measurement done first		☑ No He calibration
	Equilibration time/step:	> 10 min	Total time for measurement:	390 min (PCI absorption)	
	Temperature stability 77K	Standard deviation: not meas	Pressure Sensor Accuracy:	☑ 0.04 % of FS:	☐ % of reading:
	Equation of State:	☐ Ideal	☑ Real: Model:	GASPAK V3.32 (Cryodata, Inc.)	

CALIBRATION				
Helium Adsorption correction?	☐ Yes ☑ No	**Supplied adsorption data has no correction.**		
		If other, explain:		
Skeletal Density	☑ Not Measured	☐ Measured:	g/cm³	Method used:

Table 24 – Preparation of the sample for measurement from laboratory 3.

SAMPLE PREPARATION						
Run Number (same as "Experiment Result"):						
SAMPLE MASS	1.3227 g	0.0002				
Initial mass:	±	mg	Date:	07.0.03.2023		
After degass (optional):	±	mg	Date:	8.03		
Final mass:	±	mg	Date:	8.03		
SAMPLE DEGASS	Begin date/time:	7.03/17:00	End date/	8.03/9:00		
Base Vacuum pressure 15	units:	kP				
Degas protocol:	☑ Degas protocol Followed		☐ Degas protocol exception (Explain):			☐ Analysis repetition
Degass explanation:						
Was sample exposed to air after degas and prior to measurement?			☑ No		☐ Yes (explain):	
Air exposure explanation:						

MEASUREMENT INFORMATION					
Measurement method	☐ Gravimetric	☑ Volumetric	☐ Other:	☑ Static	Dynamic
Measurement temperature control	☑ Liquid nitrogen	☐ Other (specify):		If dynamic, flow rate:	
	Hydrogen purity:		Additional purifier used? ☐ Yes		☑ No
	Base Vacuum pressure:	15 Pa	Units:		
	Sequence order:	☑ He calibration done first	☐ H_2 measurement done first		☐ No He calibration
	Equilibration time/step:		min	Total time for measurement:	min
	Temperaature stability	Standard deviation:	K	Pressure Sensor Accuracy: ☐ % of FS:	☐% of reading:
	Equation of State:	☐ Ideal	☑ Real: Model:		

CALIBRATION			
Helium Adsorption correction?	☐ Yes ☑ No	**Supplied adsorption data has no correction.**	
		If other, explain:	
Skeletal Density	☐ Not Measured	☑ Measure 1.3 g/cm³	Method used: He

Table 25 – Preparation of the sample for measurement from laboratory 3.

SAMPLE PREPARATION						
Run Number (same as "Experiment Result"):						
SAMPLE MASS	1.0801 g	0.0002				
Initial mass:	±	mg	Date:	09/03/2023		
After degass (optional):	±	mg	Date:			
Final mass:	±	mg	Date:			
SAMPLE DEGASS	Begin date/time:	9.03/17:00	End date/	10.03/9:00		
Base Vacuum pressure 15	units:	kP				
Degas protocol:	☑ Degas protocol Followed		☐ Degas protocol exception (Explain):			☐ Analysis repetition
Degass explanation:						
Was sample exposed to air after degas and prior to measurement?			☑ No		☐ Yes (explain):	
Air exposure explanation:						

MEASUREMENT INFORMATION					
Measurement method	☐ Gravimetric	☑ Volumetric	☐ Other:	☑ Static	Dynamic
Measurement temperature control	☑ Liquid nitrogen	☐ Other (specify):		If dynamic, flow rate:	
	Hydrogen purity:		Additional purifier used?	☐ Yes	☑ No
	Base Vacuum pressure:	15 Pa	Units:		
	Sequence order:	☑ He calibration done first		☐ H_2 measurement done first	☐ No He calibration
	Equilibration time/step:		min	Total time for measurement:	min
	Temperaature stability	Standard deviation:	K	Pressure Sensor Accuracy: ☐ % of FS:	☐% of reading:
	Equation of State:	☐ Ideal	☑	Real: Model:	

CALIBRATION			
Helium Adsorption correction?	☐ Yes ☑ No	**Supplied adsorption data has no correction.**	
		If other, explain:	
Skeletal Density	☐ Not Measured	☑ Measure 1.49 g/cm³	Method used: He

Table 26 – Preparation of the sample for measurement from laboratory 3.

SAMPLE PREPARATION								
Run Number (same as "Experiment Result"):								
SAMPLE MASS	1.0347 g	0.0002						
Initial mass:	±	mg	Date:	09/03/2023				
After degass (optional):	±	mg	Date:					
Final mass:	±	mg	Date:					
SAMPLE DEGASS	Begin date/time: 20.03/17:00		End date/ 21.03/9:00					
Base Vacuum pressure 15	units:	kP						
Degas protocol:	☑ Degas protocol Followed		☐ Degas protocol exception (Explain):				☐ Analysis repetition	
Degass explanation:								
Was sample exposed to air after degas and prior to measurement?			☑ No		☐ Yes (explain):			
Air exposure explanation:								

MEASUREMENT INFORMATION							
Measurement method	☐ Gravimetric	☑ Volumetric	☐ Other:		☑ Static	Dynamic	
Measurement temperature control	☑ Liquid nitrogen	☐ Other (specify):			If dynamic, flow rate:		
	Hydrogen purity:		Additional purifier used?		☐ Yes	☑ No	
	Base Vacuum pressure:	15 Pa	Units:				
	Sequence order:	☑ He calibration done first		☐ H_2 measurement done first		☐ No He calibration	
	Equilibration time/step:		min	Total time for measurement:		min	
	Temperaature stability	Standard deviation:	K	Pressure Sensor Accuracy:	☐ % of FS:	☐% of reading:	
	Equation of State:	☐ Ideal	☑	Real: Model:			

CALIBRATION				
Helium Adsorption correction?	☐ Yes ☑ No	**Supplied adsorption data has no correction.**		
		If other, explain:		
Skeletal Density	☐ Not Measured	☑ Measure 1.5 g/cm³	Method used:	He

Table 27 – Preparation of the sample for measurement from laboratory 4.

SAMPLE PREPARATION								
Run Number (same as "Experiment Result"): 1								
SAMPLE MASS								
Initial mass: 783.07	± 0.01	mg	Date:	17/11/2022				
After degass (optional):	±	mg	Date:					
Final mass: 781.8	± 0.1	mg	Date:	21/11/2022				
SAMPLE DEGASS	Begin date/time: 17/11/2022		End date/time:	17/11/2022				
Base Vacuum pressure	units: 1E-5 mbar at pump							
Degas protocol:	☑ Degas protocol Followed		☐ Degas protocol exception (Explain):				☐ Analysis repetition	
Degass explanation:								
Was sample exposed to air after degas and prior to measurement?			☑ No		☐ Yes (explain):			
Air exposure explanation:								

MEASUREMENT INFORMATION							
Measurement method	☐ Gravimetric	☑ Volumetric	☐ Other:		☑ Static	Dynamic	
Measurement temperature control	☑ Liquid nitrogen	☐ Other (specify):			If dynamic, flow rate:		
	Hydrogen purity	99.999	Additional purifier used?		☐ Yes	☑ No	
	Base Vacuum pressure:	1E-5 mbar at pump	Units:				
	Sequence order:	☐ He calibration done first		☐ H_2 measurement done first		☑ No He calibration	
	Equilibration time/step:	10	min	Total time for measurement:		464 min	
	Temperature stability:	Ref = 23.0 +/- 0.1; Amb = 21.6 +/- 0.8 degC		Pressure Sensor Accuracy:	☑ % of FS:	☐% of reading:	
	Equation of State:	☐ Ideal	☑	Real: Model:	NIST Database 23 REFPROP		

CALIBRATION					
Helium Adsorption correction?	☐ Yes ☑ No	**Supplied adsorption data has no correction.**			
		If other, explain:	Volumes calibrated empty with hydrogen. Supplied skeletal density (1.54 g/cc) used to calculate volume of sample.		
Skeletal Density	☑ Not Measured	☐ Measured:	g/cm³	Method used:	This was measured on another instrument using He to be 1.76 g/cc but was not used (only used for error analysis)

Table 28 – Preparation of the sample for measurement from laboratory 4.

SAMPLE PREPARATION						
Run Number (same as "Experiment Result"): 1						
SAMPLE MASS						
Initial mass: 783.07	± 0.01	mg	Date:	17/11/2022		
After degass (optional):	±	mg	Date:			
Final mass: 781.8	± 0.1	mg	Date:	21/11/2022		
SAMPLE DEGASS	Begin date/time: 17/11/2022		End date/time:	17/11/2022		
Base Vacuum pressure	units: 1E-5 mbar at pump					
Degas protocol:	☑ Degas protocol Followed		☐ Degas protocol exception (Explain):		☐ Analysis repetition	
Degass explanation:						
Was sample exposed to air after degas and prior to measurement?			☑ No		☐ Yes (explain):	
Air exposure explanation:						
MEASUREMENT INFORMATION						
Measurement method	☐ Gravimetric	☑ Volumetric	☐ Other:		☑ Static	Dynamic
Measurement temperature control	☑ Liquid nitrogen	☐ Other (specify):			If dynamic, flow rate:	
	Hydrogen purity 99.999		Additional purifier used?	☐ Yes	☑ No	
	Base Vacuum pressure: 1E-5 mbar at pump		Units:			
	Sequence order:	☐ He calibration done first	☐ H_2 measurement done first		☑ No He calibration	
	Equilibration time/step:	10 min	Total time for measurement:		464 min	
	Temperature stability: Ref = 23.0 +/- 0.1; Amb = 21.6 +/- 0.8 degC		Pressure Sensor Accuracy:	☑ % of FS:	☐ % of reading:	
	Equation of State:	☐ Ideal	☑ Real: Model:	NIST Database 23 REFPROP		
CALIBRATION						
Helium Adsorption correction?	☐ Yes ☑ No	**Supplied adsorption data has no correction.**				
		If other, explain:	Volumes calibrated empty with hydrogen. Supplied skeletal density (1.54 g/cc) used to calculate volume of sample.			
Skeletal Density	☑ Not Measured	☐ Measured:	g/cm³	Method used:	This was measured on another instrument using He to be 1.76 g/cc but was not used (only used for error analysis)	

Table 29 – Preparation of the sample for measurement from laboratory 5.

SAMPLE PREPARATION						
Run Number (same as "Experiment Result"): 1st measurement						
SAMPLE MASS						
Initial mass: 0.44315	±0.00003	mg	Date:27.10			
After degass (optional):	±	mg	Date:			
Final mass:0.44207	±0.00001	mg	Date:02.11			
SAMPLE DEGASS	Begin date/time: 31.10.2022/14:26		End date/time: 31.10.2022/23:15			
Base Vacuum pressure : $6.6*10^{-2}$	units: mbar					
Degas protocol:	☑ Degas protocol Followed		☐ Degas protocol exception (Explain):		☑ Analysis repetition	
Degass explanation:	120 °C for 8h					
Was sample exposed to air after degas and prior to measurement?			☑ No		☐ Yes (explain):	
Air exposure explanation:						
MEASUREMENT INFORMATION						
Measurement method	☑ Gravimetric	☑ Volumetric	☐ Other:		☐ Static	Dynamic
Measurement temperature control	☑ Liquid nitrogen	☐ Other (specify):			If dynamic, flow rate:	
	Hydrogen purity:	0.99999	Additional purifier used?	☐ Yes	☑ No	
	Base Vacuum pressure:	$6.6*10^{-2}$	Units: mbar			
	Sequence order:	☑ He calibration done first	☐ H_2 measurement done first		☐ No He calibration	
	Equilibration time/step:	10 min	Total time for measurement:		560 min	
	Temperaature stability	Standard deviation: 0.07 K	Pressure Sensor Accuracy:	☐ % of FS:	☑ % of reading: 0.3	
	Equation of State:	☐ Ideal	☑ Real: Model:			
CALIBRATION						
Helium Adsorption correction?	☑ Yes ☐ No	**Supplied adsorption data has no correction.**				
		If other, explain:	seasand calibration (y=-9.17811E-8x+3.05356E-4)			
Skeletal Density	☑ Not Measured	☐ Measured:	g/cm³	Method used:		

Table 30 – Preparation of the sample for measurement from laboratory 5.

SAMPLE PREPARATION						
Run Number (same as "Experiment Result"): 2nd measurement						
SAMPLE MASS						
Initial mass:0.44315	±0.00003	mg	Date:27.10			
After degass (optional):	±	mg	Date:			
Final mass:0.44207	±0.00001	mg	Date:02.11			
SAMPLE DEGASS	Begin date/time: 02.11.2022/00:58		End date/time: 02.11.2022/09:53			
Base Vacuum pressure 6.6*10-2	units: mbar					
Degas protocol:	☑ Degas protocol Followed		☐ Degas protocol exception (Explain):		☑ Analysis repetition	
Degass explanation:	120 °C for 8h					
Was sample exposed to air after degas and prior to measurement?			☑ No	☐ Yes (explain):		
Air exposure explanation:						
MEASUREMENT INFORMATION						
Measurement method	☐ Gravimetric	☑ Volumetric	☐ Other:	☐ Static	Dynamic	
Measurement temperature control	☑ Liquid nitrogen	☐ Other (specify):		If dynamic, flow rate:		
	Hydrogen purity: 0.99999		Additional purifier used?	☐ Yes	☑ No	
	Base Vacuum pressure:	$6.6*10^{-2}$	Units:	mbar		
	Sequence order:	☑ He calibration done first		☐ H_2 measurement done first	☐ No He calibration	
	Equilibration time/step:	10 min	Total time for measurement:	280 min		
	Temperaature stability	Standard deviation:	0.049 K	Pressure Sensor Accuracy:	☐ % of FS:	☑ % of reading:0.3
	Equation of State:	☐ Ideal	☑ Real: Model:			
CALIBRATION						
Helium Adsorption correction?	☑ Yes ☐ No	**Supplied adsorption data has no correction.**				
		If other, explain:	seasand calibration (y=-9.17811E-8x+3.05356E-4)			
Skeletal Density	☑ Not Measured	☐ Measured:	g/cm³	Method used:		

Table 31 – Preparation of the sample for measurement from laboratory 5.

SAMPLE PREPRATION						
Run Number (same as "Experiment Result"): 3th measurement						
SAMPLE MASS						
Initial mass:0.55727	±0.00001	mg	Date:02.11			
After degass (optional):	±	mg	Date:			
Final mass:0.55580	±0.00002	mg	Date:08.11			
SAMPLE DEGASS	Begin date/time: 03.11.2022/00:14		End date/time: 03.11.2022/09:04			
Base Vacuum pressure :$6.6*10^{-2}$	units: mbar					
Degas protocol:	☑ Degas protocol Followed		☐ Degas protocol exception (Explain):		☑ Analysis repetition	
Degass explanation:	120 °C for 8h					
Was sample exposed to air after degas and prior to measurement?			☑ No	☐ Yes (explain):		
Air exposure explanation:						
MEASUREMENT INFORMATION						
Measurement method	☐ Gravimetric	☑ Volumetric	☐ Other:	☐ Static	Dynamic	
Measurement temperature control	☑ Liquid nitrogen	☐ Other (specify):		If dynamic, flow rate:		
	Hydrogen purity: 0.99999		Additional purifier used?	☐ Yes	☑ No	
	Base Vacuum pressure:	$6.6*10^{-2}$	Units:	mbar		
	Sequence order:	☑ He calibration done first		☐ H_2 measurement done first	☐ No He calibration	
	Equilibration time/step:	10 min	Total time for measurement:	275 min		
	Temperaature stability	Standard deviation:	0.063K	Pressure Sensor Accuracy:	☐ % of FS:	☑ % of reading: 0.3
	Equation of State:	☐ Ideal	☑ Real: Model:			
CALIBRATION						
Helium Adsorption correction?	☑ Yes ☐ No	**Supplied adsorption data has no correction.**				
		If other, explain:	seasand calibration (y=-9.17811E-8x+3.05356E-4)			
Skeletal Density	☑ Not Measured	☐ Measured:	g/cm³	Method used:		

Table 32 – Preparation of the sample for measurement from laboratory 5.

SAMPLE PREPARATION						
Run Number (same as "Experiment Result"): 4th measurement						
SAMPLE MASS						
Initial mass: 0.55727	±0.00001	mg	Date:02.11			
After degass (optional):	±	mg	Date:			
Final mass:0.55580	±0.00002	mg	Date:08.11			
SAMPLE DEGASS	Begin date/time: 04.11.2022/10:32		End date/time: 04.11.2022/20:03			
Base Vacuum pressure : $6.6*10^{-2}$	units: mbar					
Degas protocol:	☑ Degas protocol Followed	☐ Degas protocol exception (Explain):			☑ Analysis repetition	
Degass explanation:	120 °C for 8h					
Was sample exposed to air after degas and prior to measurement?		☑ No	☐ Yes (explain):			
Air exposure explanation:						
MEASUREMENT INFORMATION						
Measurement method	☐ Gravimetric	☑ Volumetric	☐ Other:	☐ Static	Dynamic	
Measurement temperature control	☑ Liquid nitrogen	☐ Other (specify):		If dynamic, flow rate:		
Hydrogen purity:	0.99999	Additional purifier used?	☐ Yes	☑ No		
Base Vacuum pressure:	$6.6*10^{-2}$	Units: mbar				
Sequence order:	☑ He calibration done first	☐ H_2 measurement done first	☐ No He calibration			
Equilibration time/step:	10 min	Total time for measurement:	275 min			
Temperaature stability	Standard deviation: 0.0621 K	Pressure Sensor Accuracy:	☐ % of FS:	☑ % of reading: 0.3		
Equation of State:	☐ Ideal	☑ Real: Model:				
CALIBRATION						
Helium Adsorption correction?	☑ Yes ☐ No	**Supplied adsorption data has no correction.**				
		If other, explain:	seasand calibration (y=-9.17811E-8x+3.05356E-4)			
Skeletal Density	☑ Not Measured	☐ Measured:	g/cm³	Method used:		

Table 33 – Preparation of the sample for measurement from laboratory 5.

SAMPLE PREPARATION						
Run Number (same as "Experiment Result"): 5th measurement						
SAMPLE MASS						
Initial mass: 0.36349	±0.00002	mg	Date: 08.11			
After degass (optional):	±	mg	Date:			
Final mass:0.36313	±0.00001	mg	Date: 09.11			
SAMPLE DEGASS	Begin date/time: 08.11.2022/15:39		End date/time: 09.11.2022/00:10			
Base Vacuum pressure : $6.6*10^{-2}$	units: mbar					
Degas protocol:	☑ Degas protocol Followed	☐ Degas protocol exception (Explain):			☐ Analysis repetition	
Degass explanation:	120 °C for 8h					
Was sample exposed to air after degas and prior to measurement?		☑ No	☐ Yes (explain):			
Air exposure explanation:						
MEASUREMENT INFORMATION						
Measurement method	☐ Gravimetric	☑ Volumetric	☐ Other:	☐ Static	Dynamic	
Measurement temperature control	☑ Liquid nitrogen	☐ Other (specify):		If dynamic, flow rate:		
Hydrogen purity:	0.99999	Additional purifier used?	☐ Yes	☑ No		
Base Vacuum pressure:	$6.6*10^{-2}$	Units: mbar				
Sequence order:	☑ He calibration done first	☐ H_2 measurement done first	☐ No He calibration			
Equilibration time/step:	10 min	Total time for measurement:	275 min			
Temperaature stability	Standard deviation: 0.066K	Pressure Sensor Accuracy:	☐ % of FS:	☑ % of reading: 0.3		
Equation of State:	☐ Ideal	☑ Real: Model:				
CALIBRATION						
Helium Adsorption correction?	☑ Yes ☐ No	**Supplied adsorption data has no correction.**				
		If other, explain:	seasand calibration (y=-9.17811E-8x+3.05356E-4)			
Skeletal Density	☑ Not Measured	☐ Measured:	g/cm³	Method used:		

Table 34 – Preparation of the sample for measurement from laboratory 6.

SAMPLE PREPARATION						
Run Number (same as "Experiment Result"):						
SAMPLE MASS						
Initial mass:		mg	Date:	#########	* Degassed total sample sent (1725.08 ± 0.346 mg initial)	
After degass (optional):	1057.62 ± 0.235	mg	Date:	#########		
Final mass:	1058.213 ± 0.67	mg	Date:	#########		
SAMPLE DEGASS	Begin date/time:	1/4/2023 3:42 PM MST	End date/time:	1/5/2023 7:00 AM MST		
Base Vacuum pressure	units:	1E-8 Torr				
Degas protocol:	☑ Degas protocol Followed		☐ Degas protocol exception (Explain):		☐ Analysis repetition	
Degass explanation:						
Was sample exposed to air after degas and prior to measurement?			☑ No	☐ Yes (explain):		
Air exposure explanation:						
MEASUREMENT INFORMATION						
Measurement method	☐ Gravimetric	☑ Volumetric	☐ Other:	☑ Static	Dynamic	
Measurement temperature control	☐ Liquid nitrogen	☑ Other (specify):	Cryo	If dynamic, flow rate:		
	Hydrogen purity	99.9999%	Additional purifier used?	☑ Yes	☐ No	
	Base Vacuum pressure:	1.00E-05	Units:	Torr		
	Sequence order:	☑ He calibration done first	☐ H_2 measurement done first	☐ No He calibration		
	Equilibration time/step:	30 min	Total time for measurement:	58 hours		
	Temperature sta	0.01 K	Standard deviation: K	Pressure Sensor Accuracy:	☐ % of FS:	☑ % of reading ±1.0%
	Equation of State:	☐ Ideal	☑ Real: Model:	GASPAK		
CALIBRATION						
Helium Adsorption correction?	☐ Yes ☑ No	**Supplied adsorption data has no correction.**				
		If other, explain:				
Skeletal Density	☐ Not Measured	☑ Measure 1.5535 g/cm³	Method used:	He Pycnometry		

Table 35 – Preparation of the sample for measurement from laboratory 6.

SAMPLE PREPARATION						
Run Number (same as "Experiment Result"):						
SAMPLE MASS						
Initial mass:		mg	Date:	#########	* Degassed total sample sent (1725.08 ± 0.346 mg)	
After degass (optional):	495.94 ± 0.652	mg	Date:	#########		
Final mass:	496.32 ± 0.283	mg	Date:	#########		
SAMPLE DEGASS	Begin date/time:	01/04/2023 15:42	End date/time:	#########		
Base Vacuum pressure	units:	1E-8 Torr				
Degas protocol:	☑ Degas protocol Followed		☐ Degas protocol exception (Explain):		☐ Analysis repetition	
Degass explanation:						
Was sample exposed to air after degas and prior to measurement?			☑ No	☐ Yes (explain):		
Air exposure explanation:						
MEASUREMENT INFORMATION						
Measurement method	☐ Gravimetric	☑ Volumetric	☐ Other:	☑ Static	Dynamic	
Measurement temperature control	☐ Liquid nitrogen	☑ Other (specify):	Cryo	If dynamic, flow rate:		
	Hydrogen purity:	99.9999%	Additional purifier used?	☑ Yes	☐ No	
	Base Vacuum pressure:	1.00E-05	Units:	Torr		
	Sequence order:	☑ He calibration done first	☐ H_2 measurement done first	☐ No He calibration		
	Equilibration time/step:	60 min	Total time for measurement:	190 hours		
	Temperature stability	see comment	Standard deviation: K	Pressure Sensor Accuracy:	☐ % of FS:	☑ % of reading: ±1.0%
	Equation of State:	☐ Ideal	☐ Real: Model:	GASPAK		
CALIBRATION						
Helium Adsorption correction?	☐ Yes ☑ No	**Supplied adsorption data has no correction.**				
		If other, explain:				
Skeletal Density	☐ Not Measured	☑ Measure 1.5428 g/cm³	Method used:	He Pycnometry		
COMMENTS						
The cryo shroud pressure varied form 1.2 mTorr to 3.6 mTorr impacting the temperature control of the cryo head, and thus sample temperature. We typically have sample temperature variation within only 0.01 K, but was likely on the order of magnitude of 0.1K here.						

Table 36 – Preparation of the sample for measurement from laboratory 7.

SAMPLE PREPARATION					
Run Number (same as "Experiment Result"):					
SAMPLE MASS					
Initial mass: 212.4	± 0.2	mg	Date: 26/10/2022		
After degass (optional):	±	mg	Date:		
Final mass: 211.7	± 0.2	mg	Date: 08/11/2022		
SAMPLE DEGASS	Begin date/time: 26/10/2022		End date/time: 30/10/2022		
Base Vacuum pressure: < 10e-06	units: mbar				
Degas protocol:	☐ Degas protocol Followed		☑ Degas protocol exception (Explain):		☐ Analysis repetition
Degass explanation: Sample was outgassed at 120C for 72 hours					
Was sample exposed to air after degas and prior to measurement?			☑ No	☐ Yes (explain):	
Air exposure explanation:					

MEASUREMENT INFORMATION					
Measurement method	☐ Gravimetric	☑ Volumetric	☐ Other:	☑ Static	Dynamic
Measurement temperature control	☑ Liquid nitrogen ☐	Other (specify):		If dynamic, flow rate:	
	Hydrogen purity: 99.999%		Additional purifier used? ☐ Yes	☑ No	
	Base Vacuum pressure: < 10-06		Units: mbar		
	Sequence order:	☑ He calibration done first	☐ H_2 measurement done first	☐ No He calibration	
	Equilibration time/step: 5		min	Total time for measurement: 232	min
	Temperature stability: 0.5K	Standard deviation: 0.07	K	Pressure Sensor Accuracy: 1 ☐ % of FS:	☑ % of reading:
	Equation of State:	☐ Ideal		☑ Real: Model: BWR MBWR equation of state for hydrogen of Younglove (1982)	

CALIBRATION				
Helium Adsorption correction?	☑ Yes ☐ No	**Supplied adsorption data has no correction.**		
		If other, explain:		
Skeletal Density	☑ Not Measured	☐ Measured:	g/cm³	Method used:

COMMENTS

- Void volumes of the sample holder were determined using helium (99.999%) after keeping all parts of the instrument including the sample at 30 oC. In order to avoid helium adsorption errors, sample holder void volumes at 77K were calculated from a previously constructed reference curve (volume at -196 oC vs volume at 30 oC). The curve was obtained by inserting various amounts of non-adsorbing material (Pyrex glass) and performing volume calibrations at instrument temperature (30C) and measurement temperature (instrument at 30 oC and sample at -196 oC).
- A blank measurement was carried on the empty sample holder according to the specified experimental conditions and was subtracted from the actual isotherm. Due to the configuration of the instrument, it was impossible to obtain exactly the same set of recommended equilibrium pressure points. In order to extract blank values for the actual experimental equilibrium pressure points, linear interpolation of the blank isotherm was used.
- Liquid nitrogen level was kept constant during the experiments by means of a custom made automation which consists of a Pt-100 thermocouple acting as a level sensor, an on-off controller and an electronic valve connected to an external LN2 dewar

Table 37 – Preparation of the sample for measurement from laboratory 7.

SAMPLE PREPARATION					
Run Number (same as "Experiment Result"):					
SAMPLE MASS					
Initial mass: 110.7	± 0.2	mg	Date: 08/11/2022		
After degass (optional):	±	mg	Date:		
Final mass: 109.8	± 0.2	mg	Date: 15/11/2022		
SAMPLE DEGASS	Begin date/time: 08/11/2022, 21:00		End date/time: 09/11/2022, 12:00		
Base Vacuum pressure: < 10e-06	units: mbar				
☑ egas protocol:	☑ Degas protocol Followed		☐ Degas protocol exception (Explain):		☐ Analysis repetition
Degass explanation: Sample was outgassed at 120C for 15 hours					
☐ as sample exposed to air after degas and prior to measurement?			☑ No	☐ Yes (explain):	
Air exposure explanation:					
		☐			

MEASUREMENT INFORMATION					
☑ **easurement method**	☐ Gravimetric	☑ Volumetric	☐ Other:	☑ Static	Dynamic
☑ **easurement temperature control**	☑ Liquid nitrogen	☐ ther (specify):		If dynamic, flow rate:	
☑	Hydrogen purity: 99.999%		Additional purifier used?	☐ Yes ☑ No	
	Base Vacuum pressure: < 10e-06		Units: mbar		
☐	Sequence order:	☑ He calibration done first	☐ H_2 measurement done first	☐ No He calibration	
	Equilibration time/step: 5		min	Total time for measurement: 235	min
☑	Temperature stability: 0.5K	Standard deviation: 0.07	K	Pressure Sensor Accuracy: 1 ☐ % of FS:	☑ % of reading:
☑	Equation of State:	☐ Ideal		☑ Real: Model: BWR MBWR equation of state for hydrogen of Younglove (1982)	

CALIBRATION					
☐ **elium Adsorption correction?**	☑ Yes ☐ No	**Supplied adsorption data has no correction.**			
		If other, explain:			
☐ **keletal Density**	☑ Not Measured	☐ Measured:	g/cm³	Method used:	

COMMENTS

- Void volumes of the sample holder were determined using helium (99.999%) after keeping all parts of the instrument including the sample at 30 oC. In order to avoid helium adsorption errors, sample holder void volumes at 77K were calculated from a previously constructed reference curve (volume at -196 oC vs volume at 30 oC). The curve was obtained by inserting various amounts of non-adsorbing material (Pyrex glass) and performing volume calibrations at instrument temperature (30C) and measurement temperature (instrument at 30 oC and sample at -196 oC).
- A blank measurement was carried on the empty sample holder according to the specified experimental conditions and was subtracted from the actual isotherm. Due to the configuration of the instrument, it was impossible to obtain exactly the same set of recommended equilibrium pressure points. In order to extract blank values for the actual experimental equilibrium pressure points, linear interpolation of the blank isotherm was used.
- Liquid nitrogen level was kept constant during the experiments by means of a custom made automation which consists of a Pt-100 thermocouple acting as a level sensor, an on-off controller and an electronic valve connected to an external LN2 dewarr

Table 38 – Preparation of the sample for measurement from laboratory 8.

SAMPLE PREPARATION					
Run Number (same as "Experiment Result"):					
SAMPLE MASS					
Initial mass: 110.7	± 0.2	mg	Date: 08/11/2022		
After degass (optional):	±	mg	Date:		
Final mass: 109.8	± 0.2	mg	Date: 15/11/2022		
SAMPLE DEGASS	Begin date/time: 08/11/2022, 21:00		End date/time: 09/11/2022, 12.00		
Base Vacuum pressure: < 10e-06	units:mbar				
Degas protocol:	☑ Degas protocol Followed		☐ Degas protocol exception (Explain):		☐ Analysis repetition
Degass explanation: Sample was outgassed at 120C for 15 hours					
Was sample exposed to air after degas and prior to measurement?			☑ No	☐ Yes (explain):	
Air exposure explanation:					

MEASUREMENT INFORMATION					
Measurement method	☐ Gravimetric	☑ Volumetric	☐ Other:	☐ Static	Dynamic
Measurement temperature control	☑ Liquid nitrogen	☐ Other (specify):		If dynamic, flow rate:	
	Hydrogen purity: 99.999%		Additional purifier used? ☐ Yes	☑ No	
	Base Vacuum pressure: < 10e-06		Units: mbar		
	Sequence order:	☑ He calibration done first	☐ H_2 measurement done first	☐ No He calibration	
	Equilibration time/step: 5		min	Total time for measurement: 262	min
	Temperature stability: 0.5K	Standard deviation: 0.07	K	Pressure Sensor Accuracy: 1 ☐ % of FS:	☑ % of reading:
	Equation of State:	☐ Ideal	☑ Real: Model: BWR MBWR equation of state for hydrogen of Younglove (1982)		

CALIBRATION				
Helium Adsorption correction?	☑ Yes ☐ No	**Supplied adsorption data has no correction.**		
		If other, explain:		
Skeletal Density	☑ Not Measured	☐ Measured:	g/cm³	Method used:

COMMENTS

- Void volumes of the sample holder were determined using helium (99.999%) after keeping all parts of the instrument including the sample at 30 oC. In order to avoid helium adsorption errors, sample holder void volumes at 77K were calculated from a previously constructed reference curve (volume at -196 oC vs volume at 30 oC). The curve was obtained by inserting various amounts of non-adsorbing material (Pyrex glass) and performing volume calibrations at instrument temperature (30C) and measurement temperature (instrument at 30 oC and sample at -196 oC).
- A blank measurement was carried on the empty sample holder according to the specified experimental conditions and was subtracted from the actual isotherm. Due to the configuration of the instrument, it was impossible to obtain exactly the same set of recommended equilibrium pressure points. In order to extract blank values for the actual experimental equilibrium pressure points, linear interpolation of the blank isotherm was used.
- Liquid nitrogen level was kept constant during the experiments by means of a custom made automation which consists of a Pt-100 thermocouple acting as a level sensor, an on-off controller and an electronic valve connected to an external LN2 dewar

Table 39 – Preparation of the sample for measurement from laboratory 8.

SAMPLE PREPARATION					
Run Number (same as "Experiment Result"):					
SAMPLE MASS					
Initial mass: 189.5	± 0.2	mg	Date: 30/01/2023		
After degass (optional):	±	mg	Date:		
Final mass: 188.5	± 0.2	mg	Date:02/02/2023		
SAMPLE DEGASS	Begin date/time: 30/01/2023, 21:00		End date/time:31/01/2023, 12.00		
Base Vacuum pressure: < 10e-06	units: mbar				
Degas protocol:	☑ Degas protocol Followed		☐ Degas protocol exception (Explain):		☐ Analysis repetition
Degass explanation: Sample was outgassed at 120C for 15 hours					
Was sample exposed to air after degas and prior to measurement?			☑ No	☐ Yes (explain):	
Air exposure explanation:					
	☐				

MEASUREMENT INFORMATION					
Measurement method	☐ Gravimetric	☑ Volumetric	☐ Other:	☐ Static	Dynamic
Measurement temperature control	☑ Liquid nitroge ☐	Other (specify):		If dynamic, flow rate:	
	Hydrogen purity: 99.999%		Additional purifier used?	☐ Yes	☑ No
	Base Vacuum pressure: < 10e-06		Units: mbar		
	Sequence order:	☑ He calibration done first	☐	H_2 measurement done	☐ No He calibration
	Equilibration time/step: 5		min	Total time for measurement: 220	min
	Temperature stability: 0.5K	Standard deviation: 0.07	K	Pressure Sensor Accuracy: 1 ☐ % of FS:	☑ % of reading:
	Equation of State:	☐ Ideal	☑ Real: Model: BWR MBWR equation of state for hydrogen of Younglove (1982)		

CALIBRATION				
Helium Adsorption correction?	☑ Yes ☐ No	**Supplied adsorption data has no correction.**		
		If other, explain:		
Skeletal Density	☑ Not Measured ☐	Measured:	g/cm³	Method used:

COMMENTS

- Void volumes of the sample holder were determined using helium (99.999%) after keeping all parts of the instrument including the sample at 30 oC. In order to avoid helium adsorption errors, sample holder void volumes at 77K were calculated from a previously constructed reference curve (volume at -196 oC vs volume at 30 oC). The curve was obtained by inserting various amounts of non-adsorbing material (Pyrex glass) and performing volume calibrations at instrument temperature (30C) and measurement temperature (instrument at 30 oC and sample at -196 oC).
- A blank measurement was carried on the empty sample holder according to the specified experimental conditions and was subtracted from the actual isotherm. Due to the configuration of the instrument, it was impossible to obtain exactly the same set of recommended equilibrium pressure points. In order to extract blank values for the actual experimental equilibrium pressure points, linear interpolation of the blank isotherm was used.
- Liquid nitrogen level was kept constant during the experiments by means of a custom made automation which consists of a Pt-100 thermocouple acting as a level sensor, an on-off controller and an electronic valve connected to an external LN2 dewar

Table 40 – Preparation of the sample for measurement from laboratory 9.

SAMPLE PREPARATION							
Run Number (same as "Experiment Result"):							
SAMPLE MASS							
Initial mass: 84.510	± 0.001	mg	Date: 16/02/2023				
After degass (optional):	±	mg	Date:				
Final mass: 84.085	± 0.001	mg	Date: 17/02/2023				
SAMPLE DEGASS	Begin date/time: 21:00		End date/time: 12:00				
Base Vacuum pressure: < 10e-06	units: mbar						
Degas protocol:	☑ Degas protocol Followed		☐ Degas protocol exception (Explain):				☐ Analysis repetition
Degass explanation: Sample was outgassed at 120C for 15 hrs							
Was sample exposed to air after degas and prior to measurement?				☑ No	☐ Yes (explain):		
Air exposure explanation:							
MEASUREMENT INFORMATION							
Measurement method ☑	Gravimetric		☐ Volumetric	☐ Other:	☑ Static	Dynamic	
Measurement temperature control	☑ Liquid nitrogen	☐	Other (specify):		If dynamic, flow rate:		
	Hydrogen purity: 99.999%			Additional purifier used?	☐ Yes	☑ No	
	Base Vacuum pressure: < 10e-06			Units: mbar			
	Sequence order:		☐ He calibration done first	☐	H_2 measurement done first	☑ No He calibration	
	Equilibration time/step: 5			min	Total time for measurement: 162	min	
	Temperature stability: 0.5 K		Standard deviation: 0.2	K	Pressure Sensor Accuracy: 0.05 ☑ % of FS:	☐ % of reading:	
	Equation of State:		☐ Ideal		☑ Real: Model: BWR MBWR equation of state for hydrogen of Younglove (1982)		
CALIBRATION							
Helium Adsorption correction? ☐	Yes ☑ No		**Supplied adsorption data has no correction.**				
			If other, explain:				
Skeletal Density ☐	Not Measured	☑	Measured: 1.51	g/cm³	Method used: Helium pycnometry (in situ gravimetric)		
COMMENTS							
The blank run was performed after adding to the balance bucket a non-adsorbing material (pyrex glass, m=82.994 mg, density used 2.23 g/cm3). The blank measurement was then subtracted from the ZIF-8 isotherms							

Table 41 – Preparation of the sample for measurement from laboratory 9.

SAMPLE PREPARATION							
Run Number (same as "Experiment Result"):							
SAMPLE MASS							
Initial mass: 39.965	± 0.001	mg	Date: 15/03/2023				
After degass (optional):	±	mg	Date:				
Final mass: 39.695	± 0.001	mg	Date: 16/03/2023				
SAMPLE DEGASS	Begin date/time: 21:00		End date/time: 12:00				
Base Vacuum pressure: < 10e-06	units: mbar						
Degas protocol:	☑ Degas protocol Followed		☐ Degas protocol exception (Explain):				☐ Analysis repetition
Degass explanation: Sample was outgassed at 120C for 15 hrs							
Was sample exposed to air after degas and prior to measurement?				☑ No	☐ Yes (explain):		
Air exposure explanation:							
			☐				
MEASUREMENT INFORMATION							
Measurement method ☑	Gravimetric		☐ Volumetric	☐ Other:	☑ Static	Dynamic	
Measurement temperature control	☑ Liquid nitrogen	☐	Other (specify):		If dynamic, flow rate:		
	Hydrogen purity: 99.999%			Additional purifier used?	☐ Yes	☑ No	
	Base Vacuum pressure: < 10e-06			Units: mbar			
	Sequence order:		☐ He calibration done first	☐	H_2 measurement done first	☑ No He calibration	
	Equilibration time/step: 5			min	Total time for measurement: 144	min	
	Temperaature stability: 0.5 K		Standard deviation: 0.2	K	Pressure Sensor Accuracy: 0.05 ☑ % of FS:	☐ % of reading:	
	Equation of State:		☐ Ideal		☑ Real: Model: BWR MBWR equation of state for hydrogen of Younglove (1982)		
CALIBRATION							
Helium Adsorption correction? ☐	Yes ☑ No		**Supplied adsorption data has no correction.**				
			If other, explain:				
Skeletal Density ☐	Not Measured	☑	Measured: 1.51	g/cm³	Method used: Helium pycnometry (in situ gravimetric)		
COMMENTS							
The blank run was performed after adding to the balance bucket a non-adsorbing material (pyrex glass, m=82.9944 mg, density used 2.23 g/cm3). The blank measurement was then subtracted from the ZIF-8 isotherms							

Table 42 – Preparation of the sample for measurement from laboratory 10.

SAMPLE PREPARATION						
Run Number (same as "Experiment Result"): 1						
SAMPLE MASS						
Initial mass:	±	mg	Date:			
After degass (optional):	±	mg	Date:			
Final mass: 1.4512	±0.0001	mg	Date: 18/11/2022			
SAMPLE DEGASS	Begin date/time: 16/11/2022		End date/time: 17/11/2022			
Base Vacuum pressure	units: 1x10-7 mbar					
Degas protocol:	☑ Degas protocol Followed		☐ Degas protocol exception (Explain):			☑ Analysis repetition
Degass explanation:						
Was sample exposed to air after degas and prior to measurement?			☑ No	☐ Yes (explain):		
Air exposure explanation:						

MEASUREMENT INFORMATION						
Measurement method	☐ Gravimetric	☑ Volumetric	☐ Other:	☑ Static	Dynamic	
Measurement temperature control	☑ Liquid nitrogen	☐ Other (specify):		If dynamic, flow rate:		
	Hydrogen purity: 99.9995%		Additional purifier used? ☐ Yes		☑ No	
	Base Vacuum pressure:		Units:			
	Sequence order:	☐ He calibration done first	☑ H_2 measurement done first		☐ No He calibration	
	Equilibration time/step:		min	Total time for measurement:	min	
	Temperaature stability	Standard deviation:	K	Pressure Sensor Accuracy: ☐ % of FS:	☐ % of reading:	
	Equation of State:	☐ Ideal	☑ Real: Model: mBWR-Jacobsen			

0.064931383334+C9:C47

Helium Adsorption correction?	☑ Yes ☐ No	**Supplied adsorption data has no correction.**		
		If other, explain:		
Skeletal Density	☐ Not Measured	☑ Measured:	1.43 g/cm³	Method used: He pycnometry

Table 43 – Preparation of the sample for measurement from laboratory 10.

SAMPLE PREPARATION						
Run Number (same as "Experiment Result"): 1						
SAMPLE MASS						
Initial mass:	±	mg	Date:			
After degass (optional):	±	mg	Date:			
Final mass: 1.4512	±0.0001	mg	Date: 18/11/2022			
SAMPLE DEGASS	Begin date/time: 16/11/2022		End date/time: 17/11/2022			
Base Vacuum pressure	units: 1x10-7 mbar					
Degas protocol:	☑ Degas protocol Followed		☐ Degas protocol exception (Explain):			☑ Analysis repetition
Degass explanation:						
Was sample exposed to air after degas and prior to measurement?			☑ No	☐ Yes (explain):		
Air exposure explanation:						

MEASUREMENT INFORMATION						
Measurement method	☐ Gravimetric	☑ Volumetric	☐ Other:	☑ Static	Dynamic	
Measurement temperature control	☑ Liquid nitrogen	☐ Other (specify):		If dynamic, flow rate:		
	Hydrogen purity: 99.9995%		Additional purifier used? ☐ Yes		☑ No	
	Base Vacuum pressure:		Units:			
	Sequence order:	☐ He calibration done first	☑ H_2 measurement done first		☐ No He calibration	
	Equilibration time/step:		min	Total time for measurement:	min	
	Temperaature stability	Standard deviation:	K	Pressure Sensor Accuracy: ☐ % of FS:	☐ % of reading:	
	Equation of State:	☐ Ideal	☑ Real: Model: mBWR-Jacobsen			

0.064931383334+C9:C47

Helium Adsorption correction?	☑ Yes ☐ No	**Supplied adsorption data has no correction.**		
		If other, explain:		
Skeletal Density	☐ Not Measured	☑ Measured:	1.43 g/cm³	Method used: He pycnometry

Table 44 – Preparation of the sample for measurement from laboratory 15.

SAMPLE PREPARATION							
Run Number (same as "Experiment Result"):							
SAMPLE MASS							
Initial mass:	±	mg		Date:			
After degass (optional):	±	mg		Date:			
Final mass: 1132.9	±	mg		Date:			
SAMPLE DEGASS	Begin date/time:		03/02/2023	End date/time:			
Base Vacuum pressure	units:						
Degas protocol:	☐Degas protocol Followed		☐ Degas protocol exception (Explain):			☐ Analysis repetition	
Degass explanation:							
Was sample exposed to air after degas and prior to measurement?				☐ No		☐ Yes (explain):	
Air exposure explanation:							
MEASUREMENT INFORMATION							
Measurement method	☐ Gravimetric		☑ Volumetric	☐ Other:		☑ Static	Dynamic
Measurement temperature control	☑ Liquid nitrogen		☐ Other (specify):			If dynamic, flow rate:	
	Hydrogen purity:			Additional purifier used?		☐ Yes	☐ No
	Base Vacuum pressure:			Units:			
	Sequence order:	☐		He calibration done first	☐	H_2 measurement done first	☐ No He calibration
	Equilibration time/step:			min	Total time for measurement:		min
	Temperaature stability	Standard deviation:		K	Pressure Sensor Accuracy:	☐ % of FS:	☐% of reading:
	Equation of State:	☐	Ideal	☑ Real: Model:		mBWR-Jacobsen	
CALIBRATION							
Helium Adsorption correction?	☐ Yes ☐ No		**Supplied adsorption data has no correction.**				
			If other, explain:				
Skeletal Density	☐ Not Measured		☐ Measured:	g/cm³		Method used:	

7.4.2 Hydrogen adsorption results

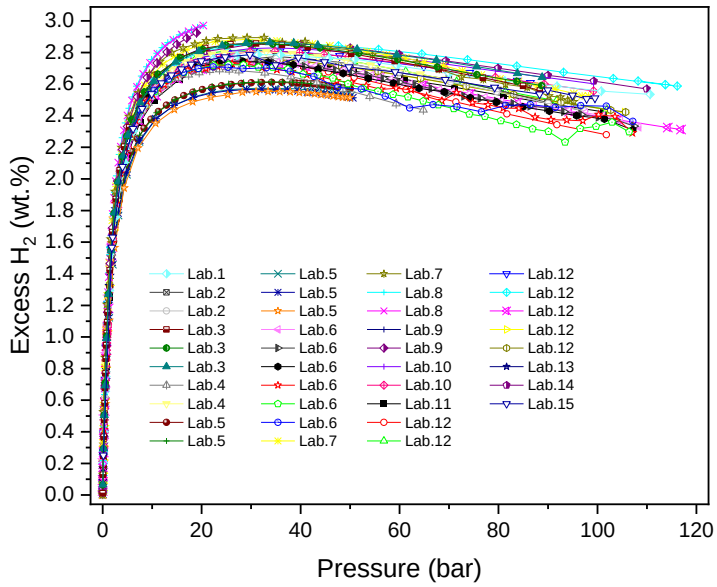

Figure 95 – Comparison of all the H_2 adsorption isotherms at 77 K from the 15 laboratories participating in this study.

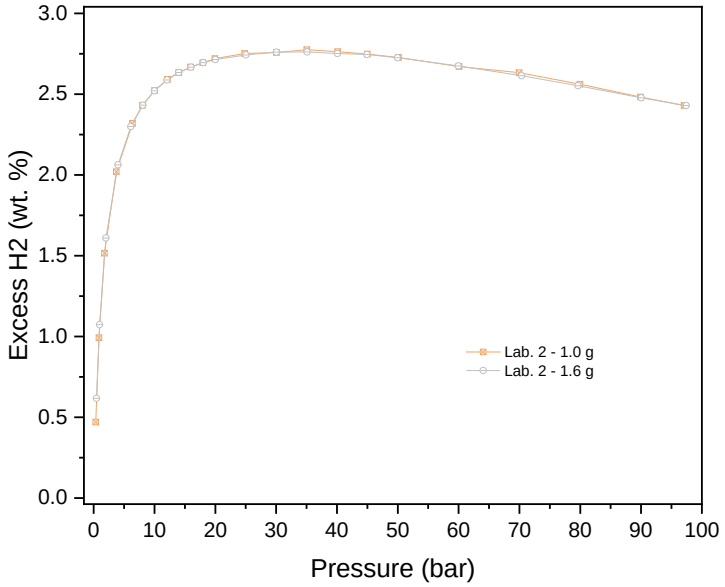

Figure 96 – Comparison of H_2 adsorption isotherms at 77 K from the laboratory 2 using different amounts of sample.

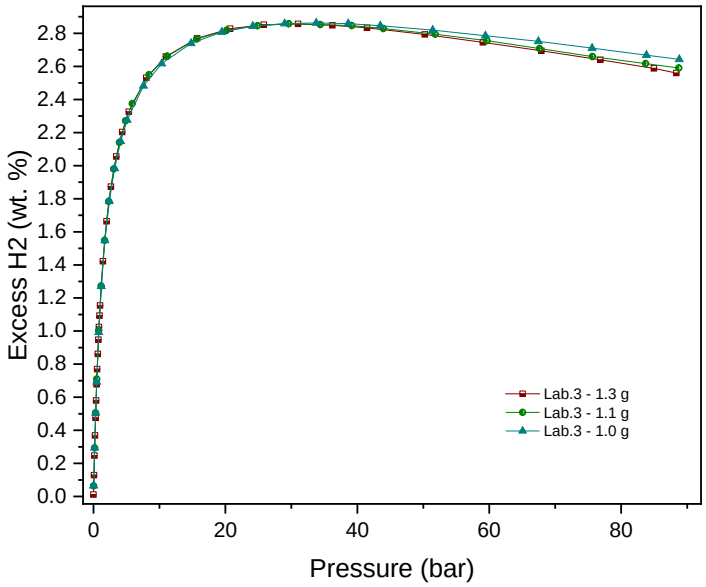

Figure 97 – Comparison of H_2 adsorption isotherms at 77 K from the laboratory 3 using similar amounts of sample.

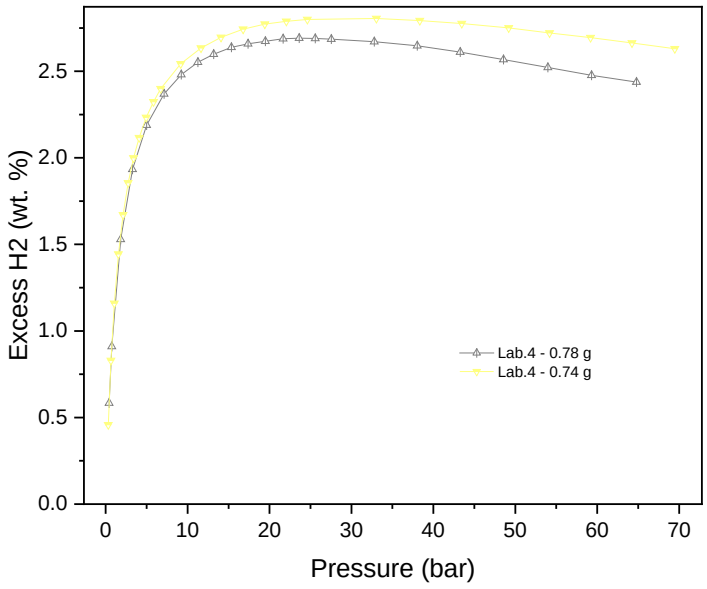

Figure 98 – Comparison of H_2 adsorption isotherms at 77 K from the laboratory 4 using similar amounts of sample.

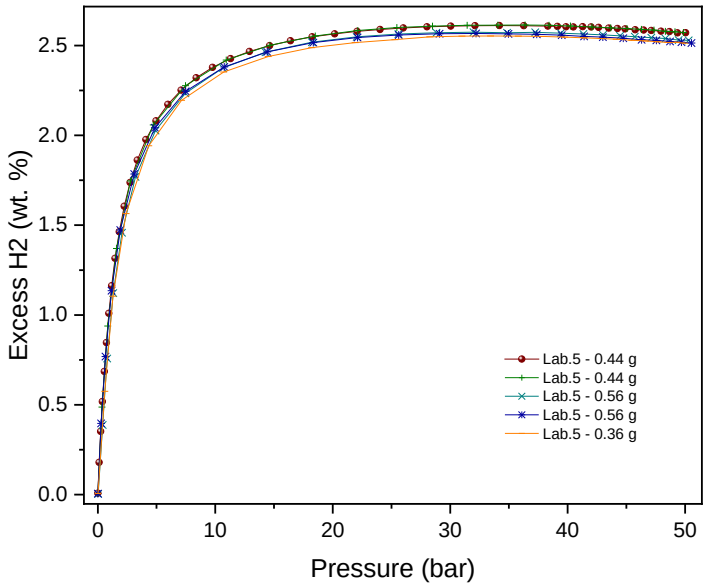

Figure 99 – Comparison of H_2 adsorption isotherms at 77 K from the laboratory 5 using different amounts of analysed sample.

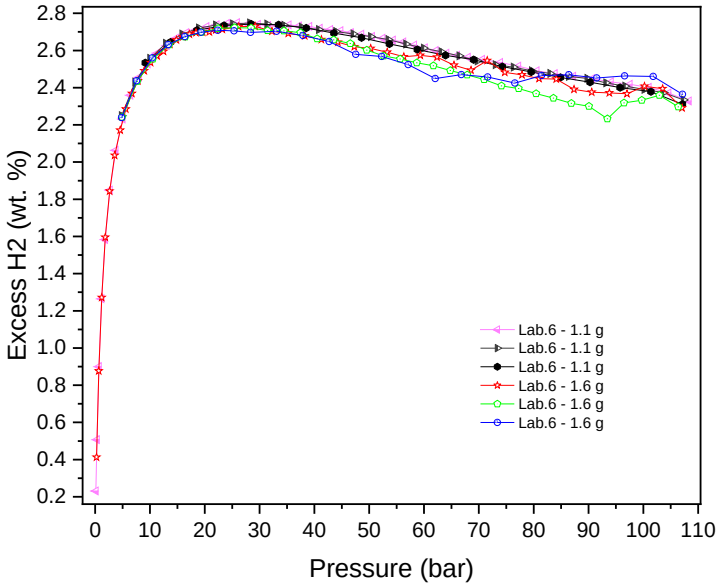

Figure 100 – Comparison of H_2 adsorption isotherms at 77 K from the laboratory 5 using different amounts of sample.

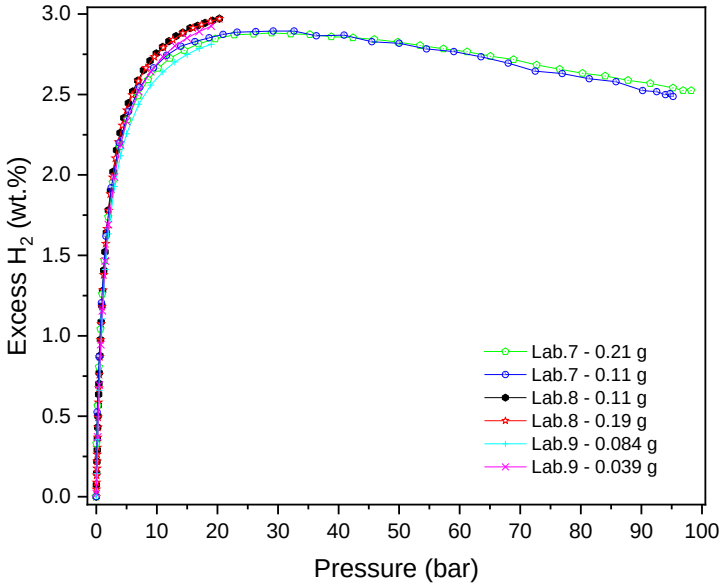

Figure 101 – Comparison of H_2 adsorption isotherms at 77 K from the laboratories 7, 8 and 9 using different amounts of sample and volumetric (7 and 8) and gravimetric (9) analysers.

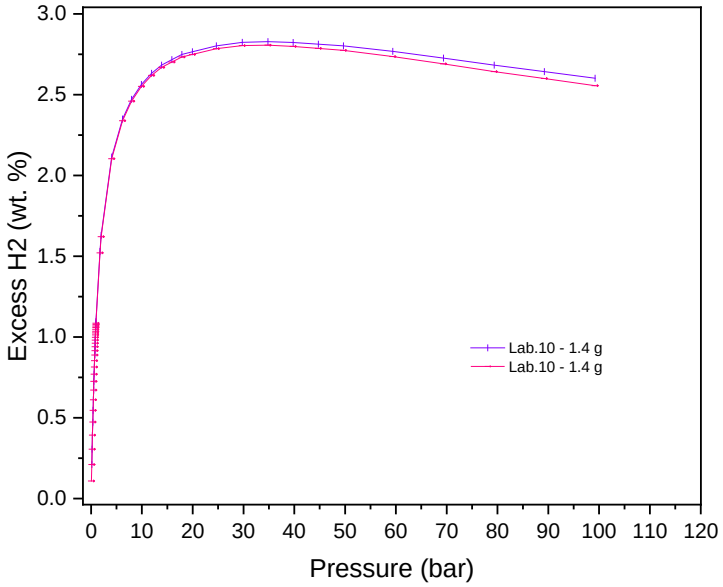

Figure 102 – Comparison of H_2 adsorption isotherms at 77 K from the laboratory 10.

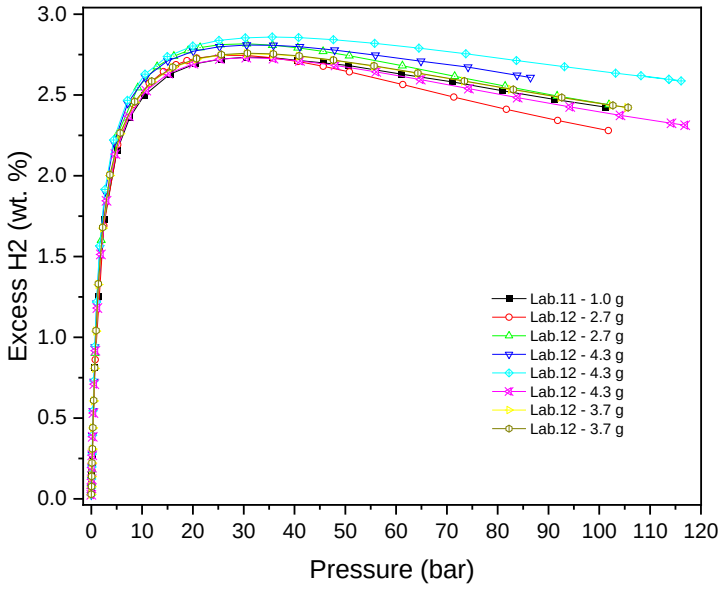

Figure 103 – Comparison of H_2 adsorption isotherms at 77 K from the laboratories 11 and 12.

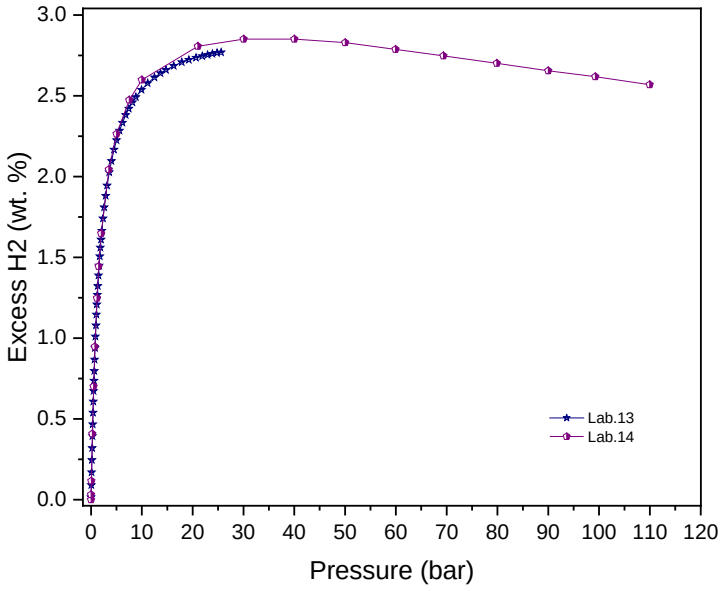

Figure 104 – Comparison of H_2 adsorption isotherms at 77 K from the laboratories 13 and 14, using volumetric and gravimetric devices, respectively, with the same operator.